**BRUNO LUAN ROSA**

# THE GENETIC BASIS OF DROUGHT RESISTANCE IN TOMATO

Thesis submitted to the Plant Physiology Graduate Program of the Universidade Federal de Viçosa in partial fulfillment of the requirements for the degree of *Doctor Scientiae*.

Adviser: Agustin Zsögön

**VIÇOSA - MINAS GERAIS**
**2022**

**Ficha catalográfica elaborada pela Biblioteca Central da Universidade Federal de Viçosa - Campus Viçosa**

T
R788g
2022

Rosa, Bruno Luan, 1988-
The genetic basis of drought resistance in tomato / Bruno Luan Rosa. – Viçosa, MG, 2022.
1 tese eletrônica (108 f.): il. (algumas color.).

Texto em inglês.
Orientador: Agustin Zsögön.
Tese (doutorado) - Universidade Federal de Viçosa, Departamento de Biologia Vegetal, 2022.
Inclui bibliografia.
DOI: https://doi.org/10.47328/ufvbbt.2022.667
Modo de acesso: World Wide Web.

1. Tomate - Genética. 2. Tomate - Resistência à seca. 3. Estresse hídrico. 4. Introgressão genética. I. Zsögön, Agustin, 1980-. II. Universidade Federal de Viçosa. Departamento de Biologia Vegetal. Programa de Pós-Graduação em Fisiologia Vegetal. III. Título.

CDD 22. ed. 635.6422

Bibliotecário(a) responsável: Alice Regina Pinto Pires CRB-6/2523

**BRUNO LUAN ROSA**

# THE GENETIC BASIS OF DROUGHT RESISTANCE IN TOMATO

Thesis submitted to the Plant Physiology Graduate Program of the Universidade Federal de Viçosa in partial fulfillment of the requirements for the degree of *Doctor Scientiae*.

APPROVED: 8th April, 2022

Assent:

Bruno Luan Rosa
Author

Agustin Zsögön
Adviser

## ACKNOWLEDGMENTS

I first thank God for giving me health, strength, and wisdom to live;

To my dear parents Marlene Rosa and Renato Rosa for educating me and teaching me a lot about love and care for plants, you are a great example for my life;

To my dear girlfriend Tatiana Gonzaga Homem, thank you for always being by my side at all times and making me so happy;

To my friends in the post-graduation program in plant physiology, Emmanuel, Juliene, Leonardo, Mateus, Maria Carolina, Bruno, Thalita, Diego, Guilherme, João, Pedro, thank you very much for the valuable companionship and the laughs;

To my brothers from República Poligono, Daniel, Moab, Ari, thanks for making these four years here in Viçosa much more pleasant, living with you was a very good experience;

To Prof. Agustin Zsögön thanks for having accepted to guide me in this journey, for having had patience and concern with my development, and for the valuable teachings;

To Prof. Samuel Cordeiro Vitor Martins for his co-Adviser and for always being willing to answer my questions;

To Prof. Eduardo Gusmão Pereira for introducing me to scientific research and for encouraging me to deepen my knowledge in plant science;

To the Universidade Federal de Viçosa (UFV) and all teachers, technicians, and other servers of PPG - Plant Physiology, thank you for teaching and for making this work possible;

This study was financed in part by the Coordenação de Aperfeiçoamento de Pessoal de Nível Superior - Brasil (CAPES) - Finance Code 001.

To the Coordenadoria de Aperfeiçoamento de Pessoal de nível Superior (CAPES) and the Fundação de Amparo a Pesquisa do Estado de Minas Gerais (FAPEMIG) for funding and assistance;

To the Brazilian people for funding this work;

My sincere thanks.

## ABSTRACT

ROSA, Bruno Luan, D.Sc., Universidade Federal de Viçosa, April, 2022. **The genetic basis of drought resistance in tomato.** Adviser: Agustin Zsögön.

The development of crop varieties capable of maintaining satisfactory yields under stressful conditions such as drought is an important step towards ensuring adequate food production in the future. In this context, natural genetic variation in tomato can be allied with modern techniques such as the production of introgression lines, as well as mutant and transgenic organisms in the search for varieties more resistant to water deficit. Here, we show that *S. pennellii* introgression lines IL2-5, IL4-3, and IL2-5/4-3 exhibit increased leaf succulence, as well as significant changes in leaf thickness and stomatal density. Together, these leaf traits contributed to the maintenance of leaf water status, which improved photosynthetic performance and plant resilience when subjected to drought conditions. In this work, we also demonstrated the physiological and hydraulic changes caused by an allelic variant of the *OBSCURAVENOSA* (*OBV*) gene. In addition to controlling the development of vascular bundle sheath extensions (BSE), this gene also resulted in significant changes in leaf insertion angle, leaf margin serration, venation density, and fruit shape. We found that BSE development is strongly linked functionally to the auxin signaling network involving *AUXIN RESPONSE FACTOR* 4 (*ARF4*). Lastly, we show that loss of function of *ARF4* alters leaf structure, resulting in a phenotype with severe leaf curling and low stomatal conductance. Loss of *ARF4* function increased water and abscisic acid content in leaves, resulting in significant improvements in tomato plant resistance to salt and osmotic stress. Our data provide evidence that anatomical and morphological changes in leaves, whether from natural genetic variation or genetically modified organisms, can help to better understand the process of resistance to abiotic stress, such as drought and salinity. Thus, we suggest that mapping and identifying the genes responsible for the leaf traits demonstrated here may help in the creation of future varieties that are more resistant to water deficit.



**Keywords:** *Solanum pennellii*. Introgression lines. Auxin. CRISPR-Cas9. Bundle sheath extensions. Drought stress.

## RESUMO

ROSA, Bruno Luan, D.Sc., Universidade Federal de Viçosa, abril de 2022. **A base genética da resistência à seca no tomateiro**. Orientador: Agustin Zsögön.

O desenvolvimento de variedades capazes de manter rendimentos satisfatórios sob condições estressantes, como a seca, é um passo importante para garantirmos a produção adequada de alimentos no futuro. Neste contexto, a variação genética natural do tomateiro pode ser aliada a técnicas modernas, como a produção de linhagens de introgressão, assim como organismos mutantes e transgênicos na busca de cultivares mais resistentes ao déficit hídrico. Aqui, mostramos que as linhagens de introgressão *S. pennellii* IL2-5, IL4-3 e IL2-5/4-3 exibem maior suculência foliar, bem como mudanças significativas na espessura da folha e na densidade estomática. Juntos, essas características foliares contribuíram para a manutenção do status hídrico foliar, o que melhorou o desempenho fotossintético e a resiliência da planta quando submetida a condições de seca. Neste trabalho, também demonstramos as alterações fisiológicas e hidráulicas causadas por uma variante alélica do gene *OBSCURAVENOSA* (*OBV*). Além de controlar o desenvolvimento de extensões de bainha vascular (BSE), este gene também resultou em mudanças significativas no ângulo de inserção da folha, na serração da margem da folha, na densidade de venação e na forma do fruto. Descobrimos que o desenvolvimento da BSE está fortemente ligada a rede de sinalização de auxina envolvendo *AUXIN RESPONSE FACTOR 4* (*ARF4*). Por fim, a perda de função de *ARF4* altera a estrutura das folhas, resultando em um fenótipo com severo enrolamento foliar e baixa condutância estomática. Aqui, mostramos que a perda da função do *ARF4* aumentou o conteúdo de água e ácido abscísico nas folhas, resultando em melhorias significativas na resistência do tomateiro ao estresse salino e osmótico. Nossos dados fornecem evidências de que alterações anatômicas e morfológicas das folhas, sejam elas provenientes da variação genética natural ou de organismos geneticamente modificados, podem ajudar a entender melhor o processo de resistência ao estresse abiótico, como a seca e a salinidade. Assim, sugerimos que o mapeamento e identificação dos genes responsáveis pelas características foliares aqui demonstradas podem ajudar na criação de futuras variedades mais resistentes ao déficit hídrico.

**Palavras-chave:** *Solanum pennellii*. Linhagens de introgressão. Auxina. CRISPR-Cas9. Extensões da bainha do feixe vascular. Estresse hídrico.

**CONTENTS**

## GENERAL INTRODUCTION

The leaf thickness is a determinant trait for photosynthetic efficiency, also playing an important role in the survivability of plants to extreme climatic factors (Ogburn and Edwards, 2010; Poorter *et al.*, 2010; Galmés *et al.*, 2013). In tomato, increased leaf thickness linked to elongation of palisade parenchyma cells may function as an adaptation to arid environments, this being a trait responsive to environmental conditions of light and water (Coneva *et al.*, 2017). High ploidy levels have been observed in thicker tomato leaves, indicating that increased endoreduplication may support larger cells and, consequently, thicker leaves (Coneva *et al.*, 2017). In this work, we investigated whether the association between increased leaf thickness and increased mesophyll cell size may result in greater succulence ensuring greater drought resistance to tomato. The term succulence can be defined as the ability of a plant to store water in living tissues becoming temporarily independent of the external water supply (Males, 2017). Succulence in plants is considered the most successful anatomical adaptation in terms of drought avoidance and has a strong link with increased ploidy and leaf thickness (Males, 2017; Lim *et al.*, 2020).

Vascular bundle sheath extensions (BSE) have a strong influence on leaf hydraulic conductance, consequently, the presence of this structure in leaves tends to increase stomatal conductance thus benefiting an improvement in photosynthetic activity (Brodribb *et al.*, 2007; Buckley *et al.*, 2011; Sack and Scoffoni, 2013; Zsögön *et al.*, 2015). Despite their functional impact, what determines the distribution of leaf BSEs in natural and agrarian environments has yet to be unraveled. Thus, identifying the genetic basis of BSEs may help to understand the ecological functions of this structure, as well as the benefits of using this structure for the development of more productive varieties.

Finally, in this work, we also address the effects of loss-of-function and a CRISPR/cas9-induced mutant in *SlARF4* on tomato resistance capacity to salinity, drought, and osmotic stress. Auxin response factors (*ARF*s) can be related to different plant responses to environmental stresses, including through significant changes in leaf morphology (Jones *et al.*, 2002). However, the role of *ARF*s in different plant responses under environmental stress conditions remains poorly understood. Here, we show through morphological, anatomical, physiological, and molecular analyses, how the involvement of *SlARF4* may affect the responses of tomato plants to these stresses.

Genetic control of leaf thickness based on natural genetic variation in tomato

Natural genetic variation, coupled with the advent of modern molecular biology techniques, such as molecular markers and gene editing, complement each other, aiding the breeding process in plants (Mascher *et al.*, 2019). Introgression lines (IL) of *S. pennellii* (*S. pen*), produced in the background of tomato (*S. lycopersicum* - *S. lyc*) cultivar M82 (Eshed and Zamir, 1995), are among the most important tools for tomato genetic mapping (Alseekh *et al.*, 2013). The complete population of *S. pen* ILs covers the entire genome of tomato cv. M82 with overlapping segments of *S. pen*. Thus, every phenotypic difference observed between ILs, or between ILs and the parents, can be attributed to one or more genes found within the introgressed chromosomal segment (deVicente and Tanksley, 1993). Thus, a multitude of quantitative trait loci (QTL), responsible for environmental adaptations, productivity, metabolism, and gene expression, are exposed (Lippman *et al.*, 2007).

Several leaf phenotypes can be observed in a population of *S. pen* IL, many of which exhibit traits with a strong influence on drought responsitvity (Chitwood *et al.*, 2013; Coneva *et al.*, 2017). Plants growing in arid environments commonly exhibit leaves with smaller areas, increased thickness, higher pilosity, and high succulence (Poorter *et al.*, 2009; Sack *et al.*, 2012; Ogburn and Edwards, 2012; Coneva *et al.*, 2017; Galdon-Armero *et al.*, 2018). Alteration of some of these leaf traits, such as thickness, stomatal and venation density can significantly influence gas exchange, photoassimilate transport, hydraulic conductance, and water use efficiency (Sack and Holbrook, 2006; Brodribb *et al.*, 2007; Sack *et al.*, 2012; Zsögön *et al.*, 2015). Some of these leaf traits observed in ILs of *S. pen* segregate independently, facilitating the selection of specific phenotypes (Chitwood *et al.*, 2013). This behavior, coupled with the strong coordination between anatomical and physiological traits in the leaf, may enable leaf anatomy to be manipulated to withstand water shortage conditions without impairing agronomic performance (Chitwood *et al.*, 2013; Muir *et al.*, 2017). In this way, leaf traits present in wild tomato species can be introduced into commercial cultivars, to make them more tolerant to climate change and better adapted to the specific conditions of current agronomic practices (Muir *et al.*, 2017).

Tomato is the most cultivated vegetable worldwide (Schwarz *et al.*, 2014) , according to FAO, the sum productivity of 175 countries in 2016 reached a total of 177 million tons of tomatoes, which were produced in approximately 4.8 million hectares of cultivated area (www.fao.org/faostat). Despite its food importance and great genetic variation, few genes conferring drought resistance have been identified in this species (Iovieno *et al.*, 2016*a*; Arms

*et al.*, 2017). IL2-5, IL4-3, and IL2-5/4-3 have thicker leaves compared to the other ILs of S. pen and its background cv. M82 (coneva eta al). However, the behavior of these ILs under drought conditions has not yet been characterized. Here, we provide the hypothesis that the increased leaf thickness of these ILs may be accompanied by increased leaf succulence. In this context, through characterization of IL2-5 and IL4-3 from *S. pen* we demonstrate the role of leaf traits, such as increased leaf thickness and succulence, in enhancing drought resistance in tomato.

Influence of BSEs on leaf functions

The spontaneous mutant *obscuravenosa* (*obv*) has a characteristic leaf phenotype, which is marked by the absence of vascular bundle sheath extensions (BSE*s*) in the leaves (Wylie, 1952). The presence of BSE*s* is commonly observed in the leaves of most tree species that reach the canopy in a forest. However, this is not a commonly observed characteristic in undergrowth species (Kenzo *et al.*, 2007). The *BSE* consists of a column of parenchymatic and sclerenchymatic cells that connects the vascular bundle to the adaxial or abaxial epidermis, or both, in leaves of many species. The presence of BSE compartmentalizes the mesophyll and creates barriers that prevent lateral diffusion of gases, especially $CO_2$ (Terashima, 1992). Compartmentalization of the mesophyll causes gas pressure along the leaf lamina to be heterogeneous. Thus, leaves that possess BSE are termed heterobaric (Terashima, 1992). The presence of BSE increases water distribution and light transfer to the inner layers of the mesophyll benefiting photosynthetic performance along the leaf and plant canopy (Karabourniotis *et al.*, 2000; Buckley *et al.*, 2015). However, the main role played by BSE is the hydraulic integration between mesophyll tissues and vascular tissues (Brodribb *et al.*, 2007; Buckley *et al.*, 2011).

On the other hand, the absence of BSE increases the lateral diffusion of gases, consequently, the gas pressure in the mesophyll along the leaf lamina can become homogeneous, and leaves with this characteristic are classified as homobaric (Terashima, 1992; Pieruschka *et al.*, 2006). In these leaves, hydraulic integration is limited and water transport faces greater resistance (Zsögön *et al.*, 2015). However, increasing lateral $CO_2$ flux, in homobaric leaves, can improve photosynthetic activity, increase water-use efficiency (*WUE*), and reduce photoinhibition damage (Pieruschka *et al.*, 2006; Xu *et al.*, 2008; Barbosa *et al.*, 2019).

The tomato is an ideal genetic model to study the ecophysiological functions of BSE, as its species and varieties exhibit variation for this leaf trait. The absence of *BSE* in tomato

was attributed to the *obv* mutation, whose locus was mapped on chromosome 5, in bin 5G, with the help of IL from *S. pen* (Jones *et al.*, 2007). The discovery of the bin where the *obv* mutation is contained facilitated the mapping of possible candidate genes (Chitwood *et al.*, 2013). Here, we identify a functional allelic variant of *OBV* and characterize its influence on physiological and hydraulic responses in tomato.

The role of auxin in abiotic stress responses

Despite being the first discovered phytohormone, the role of auxin in stress responses in plants remains poorly studied (Sharma *et al.*, 2015). The diversity of morphological and physiological responses mediated by auxin highlights its important role in plant survival (Barkoulas *et al.*, 2007; Bielach *et al.*, 2017). Recent work provides evidence that auxin can mitigate the negative effects generated by various abiotic stresses, including water deficit (Bielach et al., 2017; Hu et al., 2015; Sharma et al., 2015; Van Ha et al., 2013). Endogenous auxin levels can modulate redox homeostasis and regulate root development during drought, also causing significant morphophysiological changes in the aerial part (Wang *et al.*, 2005; Ivanchenko *et al.*, 2013; Bouzroud *et al.*, 2018).

*ARF* family genes have been identified and characterized in tomato (Zouine *et al.*, 2014) and are involved in the control of many physiological processes, such as lateral root development, fruit development, expansion, leaf senescence, and embryogenesis (Zhang *et al.*, 2015; Breitel *et al.*, 2016). For example, negative regulation of *ARF4* expression by antisense RNA (*ARF4-as*) results in severe leaf curling as well as changes in fruit ripening (Sagar *et al.*, 2013). Alterations in auxin signaling during water deficit have already been observed in many plant (Bouzroud et al., 2018; Hu et al., 2015; Kang et al., 2018; Van Ha et al., 2013). In tomato, exposure to drought stress resulted in significant increases in the expression of several *ARF* genes, including *SlARF4*, in leaves and roots (Bouzroud et al., 2018). Thus, the auxin signaling network may help explain how the suite of leaf morphological traits, such as leaf complexity, size, serration, succulence, as well as stomata, and vein density, may influence water deficit resistance in this species (Barkoulas *et al.*, 2007; Lim *et al.*, 2020). Here, we determined the influence of negative regulation and loss of function of *ARF4* on tomato plant survivability to drought, salinity, and osmotic stress. In this work, we demonstrate the role of *ARF4* in enhancing drought resistance as well as salinity resistance using *ARF4* knockout mutant (*ARF4-KO*) and transgenic lines with antisense RNA (*ARF4-as*) in the Micro-Tom background.

**REFERENCES**

**Alseekh S, Ofner I, Pleban T, Tripodi P, Di Dato F, Cammareri M, Mohammad A, Grandillo S, Fernie AR, Zamir D**. 2013. Resolution by recombination: breaking up Solanum pennellii introgressions. Trends in Plant Science **18**, 536–538.

**Arms EM, Yan Z, St Clair DA**. 2017. Differential transcriptional regulation in roots of tomato near-isogenic lines in response to rapid-onset water stress. Frontiers in plant science **8**, 166.

**Barbosa MAM, Chitwood DH, Azevedo AA, Araújo WL, Ribeiro DM, Peres LEP, Martins SCV, Zsögön A**. 2019. Bundle sheath extensions affect leaf structural and physiological plasticity in response to irradiance. Plant, Cell & Environment **42**, 1575–1589.

**Barkoulas M, Galinha C, Grigg SP, Tsiantis M**. 2007. From genes to shape: regulatory interactions in leaf development. Current Opinion in Plant Biology **10**, 660–666.

**Bielach A, Hrtyan M, Tognetti VB**. 2017. Plants under Stress: Involvement of Auxin and Cytokinin. International Journal of Molecular Sciences **18**, 1427.

**Bouzroud S, Gouiaa S, Hu N, Bernadac A, Mila I, Bendaou N, Smouni A, Bouzayen M, Zouine M**. 2018. Auxin Response Factors (ARFs) are potential mediators of auxin action in tomato response to biotic and abiotic stress (Solanum lycopersicum) (K Wu, Ed.). PLOS ONE **13**, e0193517.

**Breitel DA, Chappell-Maor L, Meir S, *et al.*** 2016. AUXIN RESPONSE FACTOR 2 Intersects Hormonal Signals in the Regulation of Tomato Fruit Ripening. PLOS Genetics **12**, e1005903.

**Brodribb TJ, Feild TS, Jordan GJ**. 2007. Leaf Maximum Photosynthetic Rate and Venation Are Linked by Hydraulics. Plant Physiology **144**, 1890–1898.

**Buckley TN, John GP, Scoffoni C, Sack L**. 2015. How Does Leaf Anatomy Influence Water Transport outside the Xylem? Plant Physiology **168**, 1616–1635.

**Buckley TN, Sack L, Gilbert ME**. 2011. The Role of Bundle Sheath Extensions and Life Form in Stomatal Responses to Leaf Water Status. Plant Physiology **156**, 962–973.

**Chitwood DH, Kumar R, Headland LR, *et al.*** 2013. A Quantitative Genetic Basis for Leaf Morphology in a Set of Precisely Defined Tomato Introgression Lines. The Plant Cell **25**, 2465–2481.

**Coneva V, Frank MH, Balaguer MA de L, Li M, Sozzani R, Chitwood DH**. 2017. Genetic Architecture and Molecular Networks Underlying Leaf Thickness in Desert-Adapted Tomato *Solanum pennellii*. Plant Physiology **175**, 376–391.

**deVicente MC, Tanksley SD**. 1993. QTL analysis of transgressive segregation in an interspecific tomato cross. Genetics **134**, 585–596.

**Eshed Y, Zamir D**. 1995. An introgression line population of Lycopersicon pennellii in the cultivated tomato enables the identification and fine mapping of yield-associated QTL. Genetics **141**, 1147–1162.

**Galdon-Armero J, Fullana-Pericas M, Mulet PA, Conesa MA, Martin C, Galmes J**. 2018. The ratio of trichomes to stomata is associated with water use efficiency in *Solanum lycopersicum* (tomato). The Plant Journal **96**, 607–619.

**Galmés J, Ochogavía JM, Gago J, Roldán EJ, Cifre J, Conesa MÀ**. 2013. Leaf responses to drought stress in Mediterranean accessions of *Solanum lycopersicum* : anatomical adaptations in relation to gas exchange parameters: Anatomical adaptations to water stress in tomato. Plant, Cell & Environment **36**, 920–935.

**Iovieno P, Punzo P, Guida G, *et al.*** 2016. Transcriptomic Changes Drive Physiological Responses to Progressive Drought Stress and Rehydration in Tomato. Frontiers in Plant Science **7**.

**Ivanchenko MG, den Os D, Monshausen GB, Dubrovsky JG, Bednářová A, Krishnan N**. 2013. Auxin increases the hydrogen peroxide (H2O2) concentration in tomato (Solanum lycopersicum) root tips while inhibiting root growth. Annals of Botany **112**, 1107–1116.

**Jones B, Frasse P, Olmos E, Zegzouti H, Li ZG, Latché A, Pech JC, Bouzayen M**. 2002. Down-regulation of DR12, an auxin-response-factor homolog, in the tomato results in a pleiotropic phenotype including dark green and blotchy ripening fruit. The Plant Journal **32**, 603–613.

**Jones CM, Rick CM, Adams D, Jernstedt J, Chetelat RT**. 2007. Genealogy and fine mapping of obscuravenosa, a gene affecting the distribution of chloroplasts in leaf veins, and evidence of selection during breeding of tomatoes (Lycopersicon esculentum; Solanaceae). American Journal of Botany **94**, 935–947.

**Karabourniotis G, Bornman JF, Nikolopoulos D**. 2000. A possible optical role of the bundle sheath extensions of the heterobaric leaves of *Vitis vinifera* and *Quercus coccifera*. Plant, Cell & Environment **23**, 423–430.

**Kenzo T, Ichie T, Watanabe Y, Hiromi T**. 2007. Ecological distribution of homobaric and heterobaric leaves in tree species of Malaysian lowland tropical rainforest. American Journal of Botany **94**, 764–775.

**Lim SD, Mayer JA, Yim WC, Cushman JC**. 2020. Plant tissue succulence engineering improves water-use efficiency, water-deficit stress attenuation and salinity tolerance in Arabidopsis. The Plant Journal **103**, 1049–1072.

**Lippman ZB, Semel Y, Zamir D**. 2007. An integrated view of quantitative trait variation using tomato interspecific introgression lines. Current Opinion in Genetics & Development **17**, 545–552.

**Males J**. 2017. Secrets of succulence. Journal of Experimental Botany **68**, 2121–2134.

**Mascher M, Schreiber M, Scholz U, Graner A, Reif JC, Stein N**. 2019. Genebank genomics bridges the gap between the conservation of crop diversity and plant breeding. Nature Genetics **51**, 1076–1081.

**Muir CD, Conesa MÀ, Roldán EJ, Molins A, Galmés J**. 2017. Weak coordination between leaf structure and function among closely related tomato species. New Phytologist **213**, 1642–1653.

**Ogburn RM, Edwards EJ**. 2010. The Ecological Water-Use Strategies of Succulent Plants. Advances in Botanical Research. Elsevier, 179–225.

**Ogburn RM, Edwards EJ**. 2012. Quantifying succulence: a rapid, physiologically meaningful metric of plant water storage: Quantifying succulence. Plant, Cell & Environment **35**, 1533–1542.

**Pieruschka R, Schurr U, Jensen M, Wolff WF, Jahnke S**. 2006. Lateral diffusion of $CO_2$ from shaded to illuminated leaf parts affects photosynthesis inside homobaric leaves. New Phytologist **169**, 779–788.

**Poorter H, Niinemets Ü, Poorter L, Wright IJ, Villar R**. 2009. Causes and consequences of variation in leaf mass per area (LMA): a meta-analysis. New Phytologist **182**, 565–588.

**Poorter H, Niinemets Ü, Walter A, Fiorani F, Schurr U**. 2010. A method to construct dose–response curves for a wide range of environmental factors and plant traits by means of a meta-analysis of phenotypic data. Journal of Experimental Botany **61**, 2043–2055.

**Sack L, Holbrook NM**. 2006. Leaf hydraulics. Annu. Rev. Plant Biol. **57**, 361–381.

**Sack L, Scoffoni C**. 2013. Leaf venation: structure, function, development, evolution, ecology and applications in the past, present and future. New Phytologist **198**, 983–1000.

**Sack L, Scoffoni C, McKown AD, Frole K, Rawls M, Havran JC, Tran H, Tran T**. 2012. Developmentally based scaling of leaf venation architecture explains global ecological patterns. Nature Communications **3**, 837.

**Sagar M, Chervin C, Mila I, *et al.*** 2013. SlARF4, an Auxin Response Factor Involved in the Control of Sugar Metabolism during Tomato Fruit Development. Plant Physiology **161**, 1362–1374.

**Schwarz D, Thompson AJ, Kläring H-P**. 2014. Guidelines to use tomato in experiments with a controlled environment. Frontiers in plant science **5**, 625.

**Sharma E, Sharma R, Borah P, Jain M, Khurana JP**. 2015. Emerging Roles of Auxin in Abiotic Stress Responses. In: Pandey GK, ed. Elucidation of Abiotic Stress Signaling in Plants. New York, NY: Springer New York, 299–328.

**Terashima I**. 1992. Anatomy of non-uniform leaf photosynthesis. Photosynthesis Research **31**, 195–212.

**Wang H, Jones B, Li Z, Frasse P, Delalande C, Regad F, Chaabouni S, Latché A, Pech J-C, Bouzayen M**. 2005. The Tomato *Aux / IAA* Transcription Factor *IAA9* Is Involved in Fruit Development and Leaf Morphogenesis. The Plant Cell **17**, 2676–2692.

**Wylie RB**. 1952. The bundle sheath extension in leaves of dicotyledons. American Journal of Botany, 645–651.

**Xu X, Martin B, Comstock JP, Vision TJ, Tauer CG, Zhao B, Pausch RC, Knapp S**. 2008. Fine mapping a QTL for carbon isotope composition in tomato. Theoretical and Applied Genetics **117**, 221–233.

**Zhang X, Yan F, Tang Y, Yuan Y, Deng W, Li Z**. 2015. Auxin Response Gene SlARF3 Plays Multiple Roles in Tomato Development and is Involved in the Formation of Epidermal Cells and Trichomes. Plant and Cell Physiology **56**, 2110–2124.

**Zouine M, Fu Y, Chateigner-Boutin A-L, Mila I, Frasse P, Wang H, Audran C, Roustan J-P, Bouzayen M**. 2014. Characterization of the Tomato ARF Gene Family Uncovers a Multi-Levels Post-Transcriptional Regulation Including Alternative Splicing (S Maas, Ed.). PLoS ONE **9**, e84203.

**Zsögön A, Alves Negrini AC, Peres LEP, Nguyen HT, Ball MC**. 2015. A mutation that eliminates bundle sheath extensions reduces leaf hydraulic conductance, stomatal conductance and assimilation rates in tomato (*S olanum lycopersicum*). New Phytologist **205**, 618–626.

CHAPTER I

# Natural genetic variation improves tomato drought resistance through anatomical changes and increased leaf succulence

Bruno L. Rosa[1]; Leonardo A. Oliveira[1]; Moab T. Andrade[1]; Samuel C. V. Martins[1]; Agustin Zsögön[1]

[1]*Departamento de Biologia Vegetal, Universidade Federal de Viçosa, 36570-900, Viçosa, MG, Brazil*

E-mail of authors: brunoluanr@hotmail.com; leonardo.a.oliveora@gmail.com; moab.agro@gmail.com; samuel.martins@ufv.br; agustin.zsogon@ufv.br

## ABSTRACT

Natural genetic variation in tomato is an important tool for the breeding of cultivars resilient to adverse climatic conditions such as drought. In this context, the wild tomato *S. pennellii* has several adaptations that make it a major source of drought resistance genes. Introgression lines of *S. pennellii* produced in the background of *S. lycopersicum* cv. M82 has enabled the mapping of different leaf traits related to increased resistance to water deficit. In this work, we demonstrate how leaf morphological and anatomical traits found in IL2-5, IL4-3, and the combined IL2-5/4-3, such as increased thickness and succulence, can aid in the drought resistance capacity of tomato. These lines showed significantly increased leaf succulence, improved maintenance of water status under drought conditions, delayed wilting, and increased tolerance to leaf desiccation. In addition, we found that IL2-5/4-3 avoids damage to photosynthetic machinery and chlorophyll degradation even after a severe drought. Our data showed that increasing leaf thickness and leaf mass did not alter $CO_2$ diffusion and assimilation under normal conditions. On the other hand, these lines showed a higher photosynthetic capacity compared to cv. M82. The weak coordination between leaf anatomical and physiological traits in these lines may be a starting point for breeding plants with water-saving strategies, thereby improving photosynthetic performance and plant resilience under drought conditions.

**Keywords:** Gas exchange, leaf anatomy, water stress, water saving adaptations

# INTRODUCTION

Wild tomato species can survive in harsh environmental conditions, such as aridity, high-temperature range, and soil salinity (Zhou *et al.*, 2018; Pailles *et al.*, 2020). These environments have allowed the evolution of an important germplasm bank, which contains species with traits that can improve the resistance of cultivated tomato to stressful environmental conditions (Van Oosten *et al.*, 2016). Among such species, *Solanum pennellii* (*S. pen*) stands out as a source of drought resistance genes for the improvement of the cultivated tomato *Solanum lycopersicum* (*S. lyc*) (Rick, 1973). Several features conferring drought resistance have already been identified in *S. pen*, for example, increased lipid biosynthesis aimed at cuticle waterproofing (Fernandez-Moreno *et al.*, 2017) and increased expression of genes that conferring desiccation resistance (Koenig *et al.*, 2013).

Plants growing in arid environments exhibit characteristic phenotypes, which enable different drought coping strategies, such as smaller and thicker leaves, higher pilosity due to increased trichome density, and succulence (Poorter *et al.*, 2009; Sack *et al.*, 2012; Ogburn and Edwards, 2012; Coneva *et al.*, 2017; Galdon-Armero *et al.*, 2018). Succulence of plant tissues is considered one of the most successful drought adaptations in the plant kingdom (Grace, 2019). Overall, succulent plant tissues are composed of a series of anatomical adaptations that allow plants to become temporarily independent of external water supply (Ogburn and Edwards, 2010). Increasing succulence using genetic engineering has been shown to have positive effects on improving drought resistance in *Arabidopsis thaliana* (Lim *et al.*, 2020). However, studies involving the enhancement of this trait in tomato have not yet been conducted.

Tomato lines involving crosses between *S. pen* and *S. lyc* (Eshed and Zamir, 1995) have enabled the mapping and characterization of a diversity of phenotypes and may serve as an advantageous tool for enhancing succulence in this species. The near-isogenic introgression lines (IL) of *S. pen* in the background of *S. lyc* (cv. M82) (Eshed and Zamir, 1995) have facilitated the mapping of several Quantitative Trait Loci (QTL) responsible for numerous phenotypes in tomato and other plant species (Lippman *et al.*, 2007; Balakrishnan *et al.*, 2019). A complete population of IL covers virtually the entire genome of cv. M82 with discrete, overlapping *S. pen* segments (Chitwood *et al.*, 2013). Thus, phenotypic differences observed between ILs, or between ILs and parents, can be attributed to one or more genes found within the introgressed chromosomal segment (deVicente and Tanksley, 1993). This approach has been used to describe many characteristics of the modern tomato plant, such as

the diversity of fruit and leaf traits (Paterson *et al.*, 1990; Frary *et al.*, 2000; Chitwood *et al.*, 2013).

Leaves are the main target organs for both improving drought resistance and increasing the photosynthetic capacity of plants (Galmés *et al.*, 2013; Ren *et al.*, 2019; Lana-Costa *et al.*, 2020*a*). However, domestication and breeding of the tomato, aimed at increasing productivity, has led to the loss of several leaf adaptations that confer greater resistance to stressful environmental conditions (Chitwood *et al.*, 2013). Wild tomato plants exhibit a number of leaf traits that confer resistance to water deficit (Egea *et al.*, 2018; Pailles *et al.*, 2020). Such traits are able to manifest themselves without compromising gas exchange (Muir *et al.*, 2017), and can segregate independently (Chitwood *et al.*, 2013). Characterization of the effect of leaf structure on diffusive and biochemical limitations to photosynthesis, as well as its effects on water-use efficiency (*WUE*), have been conducted in wild tomato relatives and in improved cultivars (Galmés *et al.*, 2013; Muir *et al.*, 2017). However, the impacts of leaf structural changes within the same genetic background are still poorly studied. Thus, we propose that the characterization of *S. pen* ILs may allow the identification and provision of important genetic material for the development of new tomato cultivars resistant to water deficit.

Here, we used ILs from *S. pen* that exhibit a significant increase in leaf thickness, as well as changes in leaf shape (Coneva *et al.*, 2017). IL2-5 has an expressive increase in leaf thickness, more serrated leaflets, and reduced circularity. IL4-3, on the other hand, in addition to thicker leaves than cv. M82, has less serration and rounder leaflets. Previous work described the effect of each introgression on leaf architecture patterns by creating a double homozygous line (Coneva et al 2017). The homozygous double IL2-5/4-3 has thicker leaves than cv. M82 at both vegetative and reproductive stages and its leaflets have less serrated borders than either parent (Coneva *et al.*, 2017). In addition to exhibiting common characteristics of drought-adapted plants, this IL also exhibits leaf modifications that may increase diffusion and uptake of $CO_2$ and light into mesophyll tissues, promoting increased photosynthetic efficiency (Niinemets *et al.*, 2009; Poorter *et al.*, 2009; Terashima *et al.*, 2011). Our main objective is to provide a detailed investigation of the influence of leaf architecture on the ability of tomato plants to resist drought. Based on this, in this work, we characterized the main functional traits of drought resistance in the IL2-5, IL4-3, and IL2-5/4-3. We hypothesize that increased leaf thickness may be accompanied by increased tissue succulence, thus resulting in significant improvements in drought resistance capacity.

## MATERIALS AND METHODS

### Plant material and growth conditions

All assays were conducted in a greenhouse at the Federal University of Viçosa, Viçosa, Minas Gerais, (20°45'S, 42°54'W, 650 m altitude). The growth conditions inside the greenhouse were as follows: average temperature of 20.5 ± 1.8 ºC; average relative humidity of the ambient air of 75 ± 3.5 %; and maximum photosynthetically photon flux density (PPFD), measured at midday with a clear sky, varying around 1500 µmol $m^{-2}$ $s^{-1}$ in summer and 1200 µmol $m^{-2}$ $s^{-1}$ in winter. The cultivation was carried out in 5 L pots containing Tropstrate substrate (Vida Verde, Mogi Mirim, SP, Brazil) supplemented with 2 g $L^{-1}$ of NPK 10:10:10 and 4 g L of dolomitic limestone ($MgCO_3$ + $CaCO_3$ ).

Sowing was carried out in plastic trays filled with the substrate described above. Transplanting to larger pots was carried out 20 days after sowing, when the seedlings had a fully developed first pair of leaves. Topdressing fertilization, after transplanting, was performed weekly via foliar application of Hoagland's solution. Fertilization was topped fortnightly with 5 g NPK 10:10:10 applied close to the edge of the pots. Drought experiments were carried out through the total suspension of irrigation for 10 or 12 continuous days. After this period, irrigation was resumed and the recovery capacity was evaluated until the pre-dawn $\Psi_w$ showed values close to those observed in well-watered treatments.

In this work, we first performed a characterization of the photosynthetic and hydraulic responses of M82, IL2-5, IL4-3 and IL2-5/4-3 under optimal conditions. In the second experiment, we characterized the behavior of IL2-5/4-3 compared to cv. M82 under drought conditions; In the third experiment, we also subjected the parental ILs (IL2-5 and IL4-3) to water deficit conditions to identify the contribution of each IL to drought responses; Finally, we acclimated the genotypes M82, IL2-5, IL4-3 and IL2-5/4-3 to moderate drought, 60% of soil field capacity (SFC), for a period 40 days to characterize plant anatomy and productivity. For SFC determination each pot was filled with 2 kg of the previously described wet substrate and its dry weight was determined after drying for 96 h in an oven at 70 °C. The total water holding capacity of this substrate (100% SFC) was determined by weighing pots containing substrate completely saturated with water, after they had stopped dripping from the bottom. Initially, irrigation was suspended for eight consecutive days and pot weight was monitored until they were at 60% SFC. From there, the amount of water applied was estimated based on the daily determination of SFC by weighing the pots. The drought treatment was started at 43 days after germination (DAG) on plants with ≈ of four pairs of leaves, with the deficit

maintained until 83 DAG to ensure leaf development in this condition. After this cycle, the plants were re-watered to full SFC and fruit yield was determined 93 DAG.

Gas exchange, chlorophyll *a* fluorescence, $A/C_i$ curves, and SPAD index

Gas exchange analyses were performed in adult plants of cv. M82, IL2-5, IL4-3, and IL2-5/4-3. All the evaluations described below were measured in fully expanded apical leaflets. Gas exchange and chlorophyll *a* fluorescence parameters were determined simultaneously between 8 a.m. and 12 p.m. using an open-flow infrared gas analyzer (IRGA) system (model LI-6400XT, Li-Cor Inc., Lincoln, NE, EUA) equipped with an integrated fluorescence chamber of 2 $cm^2$ (6400-40 Leaf Chamber, Li-Cor Inc.). The equipment was configured to provide a light intensity of 1000 μmol $m^{-2}$ $s^{-1}$ and $CO_2$ concentration of 400 μmol $mol^{-1}$, with the airflow in the chamber regulated to 300 μmol $s^{-1}$. For evaluation of dark respiratory activity ($R_d$), a 6 $cm^2$ leaf chamber with airflow set at 100 μmol $s^{-1}$ was used. The effective quantum yield of photosystem II ($\phi PSII$) was determined by measuring the steady-state fluorescence ($F$s) and the maximum fluorescence ($F$m′), applying a saturating light pulse of 8000 μmol $m^{-2}$ $s^{-1}$ photons (Genty *et al.*, 1989):

$$\phi PSII = (F_m' - F_s) / F_m' \qquad \text{Eqn 2}$$

The apparent rate of electron transport (*ETR*) was calculated as described by (Melis et al., 1987):

$$ETR = \beta \times \alpha \times \phi PSII \times \text{PPFD} \qquad \text{Eqn 3}$$

Where β is the fraction of the excitation energy distribution in the PSII, α is the fraction of light absorbed by leaves, and PPFD is the photosynthetically photon flux density.

The maximum quantum yield of PSII ($F_v/F_m$) was quantified on cv. M82 and IL2-5/4-3 using a pulse modulated Mini-PAM fluorometer (Heinz Walz, Effeltrich, Germany). Analyzes were performed at midday on leaflets previously acclimated to the dark for thirty minutes. The $F_v/F_m$ was determined as described by Kitajima and Butler (1975):

$$F_v/F_m = (F_m - F_0) / F_m \qquad \text{Eqn 4}$$

Where $F_0$ is the initial fluorescence and $F_m$ is the maximum fluorescence of the dark-acclimated tissue. $F_0$ and $F_m$ were determined using measuring light less than 1 μmol $m^{-2}$ $s^{-1}$ and a saturating light pulse of 8000 μmol $m^{-2}$ $s^{-1}$ for 0.8 seconds, respectively.

Photosynthetic $CO_2$ response ($A/C_i$) curves were measured under ambient $O_2$ and temperature, using PPFD of 1000 μmol $m^{-2}$ $s^{-1}$ and injection of incremental $CO_2$ concentrations into the chamber (50, 100, 200, 300, 400, 500, 600, 700, 800, 900, 1000, 1200, 1400, 1600, 1800 μmol $mol^{-1}$). $CO_2$ and water vapor leaks were corrected according to the methodology described by Rodeghiero et al. (2007). Calculations of chloroplast concentrations of $CO_2$ ($C_c$) and mesophyll conductance ($g_m$) were performed using the Harley method (Harley *et al.*, 1992):

$$g_m = A_{area} / [C_i - (\Gamma^* (ETR + 8(A_{area} + R_d))) / (ETR - 4(A_{area} + R_d))] \quad \text{Eqn 5}$$

Where $A_{area}$ is the net assimilation rate, $ETR$ is the rate of photosynthetic electron transport derived from chlorophyll fluorescence measurements, $C_i$ is the $CO_2$ concentration in substomatic cavities and $R_d$ is the rate of non-photorespiratory respiration in the light. To calculate $g_m$ and $C_c$ we used the $CO_2$ compensation point (Γ*) of tomato plants quantified by Muir et al. (2017). The $g_m$ data were used to convert the $A/C_i$ curves into $A/C_c$ curves according to the following equation:

$$C_c = C_i - (A/g_m) \quad \text{Eqn 6}$$

The maximum Rubisco carboxylation velocity ($V_{cmax}$), the maximum capacity for electron transport rate ($J_{max}$), and triose phosphate utilization (TPU) were estimated on $C_c$ basis and normalized to 25°C (Long and Bernacchi, 2003). Stomatal ($l_s$), mesophyll ($l_m$), and biochemical ($l_b$) limitations were calculated as described by Grassi and Magnani (2005).

Light response curves were measured in $O_2$ and at room temperature, with a concentration of 400 μmol $mol^{-1}$ de $CO_2$ maintained at both points. After stabilization of stomatal conductance ($g_s$), photosynthetic activity ($A$) was determined in the following PPFD (1000, 1500, 1200, 900, 800, 700, 600, 500, 400, 300, 200, 150, 75, 50 and 0 μmol $m^{-2}$ $s^{-1}$).

The determination of photosynthetic pigments in cv. M82 and IL2-5/4-3 were performed non-destructively using a portable chlorophyll meter model SPAD-502 Plus (Konica Minolta, Japan). Each leaf was characterized by the average of three measurements taken on the same leaflet as the gas exchange measurements.

Water potential and relative water content

Leaf water potential ($\Psi_w$) was evaluated using a Scholander portable pressure chamber (1000, PMS Instruments, Albany, NY, USA) in the early morning (pd $\Psi_w$ = pre-dawn, 5 a.m.) and at noon (md $\Psi_w$ = midday, 12 p.m.). The leaflets were sectioned at the base of the petiole

with the aid of a blade and quickly inserted into the pressure chamber previously moistened with humid filter paper.

The leaf relative water content (RWC) was quantified on the same leaflet used for the $\Psi_w$ measurements. Immediately after $\Psi_w$ quantification, leaflets were stored in zip-lock bags with high humidity and transported to the laboratory in polystyrene boxes in the dark. After quantification of the fresh mass (FM), the leaflets were placed to rehydrate in distilled water at room temperature for 12 h in the dark for turgid mass (TM) determination. The dry mass (DM) was determined after oven-drying the leaflets at 70 ºC for 72 h. The RWC was calculated according to the following formula:

$$RWC = (FM - DM) / (TM - DM) \times 100 \quad \text{Eqn 1}$$

Leaf anatomy determinations

The terminal leaflets of the fifth leaf of plants grown under well-watered conditions were used to compare the anatomical differences between cv. M82 and IL2-5/4-3. The anatomical characterization of leaflets of cv. M82, IL2-5, IL4-3 and IL2-5/4-3 that expanded completely under drought conditions was performed on the seventh leaf. To obtain leaf cross-sections, a 1 × 0.5 cm fragment was excised from the leaf lamina and fixed in FAA70 (70% formalin-acetic acid-alcohol) for 24 h. Subsequently, the samples were dehydrated in an ethanol series (70%, 85% e 95%), under vacuum (-20 polHg). Pre-infiltration was performed with resin (Historesin® Leica Microsystems, Wetzlar, Germany) and ethanol 95% (1:1) for 2 h under vacuum (-20 polHg), and infiltration was done in resin for one week. Cross-sections of 5 μm thickness made on an automatic microtome (RM2155, Leica Microsystems) were mounted on blades and stained with 0.05% toluidine blue.

Vein density ($V_d$) and stomatal density ($S_d$) were measured in apical leaflets of the seventh fully expanded leaf in the drought treatment using six replicates per genotype. The leaflets were collected and fixed in methanol 95 % for 48 h, then the solution was changed to lactic acid 100 % and incubated at 100 °C until complete clarification (5-6 hours). The theoretical hydraulic conductance ($K_t$), which indicates the axial water transport capacity through the xylem, was calculated according to Tyree and Ewers (1991). The slides and diaphanized leaflets were photographed under a light microscope (AX70 TRF, Olympus Optical, Tokyo, Japan) coupled with a digital camera (Zeis AxioCan HRc, Göttingen, Germany) and a microcomputer with the image capture program Axio Vision. For image

measurements, we used Image-Pro Plus® software (Media Cybernetics, Silver Spring, MD, USA).

Saturated water content, fresh leaf thickness, leaf volume and leaf density

Saturated water content (SWC) was calculated according to Ogburn and Edwards (2012) using five leaflets per individual, which were collected from the seventh fully expanded leaf of six replicates per genotype. The water mass of the saturated tissue was quantified after 12 h of rehydration in distilled water. After this step, the leaflets was scanned to determine the leaf area ($L_a$) and subsequent calculation of the SWC. The dry mass was then quantified after drying in an oven at 70 °C for 72 h. The SWC was calculated on an area and mass basis according to the following formulas:

SWC (g $m^2$) = (leaflet mass (g) at full hydratation - dried leaflet mass (g)) / leaflet area ($m^2$) Eqn 7

SWC (g g) = (leaflet mass (g) at full hydratation - dried leaflet mass (g)) / dried leaflet mass Eqn 8

Five leaflets from the fourth and fifth leaves of six replicates per genotype were excised and immediately put to rehydrate for 12 h to determine the TM. After this step, the leaflets were scanned for later determination of the leaf area ($L_a$). The leaflet DM was determined after drying in an oven at 70 ºC for 72 h. We removed the petioles completely before determining the TM and DM, and rehydration was carried out by placing the base of the leaflet midrib in contact with distilled water. The estimation of leaf thickness ($L_t$) in µm was performed using the method of Vile et al. (2005) according to the equation proposed by Muir et al. (2017):

$$L_t = LMA / LDMC \quad \text{Eqn 9}$$

Where LDMC is the leaf dry matter content (ratio of leaf DM to saturated TM) and LMA is the Leaf dry mass per area (ratio of Leaf DM to leaf area $L_a$).

To calculate the volume of leaves and roots, a graduated cylinder partially filled with water was used. The volume was quantified by the water displacement caused by the insertion of the material in the container. The leaflets used to quantify the volume were dried in an oven at 70 C for 72 h, and their mass divided by the volume to quantify the leaf density.

Leaf hydraulic conductance

Leaf hydraulic conductance ($K_{leaf}$) was determined in plants of cv. M82, IL2-5, IL4-3, and IL2-5/4-3 by the evaporative flow method (Brodribb and Holbrook, 2006). $K_{leaf}$ determination was performed using apical leaflets from the fully expanded fifth leaf. These leaflets had their petioles cut under water and their lamina positioned in a conifer chamber coupled to the IRGA (6400-22L Lighted Conifer Chamber) for quantification of transpiration rates, E. The equipment was configured to provide 1000 μmol $m^{-2}$ $s^{-1}$ of light intensity, $CO_2$ concentration of 400 μmol $mol^{-1}$, and chamber airflow of 500 μmol $m^{-2}$ $s^{-1}$. All measurements were performed at 25°C and the vapor pressure deficit was maintained around 1.0 kPa. The leaves remained in the chamber under these conditions until they reached a steady state of transpiration (less than 10% variation over 180 s). Quantification of *E* was performed using the entire area of leaflets between 8 a.m. and 12 p.m.. Immediately after *E* quantification, $\Psi_w$ of the transpiring leaflet was determined using a Scholander-type pressure chamber. The leaf area of the transpiring leaflet was quantified using ImageJ (National Institutes of Health, Bethesda, USA). $K_{leaf}$ was calculated as:

$$K_{leaf} = -E / \Psi_{leaflet} \quad \text{Eqn 10}$$

$K_{leaf}$ values were normalized by the area of the leaflets ($L_a$). The parameters were determined in six plants per genotype.

Pressure-volume curves and rehydration capacity determinations

Pressure-volume curves (Tyree and Hammel, 1972) were performed on fully expanded apical leaflets of the fifth leaf (n = 4). The leaflets were excised underwater and rehydrated overnight for 12 h. In the next morning, leaves were allowed to slowly desiccate, while leaf weight and $\Psi_w$ were regularly assessed until $\Psi_w$ stopped falling due to cellular damage. In the end, the leaflets were scanned for leaf area ($L_a$) measurement and oven-dried at 70ºC for 72 h. Dry weights were utilized to calculate RWC (Eqn 1), which was plotted against $\Psi_w$. From each curve, we estimated the water potential and the RWC at turgor loss point ($\Psi_{TLP}$ and $RWC_{TLP}$, respectively), the osmotic potential at full turgor (Πo), the global modulus of elasticity (ε), and the leaf capacitance at full turgor ($C_{FT}$) and turgor loss point ($C_{TLP}$) normalized by $L_a$.

The percentage loss of leaf rehydration capacity (PLRC) was calculated as described by Trueba et al. (2019). PLRC was calculated at 50 DAG using six replicates per genotype. Five leaflets of the seventh leaf were collected per individual and placed to hydrate for 12 h to

determine the turgid mass. To isolate the effect of water scarcity on the leaf, dehydration was performed at 25°C, humidity of 50%, and low levels of irradiance (< 20 µmol $m^{-2}$ $s^{-1}$ PPFD). To estimate the RWC during dehydration, we considered that the leaflet dried mass corresponded to 10% of the turgid leaflet mass. This value was determined based on previous RWC quantifications of the respective genotypes. As they reached RWC around 100-90%, 80-70%, 60-50%, 40-30%, and 20-10%, the leaflets were removed from dehydration and placed to rehydrate for another 12 h to determine the rehydrated mass. After this step, the leaflets were oven-dried at 70 ºC for 72 h and the dry mass was quantified for later determination of the PLRC.

Minimal leaf conductance

The minimal leaf conductance ($g_{min}$) was measured in apical leaflets of the fifth leaf using the detached leaf mass loss method (Duursma *et al.*, 2019). Seven leaflets per genotype were used, previously hydrated for 12 h by immersion of the petiole in water. After this period, the petioles were sealed with parafilm and weighed on an analytical balance every 15 minutes for 4 hours. During weighing, the temperature and humidity of the environment were monitored for later calculation of leaf-to-air vapour pressure deficit (*VPD*). The $g_{min}$ was estimated from the slope of the linear relationship between leaf mass versus time and normalized by *VPD* and $L_a$. The leaves were scanned before and after the dehydration period and the average of both values was used as $L_a$ for $g_{min}$ calculations.

Growth parameters, dry mass, fruit yield, and total leaf area

The total leaf area of each plant was determined at the end of each experiment with the aid of a meter (LI-COR 3100). The parameters, height, stem diameter, and internode length were determined using a ruler and digital caliper. Fruit harvest for yield and determination of harvest index ($H_i$) was performed at 93 DAG. Fresh vegetative mass (leaves and stems) was determined after fruit harvest, and HI was calculated as the ratio of total fruit yield to total above-ground biomass (fruit and vegetative). To quantify the dry mass, the plant tissues (leaf, stem, and root) were dried in an oven at 70 °C for 72 h and the dry mass was determined on a precision analytical balance.

Experimental design and statistical analysis

The experiments were set up in completely randomized blocks. The first experiment comparing cv. M82 with IL2-5/4-3 was analyzed in a 2 × 2 factorial scheme (genotypes ×

water condition). The other drought experiments using the parental IL were analyzed in a 2 × 4 factorial scheme (water condition × genotypes). We used principal component analysis (*PCA*) to identify the main axes of variation between fifteen traits related to leaf anatomy and productivity of well-watered plants and plants submitted to drought conditions. Since the variables have different units, they were scaled to have a variance of 1 and a mean of 0 by subtracting the mean and dividing by the $S_d$, using the standardized method in GraphPad Prizm 9. *PCA* analysis was carried out using the GraphPad Prizm 9. The generated data were submitted to analysis of variance (ANOVA) and the means were compared using Tukey and Šídák's multiple comparison tests ($p < 0.05$). All statistical analyzes were performed using GraphPad Prism software (GraphPad Software Inc., San Diego CA, USA).

## RESULTS

### The double introgression line is more drought resistant than M82

We confirmed the phenotype of thicker leaves in IL2-5/4-3 by evaluating cross-sections of leaflets grown under well-watered conditions. The mean leaf thickness of IL2-5/4-3 was significantly greater than that observed in M82 ($p$-value = 0.002) (Fig. 1 B). The palisade and spongy parenchyma of IL2-5/4-3 were significantly larger than the respective tissues observed in M82 (Fig. 1E and F). Combined with the increment observed in the tissues that make up the leaf mesophyll, IL2-5/4-3 also increased the thickness of the adaxial and abaxial epidermis (Fig. 1C and D).

To better understand how the foliar traits of the IL2-5/4-3 line can influence the performance of tomato plants under drought conditions, we conducted a new experiment comparing it to the cv. M82. On the third day of deficit imposition, M82 plants under drought showed significant reductions in $A$ (31%) and $g_s$ (40%) (Fig. 2B and C). On the other hand, on that same day, IL2-5/4-3 maintained $A$ and $g_s$ values similar to the values found in the M82 control plants. Seven days after the onset of drought M82 and IL2-5/4-3 showed reductions of 81% and 70% in $A$; 87% and 83% in $g_s$; and 81% and 77% in $E$, respectively, compared to the control treatment (Fig. 2B, C, and D). On the tenth day, $A$ was reduced to values close to zero in both genotypes under drought conditions. However, less negative values of $\Psi_w$ were observed in IL2-5/4-3 at this point, showing that this genotype would take longer to reach $\Psi_w$ to values close to those observed in M82 in drought (Fig. 2G). Three days after the resumption of irrigation, both genotypes presented $A$ and $g_s$ equivalent to controls. However, $E$ recovery after the resumption of irrigation was observed only in IL2-5/4-3 (Fig. 2D).

The ten days of drought significantly reduced the maximum quantum yield of *PSII* ($F_v/F_m$) in M82 to 0.67 ($p$-value < 0.0001), which indicates the occurrence of significant damage to the photosynthetic apparatus (Fig. 2E). However, even subjected to a severe water condition, but less negative compared to M82, IL2-5/4-3 maintained the $F_v/F_m$ around 0.8 on the tenth day of drought (Fig. 2E). Similarly, IL2-5/4-3 also did not show significant reductions in the SPAD total chlorophyll index in response to drought. M82, on the other hand, presented significant reductions in the total chlorophyll index from the fifth day of drought, which remained low even after the resumption of irrigation (Fig. 2F).

The contribution of the parental ILs to drought responses

To explore the specific contributions of each introgressed *S. pennellii* genome segment, the parental lines IL2-5 and IL4-3 were evaluated in a second drought experiment. In general, ILs showed a behavior of greater drought tolerance compared to M82, with significant delays in wilting (Fig. S1), delay in the decrease of gas exchange, and *ETR*, in addition to improvement in water condition being observed in ILs (Fig. 3). It is noteworthy that, despite their more tolerant behavior, these lines also showed decreases in water status and gas exchange. In the first gas exchange measurements, taken before irrigation suspension, we observed a significant increase in *A* of IL2-5 relative to the other genotypes (Fig. 3A). After four days of drought, both ILs maintained A higher than M82, however, on the sixth day, only IL2-5/4-3 showed *A* higher than M82. After four days of recovery (16 days after treatment (DAT)), IL2-5/4-3 showed higher *A* than the other genotypes (Fig. 3A).

We observed that, compared to M82 and the parental ILs, IL2-5/4-3 recovers *A* faster after going through a severe period of water deficit. Recovery of *A* to levels close to the control was not observed in both genotypes (Fig. 3A). After four days of drought, IL4-3 and IL2-5/4-3 stood out in relation to $g_s$ maintenance, showing the lowest rates of stomatal resistance compared to IL2-5 and M82. IL2-5/4-3 showed higher $g_s$ and faster recovery after being rehydrated, being also able to recover $g_s$ at the level of control treatments. However, among the parental ILs, the lowest capacity for gas recovery was observed in IL2-5 (Fig. 3B). The *E* rates of the genotypes followed the same behavior observed for $g_s$, which was to be expected since $g_s$ is the parameter that most influences water loss through leaves (Fig. 3C).

In the control condition, the highest *ETR* values were observed in IL2-5 and IL2-5/4-3 lines. Under drought, the IL2-5 and IL2-5/4-3 lines maintained higher *ETR* values compared to M82 even after four days without irrigation, whereas six DAT, both ILs showed higher *ETR* values than M82. After four days of rehydration, the highest *ETR* values were observed

in IL2-5/4-3. On the sixth day of recovery (DAT 18) the *ETR* values of plants subjected to drought showed differences (Fig. 3D). At some points throughout the drought, we found that ILs lost water at slower rates compared to M82.

To understand the contribution of each of the ILs in this behavior, we carried out point measurements of RWC and $\Psi_w$ over 12 days of drought and after the resumption of irrigation. All genotypes reached $\Psi_w$ around -2 Mpa on the last day of drought (DAT 12) (Fig. 3E and H). However, IL4-3 and IL2-5/4-3 managed to keep $\Psi_w$ values less negative than M82 until DAT 12 in pd, and up to DAT 6 in md. Significant differences between the pd $\Psi_w$ and md $\Psi_w$ of the parental ILs were also observed throughout the drought. The pd $\Psi_w$ of IL4-3 was higher than that observed in IL2-5 in DAT 9, and the same behavior was observed in pd $\Psi_w$ of DAT 6 and in md $\Psi_w$ of DAT 4. Six days after the start of recovery, all genotypes reached pd $\Psi_w$ equivalent to the control treatment. This behavior suggests that the different $g_s$ recovery capacities, which occurred among the genotypes, may be linked to differences in the production capacity and degradation of ABA. IL4-3 and IL2-5/4-3 showed pd RWC higher than IL2-5 and M82 six DAT under dry conditions. After 9 days of drought, both ILs presented RWC pd higher than M82. In DAT 12, only parental ILs showed pd RWC higher than M82 in the drought conditions. All genotypes showed pd RWC similar to the control on the last day of recovery (DAT 18). Until the sixth day of drought, the highest values of md RWC were observed in IL4-3. From DAT 9, IL4-3 continued to maintain md RWC higher than M82, being also significantly higher in relation to the other ILs evaluated. At this point, the md RWC values were also higher in IL2-5/4-3 compared to M82. However, no significant differences were observed between IL2-5 and M82. At DAT 12, even reaching very negative pd $\Psi_w$ for tomato plants, the RWC of ILs did not reach valuesmuch lower than 50%. On the other hand, the lower RWC in M82 showed that drought drastically affected its water holding capacity (Fig. 3 G).

Growth and productivity parameters are differentially affected in ILs

Next, we sought to understand how IL2-5 and IL4-3 introgressions affect the phenotype and productivity of plants under optimal conditions and in the absence of irrigation. Even under well-irrigated conditions, significant differences in dry matter production were observed between ILs, as well as between ILs and M82 (Fig. 4A, B, C, and D). Comparing the isolated effect of the control treatment between the genotypes, IL2-5 showed a dry mass of leaves, stems, roots, and total dry mass similar to M82. In relation to the other ILs, both the leaf dry mass and the total dry mass of IL2-5 were significantly higher

compared to the IL4-3 and IL2-5/4-3 lines. Unlike IL2-5, IL4-3 had lower root dry mass, as well as lower total dry mass, compared to M82 under irrigated conditions. The dry mass of leaves, stem, and total was higher in IL2-5 compared to IL4-3 in the same condition. IL2-5/4-3 had the lowest leaf mass, which was significantly lower compared to IL2-5 and M82.

Under irrigated conditions, IL4-3 showed the lowest investment in root dry mass among the genotypes (Fig. 4C). Compared to M82 and IL2-5, IL2-5/4-3 was the genotype with the lowest total dry mass, however, differences between IL4-3 and IL2-5/4-3 were not observed (Fig. 4D). Under drought, IL2-5/4-3 significantly increased its root dry mass compared to other genotypes, also increasing the root/shoot ratio and root volume (Fig. 4C, E, and F). IL4-3 and IL2-5/4-3 showed the same total leaf area under irrigated conditions but were significantly smaller compared to M82 (Fig. 4G). IL2-5, on the other hand, had intermediate values, which were compared to both the other ILs and M82 (Fig. 4G). Under drought, no change in leaf area was observed between genotypes (Fig. 4G). IL2-5 showed the highest LMA values in both control and drought treatments (Fig. 4H). We verified that drought negatively affected the total dry mass production of both genotypes (Fig. 4D). However, IL4-3 and IL2-5/4-3 lines showed equal root volume and total leaf area, respectively, between control and dry treatments (Fig. 4F and G).

Natural genetic variation affects leaf architecture and productivity in tomatoes.

We explored the contribution of each parental ILs to altered leaf morphology, as well as the occurrence of phenotypic plasticity, using leaflets from drought-acclimated plants (Fig. 5). IL2-5/4-3 maintained the greatest leaf thickness compared to M82, however, thickness of the leaves of either IL2-5 or IL4-3 were similar to M82 (Fig. 5C). Because of this, we also used the method described by Vile et., al (2005) (supplemental Fig. S2) to provide an integrated measurement of leaf thickness using live tissue. Through this method, we observed that, regardless of the water condition, both ILs had thicker leaflets than M82. Except for the adaxial $S_d$ of IL4-3, the means of the dry and control treatments in the other parameters, within each IL, did not show statistical differences (Fig 5. D, E, H, and I). On the other hand, we observed a significant increase in adaxial and abaxial $S_d$ of cv. M82 in the drought, with the lowest IAS and SWC observed in this treatment (Fig 5. D, E, I, and J).

In the drought condition, IL2-5/4-3 significantly increased the number of vessel elements (Fig. 6B). Both genotypes reduced the mean diameter of vessel elements when subjected to drought (Fig. 6C). However, in the control condition, the largest vessel element

diameter was observed in IL4-3, which corroborated the highest $K_t$ values observed for this genotype (Fig. 6C and E).

After 40 days of acclimation to 60% of soil field capacity, we analyzed the effect of drought on the fruit production capacity of each of the ILs (Fig. 7). In the irrigated condition, IL2-5 had a smaller number of fruits among the ILs, as well as fruits with lower weight and lower $H_i$ compared to the other genotypes (Fig. 7). On the other hand, IL4-3 and IL2-5/4-3 achieved fruit yield rates equivalent to M82 (Fig. 7C and D) under irrigated conditions, also significantly increasing the number of fruits in relation to M82 (Fig. 7B). Under drought conditions, the largest number of fruits produced were observed in the IL4-3 and IL2-5/4-3 lines, with the smallest numbers observed in IL2-5 and M82, respectively. IL4-3 stood out in relation to the other genotypes, presenting a higher individual fruit weight, as well as a higher $H_i$ under drought conditions. However, both fruit yield parameters were significantly reduced by drought in M82 (Fig. 7A, B, and C).

Relationship between structural, physiological, and productive traits

We performed a PCA using the data from drought acclimated plants to identify the variables that contributed most to the differences in drought resistance between genotypes (Fig. 8). The drought and control treatments were well separated by the first main component (PCA 1), which explained 48.53% of the variation. PCA 2 was responsible for 16.18% of the variation and more effectively separated the evaluated genotypes (Fig. 8). The $V_d$ and $S_d$ had a strong positive correlation with PC1, with M82 in the dry condition the main responsible for this behavior. On the other hand, anatomical leaf thickness, root/shoot ratio, and SWC had a strong positive correlation with PC2. The distribution of genotypes along PC2 showed that IL2-5/4-3 was the line that most positively contributed to the correlation between the aforementioned traits and PC2. The alignment between the SWC vectors and the $H_i$ indicates a strong correlation between these traits.

PCA also showed that conservative traits related to drought tolerance (SWC, leaf thickness, root/shoot) were negatively correlated with $S_d$ and $V_d$ (Fig. 8). On the other hand, negative correlations between $S_d$ and IAS were also found, indicating that a probable increase in stomatal limitation by $S_d$ can be compensated with more IAS increasing $CO_2$ diffusion in the mesophyll. The right angle between LMA and $L_t$ indicates a null correlation between these traits. In addition to influencing drought tolerance, SWC, $L_t$, and Root/Shoot were the traits that most positively correlated with fruit yield in PC2. However, $H_i$ contributed more effectively (31.6%) to PC3, which explained 11.11% of the total variation (Table S1 and S3).

ILs show increased photosynthesis-related parameters

Given the significant anatomical changes observed in the ILs, *A*/$C_c$, *A*/PPFD, *ETR*/ $C_c$, and *ETR*/PPFD curves were performed to characterize the photosynthetic efficiency of the plants (Fig. 9). Relative to cv. M82, the ILs studied here were able to achieve higher *A* and higher *ETR* when exposed to elevated $CO_2$ pressures in the chloroplast (Fig. 9A and B). Parental ILs showed a contrasting photosynthesis behavior in response to light, where the *A* values observed in IL4-3 were lower compared to IL2-5 and IL2-5/4-3 at 1000 µmol $m^{-2}$ $s^{-1}$ of PPFD (Fig. 9C). Significant *ETR* reductions in IL4-3 and M82, in relation to the other ILs, were observed from 800 µmol $m^{-2}$ $s^{-1}$ of PPFD (Fig. 9D). IL2-5/4-3 stood out among the other genotypes, being able to perform higher *A* and *ETR* when subjected to high concentrations of $CO_2$ and light. Such behavior makes it clear that the interaction between traits from IL2-5 and IL4-3 also improves the photosynthetic activity of tomato plants. Regarding the *A*/PPFD curve, no differences in compensation point and saturation were observed between genotypes (Supplementary Tab. S4).

Since anatomical changes in the leaf can directly influence the ability to carry out gas exchange, we also estimated leaf limitations using parameters obtained from *A*/$C_c$ curves. Table 1 shows the data collected in the ambient concentration of $CO_2$ (400 ppm). Values of $p > 0.05$ showed that there was no significant change in gas exchange parameters and leaf limitations between genotypes. Although we did not find significant differences in $l_b$, the lower $C_c$ /$C_i$ ratio observed in IL2-5 may reveal a significant improvement in biochemical activity. Under well-irrigated conditions and under saturating light, we noticed that both ILs contributed to increasing the biochemical parameters of Rubisco activity, $V_{cmax}$, $J_{max}$, as well as *TPU* on a $C_c$ basis.

Influences of IL2-5 and IL4-3 on leaf hydraulics

The leaf anatomical traits observed in ILs are commonly correlated with significant changes in hydraulic transport (Li *et al.*, 2021). Thus, we compared the hydraulic traits of the genotypes using leaflets from well-watered plants. IL4-3 leaflets are more voluminous and were able to maintain a higher SWC per mass unit compared to other genotypes (Table 2). The SWC, volume, and density of IL2-5 leaflets were similar to M82. Thus, we noticed that the combination of the two lines in IL2-5/4-3 resulted in leaflets with greater volume and reduced density compared to M82. As seen in Fig. 5, IL4-3 showed higher $K_t$ than the other

genotypes. However, the $K_{leaf}$ of IL4-3 showed no differences compared to cv. M82 and IL2-5, but it was lower compared to IL2-5/4-3 (Table 2).

Relative losses in leaf rehydration capacity (PLRC) were compared between genotypes (Supplementary Fig. S4). We noted that the decline in RWC strongly increased the PLRC of both genotypes evaluated. A 10% PLRC was only observed when the RWC reached values below 60%. The mean RWC values that induced losses of 10, 20, and 50% of the rehydration capacity, for both genotypes, were around 60%, 50%, and 31%, respectively. However, the leaflets of the different genotypes have similar PLRC (Supplementary Fig. S4). This may indicate that the alterations generated by ILs in leaf architecture did not compromise their rehydration capacity.

Pressure-volume (PV) curves were also measured in leaflets grown under well-watered conditions (Supplementary Fig. S5). Most of the parameters quantified through the PV curve did not show differences between the genotypes, with the exception of the modulus of elasticity (ε). IL4-3 showed significant reductions in ε compared to IL2-5, but it was similar to IL2-5/4-3 and M82. IL2-5/4-3, in particular, had the most robust root system among the ILs under drought conditions (Fig. 6). Thus, the root system of the IL2-5/4-3 may have served as a buffer, helping to maintain the water status and, possibly, recovery after drought.

## DISCUSSION

Most studies involving ILs of *S. pen* have focused on yield and fruit traits (Lippman *et al.*, 2007; Calafiore *et al.*, 2019). On the other hand, few papers offer approaches on the wide range of leaf phenotypes of *S. pen* ILs and their benefits for developing abiotic stress-resistant varieties (Chitwood *et al.*, 2013; Coneva *et al.*, 2017). *S. pen* has leaves that respond rapidly to variations in air humidity and can withstand desiccation under extremely arid conditions (Egea *et al.*, 2018). Thus, its enhanced drought resistance ability can be attributed mainly to changes in the anatomy and morphology of its leaves (Kebede *et al.*, 1994; Egea *et al.*, 2018). Through the characterization of ILs of *S. pen*, we sought to elucidate which key leaf traits confer resistance to water deficit in tomato plants. In this work, we sought to understand, by analyzing anatomical, physiological and hydraulic parameters, how changes in leaf thickness, LMA, as well as vein and stomatal density can influence the drought performance of tomato plants. Here, we also seek to provide concise information on how increasing leaf succulence in tomato can affect its ability to resist drought. The ability to store water in tissues to mitigate the effects of drought plays a prominent role among the most successful plant adaptations (Eggli and Nyffeler, 2009). When storage occurs in photosynthetic cells, this adaptation is

called cell succulence, which is associated with increased cell size and relative vacuole volume (Gibson, 1982; Willert *et al.*, 1992). The imposition of succulence in plants is also a key step towards the introduction of CAM metabolism in cultivated plants; for this, it is essential to discover a functional leaf anatomical system that presents traits such as increased thickness and larger volume (Males, 2017). However, succulence has received little attention in the process of developing plant varieties resistant to drought conditions, and few studies have addressed increasing succulence by manipulating leaf tissue anatomy (Han *et al.*, 2013; Lim *et al.*, 2020).

Leaf succulence in IL of *S. pen* as a drought avoidance strategy

The turgor maintenance capacity and drought resistance observed in IL2-5/4-3 demonstrate the important role of *S. pen* in the improvement of cultivated tomato plants. The absence of photoinhibitory damage to the photosynthetic apparatus observed in IL2-5/4-3 demonstrates its greater ability to resist drought (Mishra *et al.*, 2012). The fact that we observed significant delays in leaf wilting, only in IL, can be explained by the maintenance of less negative potentials and higher % RWC exhibited by them during drought. The greater leaf thickness of IL2-5/4-3 (Coneva *et al.*, 2017), and showed that this IL exhibits increased thickness of the mesophyll and epidermal tissues. Later, we saw that the alteration of these leaf traits in this line may be linked to the expressive increase in leaf succulence and reduced stomatal density.

The ability of succulent plants to store water in living tissues to avoid drought is among the most successful adaptations in the plant kingdom (Lim *et al.*, 2020). Naturally, succulence has ensured the survival of many species to drought in arid, semi-arid regions and in epiphytic environments around the world (Ogburn and Edwards, 2010; Grace, 2019). However, the beneficial effect of succulence on drought avoidance has also been projected in model species through transgenic breeding (Lim *et al.*, 2020). The increased leaf SWC of the ILs studied here corroborates with the enhanced drought avoidance ability exhibited by them. The manifestation of leaf succulence only in IL2-5, IL4-3, and IL2-5/4-3 provide evidence that we can improve leaf traits that confer drought avoidance through natural genetic variation, and the introgressions studied here are a likely venue for such a search.

Increasing ploidy levels have been associated with increased leaf thickness, tissues comprising the mesophyll and epidermis, and leaf trichomes, leading to greater resistance to water deficit (Li *et al.*, 2009). Consistently, the increased leaf thickness observed in IL2-5/4-3 were also associated with increased ploidy levels (Coneva *et al.*, 2017). Succulent plant

tissues are based on anatomical adaptations that enable plants to be temporarily independent of external water supply (Ogburn and Edwards, 2010). In this work, the increase in leaf thickness was primarily responsible for the increase in succulence, as they were strongly correlated by the same axis of the PCA (PC2). Succulence can increase RWC, under acute and chronic drought conditions, due to increased water-holding capacity per unit leaf area. In addition, reductions in whole-plant water loss rates, as well as in detached leaves, can be observed in plants with succulent leaves (Lim *et al.*, 2020).

The leaf succulence displayed by IL may also explain their higher leaf RWC and $\Psi_w$, as well as their ability to maintain gas exchange longer after being subjected to drought (Nobel, 2006). The arrangement of cells that make up the leaf mesophyll of succulent plants can significantly influence $g_m$ (Ripley *et al.*, 2013). However, the greater leaf succulence demonstrated here came accompanied by increased *IAS* in the drought, which may have enabled better exposure of chloroplasts to intercellular $CO_2$, increasing diffusion (Tomás *et al.*, 2013). Succulence per leaf area base increased in all ILs in the drought (Fig. 5J), but the same behavior was not observed when this comparison was performed in well-watered conditions per mass base (Tab. 2). The data also suggest that the *S. pen* segments present in IL2-5 and IL4-3 harbor genes responsible for leaf anatomical changes related to adaptation and avoidance to drought, such as SWC. Differences in leaf SWC, make it clear that ILs have a greater capacity for leaf hydration by area basis and that, unlike M82, the applied water deficit did not change the degree of leaf succulence of its leaves (Fig. 5J).

Improving water status and gas exchange during drought using leaf anatomical traits of *S. pen* lines

Changes in leaf architecture and stomatal density can enhance photosynthetic efficiency and drought resistance in tomato (Fullana-Pericàs *et al.*, 2017; Ren *et al.*, 2019). However, the molecular mechanisms controlling these traits are still poorly understood (Batista-Silva *et al.*, 2020). Leaf architecture is a complex genetic trait that is greatly influenced by environmental factors such as water availability, temperature, and light (Carins Murphy *et al.*, 2012, 2014). Elongation of palisade parenchyma cells has been shown to contribute significantly to greater leaf thickness in IL2-5/4-3 (Coneva *et al.*, 2017). This may have significantly benefited carbon assimilation since elongation of the palisade parenchyma increases the contact area with the intercellular airspace (Terashima *et al.*, 2011). Changes in leaf architecture can come accompanied by a consequent increase in LMA and can generate great influence on the capacity for $CO_2$ interception and fixation (Flexas *et al.*, 2014;

Peguero-Pina *et al.*, 2017). However, even though IL2-5 showed a significant increase in LMA, compared to the other IL and cv. M82, greater resistance to $CO_2$ diffusion did not observe.

Water deficit reduces gas exchange, PSII efficiency, and also negatively regulates several photosynthesis-related genes in cv. M82 (Iovieno *et al.*, 2016*b*). In the first experiment, critical levels of $\Psi_w$ reduced leaf gas exchange in cv. M82 and IL2-5/4-3 to near-zero values on the tenth day of drought. However, damage to the photosynthetic apparatus and degradation of total chlorophylls were observed only in cv. M82 subjected to drought. Reduced synthesis of the photosynthetic machinery components under water deficit (Iovieno *et al.*, 2016*b*) may have significantly contributed to the reduction of $F_v/F_m$ values and occurrence of dynamic photoinhibition in M82 (Adams *et al.*, 2013). The absence of photoinhibition and chlorophyll degradation in IL2-5/4-3 corroborates its greater ability to maintain leaf water status, which ensured that the integrity of the photosynthetic machinery was maintained (Mishra *et al.*, 2012; Iovieno *et al.*, 2016*b*).

Recovery of gas exchange after the resumption of irrigation is an important step for understanding the effects of drought (Chen *et al.*, 2016). Photosynthetic rates, $F_v/F_m$, and leaf $\Psi_w$ (pd and md) were recovered on the third day after the resumption of irrigation, however, both M82 and IL2-5/4-3 still had low $g_s$ and $E$ values. Mishra et al. (2012) demonstrated that the $F_v/F_m$ variable can be a potential tool for monitoring and quantifying drought resistance in tomato plants. Corroborating with this statement, our data indicate that the anatomy of IL2-5/4-3 may enable significant improvements in drought resistance capacity.

Light and $CO_2$ are the main external factors that limit photosynthesis in plants. However, maximum utilization of these resources can be achieved by altering leaf anatomy (Ren *et al.*, 2019). In this work, we showed that the greater leaf thickness of IL resulted in a consequent increase in chlorophyllated tissues, as well as increased exposure of cells in this tissue to $CO_2$. The ability of IL, especially if dealing with IL2-5/4-3, to perform greater photosynthesis and electron transport was enhanced by this anatomical condition. The changes in leaf morphology of IL2-5, IL4-3, and IL2-5/4-3, also contributed significantly to the increase in $Vc_{max}$ and $J_{max}$, since these variables increased significantly in these lines under high $CO_2$ conditions. The higher $Vc_{max}$ values may indicate increased Rubisco concentration and greater nitrogen allocation in the leaves of the IL2-5, IL4-3, and IL2-5/4-3 lines (Centritto and Jarvis, 1999). Furthermore, the high ETR and $J_{max}$ rates of these IL may indicate an enhanced capacity for regeneration of ribulose 1,5 bisphosphate carboxylase oxygenase (RuBisCO) (Lana-Costa *et al.*, 2020*b*). Thus, the photosynthetic variation of IL can be

explained by both anatomical changes and differences in the biochemical capacity of RuBisCO, $Vc_{max}$, and $J_{max}$.

Changes in $g_s$ and $g_m$, as well as changes in stomatal density during drought, can lead to significant increases in intrinsic *WUE* (Galmés *et al.*, 2013; Lana-Costa *et al.*, 2020*b*). Normally, an increase in photosynthesis requires a coordinated increase in $g_s$ with a consequent increase in *E* and a reduction in *WUE* (Condon, 2004). However, anatomical modifications that enable higher $g_m$ and higher biochemical activity can increase photosynthesis enabling higher *WUE* (Muir *et al.*, 2017). M82 and IL have amphi-hypostomatic leaves, with the greatest amount of stomatal cells being located on the abaxial face. Except for M82, both IL showed reduced stomatal densities, mainly, on the abaxial face under drought conditions. This leaf trait has been associated with higher *WUE* in its wild relative *S. pen* (Egea *et al.*, 2018). We observed that despite the reduced stomatal density, under well-watered conditions, the IL studied here did not differ from cv. M82 in terms of *WUE*. However, the reduced stomatal density may explain the better performance of the IL during drought.

Water deficit can lead to significant increases in the root/shoot ratio, with root growth benefiting to the detriment of plant shoots as a strategy to search for water (Poorter *et al.*, 2012). In this work, IL2-5/4-3 showed significant increases in dry mass and root volume, considerably increasing the root/part ratio after undergoing a period of soil water deficit. This specific alteration may have served as a buffer improving the resistance of this genotype to drought and, combined with greater succulence and reduced stomatal density, may be related to its greater ability to recover after stress.

IL2-5 and IL4-3 lines have significantly increased the expression of genes related to leaf development and desiccation resistance (Coneva *et al.*, 2017). A smaller leaf area may enable greater water saving and reduction of the water potential gradient between leaves and roots. Moreover, unlike stomatal closure, reduced leaf area may function as a strategy for reducing heat stress (Tardieu *et al.*, 2018). In the second experiment, we observed that M82 has a significantly higher total leaf area than IL2-5/4-3. We saw that the smaller total leaf area is a characteristic phenotype of IL4-3 and IL2-5/4-3 only, with no differences observed between IL2-5 and cv. M82 under well-watered conditions. This phenotype, coupled with higher leaf succulence, may explain both the delayed wilting and the higher desiccation resistance shown by IL2-5/4-3 in the first experiment. On the other hand, we observed that the rate of leaf expansion was not significantly affected among the genotypes after the imposition of the water deficit.

In this work, no significant differences were found in the ability of IL to perform gas exchange in ambient $CO_2$ concentration. Our results showed that intrinsic changes in leaf architecture in tomato plants grown under well-irrigated conditions do not limit gas exchange. However, when we increased $CO_2$ partial pressures, IL significantly increased photosynthetic rates, which may be an interesting feature in times of global climate change (Gornall *et al.*, 2010).

Leaf traits of IL2-5 and IL4-3 as a basis for increasing resilience and maintaining productivity under drought conditions

$CO_2$ diffusion between the atmosphere and chloroplasts, via stomata and the leaf mesophyll, has a great influence on photosynthetic rates (Flexas *et al.*, 2018). However, intrinsic photosynthesis can vary widely among C3 species, and both $CO_2$ diffusion and biochemical capacity of the leaf can be worked out in search of the best performance and fitness of plants to different environments and growing conditions (Muir *et al.*, 2017). For example, compensatory alteration of stomatal density to inhibit the rapid diffusion of $CO_2$ and benefit the water economy has shown good results in improving the drought resistance of some species (Hughes *et al.*, 2017; Lim *et al.*, 2020). Our work demonstrated that the survivability of tomato plants to drought stress can be altered at the leaf level through anatomical modifications without compromising $CO_2$ diffusion.

The variation in leaf traits was explained by more than one axis of the PCA, overall, this indicates that there was weak coordination among the anatomical, physiological, and productive traits evaluated in this work (Muir *et al.*, 2017). The adaptive anatomical traits observed in this work such as SWC and $L_t$ may help in the development of varieties that are more tolerant to abiotic stressors such as drought (Ogburn and Edwards, 2010; Chitwood *et al.*, 2013). For example, by modifying SWC we can improve the cultivation of tomato plants in arid regions, as well as the ability to grow them by people with lower purchasing power. The other leaf anatomical traits observed in IL2-5 and IL4-3, associated with their higher photosynthetic capacity, can ensure higher productivity, for example, in greenhouse cultivation with high $CO_2$. PCA showed that there are significant differences between IL and cv. M82 mainly in drought. In this condition, IL2-5 and IL4-3 share traits that, added together in a single IL2-5/4-3 individual, may further increase resistance to water deficit. PCA revealed the leaf anatomical traits that contributed the most to the variation between IL and cv. M82 were stomata and vein density, as well as leaf thickness and succulence.

It is noteworthy that the future use of sublines containing smaller chromosomal segments of IL2-5 and IL4-3 may provide a more accurate characterization of the contribution of these leaf traits. Here, we saw that the larger LMA of IL2-5 segregates in concert with higher leaf complexity and greater leaflet serration. On the other hand, leaf succulence, although seen in IL2-5 under drought conditions, was shown to be a phenotype more associated with leaves lower complexity and less serrated leaflets, as in the case of IL4-3 and IL2-5/4-3. IL2-5 shows differential expression of about 400 genes when subjected to water deficit, and its gene expression profile is very similar to *S. pen* (Gong *et al.*, 2010). Currently, IL2-5 has dispersed the interest of researchers due to its higher biochemical capacity, which can increase photosynthetic rates by up to 20% compared to cv. M82 under conditions of high atmospheric $CO_2$ (Lana-Costa *et al.*, 2020*b*). Elevating photosynthetic rates along with improved drought survivability, are indispensable traits in times of climate-changing and increased demand for food (Ren *et al.*, 2019; Leng and Hall, 2019). Thus, characterization and mapping of the genes contained in IL2-5 and IL4-3 may provide significant improvements for tomato cultivation in the future.

An agronomic determinant of IL2-5 is its low intrinsic fruit yield. Thus, the reduction in fruit dry mass and Hi of IL2-5/4-3 relative to its IL4-3 parent in drought may have been caused by the action of dominant genes contained in IL2-5. However, the interaction between IL4-3 and IL2-5 resulted in additive effects that enabled IL2-5/4-3 to manifest yields comparable to cv. M82 when well-watered. It is worth noting that when subjected to drought, IL4-3 was able to maintain Hi, individual fresh mass, and fruit numbers superior to cv. M82. Our data suggest that this greater productive capacity observed in IL4-3 was passed on to IL2-5/4-3, which improved the productive fruit yield of this genotype in both control and drought treatments.

## CONCLUSION

We show that dissection of the genetic basis of drought resistance can be achieved through the analysis of natural genetic variation. In this work, we proved that leaf traits contained in IL2-5 and IL4-3 can alter leaf thickness and succulence, and that such changes can mitigate the effects caused by water deficit in tomato plants. The anatomical changes contained in these ILs made it possible to maintain leaf water status, contributed to better photosynthetic performance, and improved the resilience of plants subjected to drought. In this work, we demonstrated that the increased drought resistance observed in IL2-5/4-3 occurred due to the combined effect of changes in leaf anatomy, associated with a reduction

in total leaf area and an increase in root system. Our data showed that increased thickness and LMA, as well as reduced stomatal density, did not alter $CO_2$ diffusion in IL2-5/4-3 and IL2-5, respectively. The independent segregation of morphological and anatomical characteristics observed in *S. pen* IL may enable the identification of important leaf traits to improve tomato resistance to drought conditions. Because they do not affect leaf resistance to $CO_2$ diffusion in tomato, we believe that we can work simultaneously, or in isolation, on several leaf anatomical traits that confer drought resistance, including reducing their impact on productivity. Finally, we suggest the existence of *S. pen* genes responsible for changes in leaf traits that may improve the resistance of commercial tomato to water deficit conditions. However, future work is needed to identify the genes responsible for the behaviors demonstrated here.

REFERENCES

**Adams WW, Muller O, Cohu CM, Demmig-Adams B**. 2013. May photoinhibition be a consequence, rather than a cause, of limited plant productivity? Photosynthesis Research **117**, 31–44.

**Balakrishnan D, Surapaneni M, Mesapogu S, Neelamraju S**. 2019. Development and use of chromosome segment substitution lines as a genetic resource for crop improvement. Theoretical and Applied Genetics **132**, 1–25.

**Batista-Silva W, da Fonseca-Pereira P, Martins AO, Zsögön A, Nunes-Nesi A, Araújo WL**. 2020. Engineering Improved Photosynthesis in the Era of Synthetic Biology. Plant Communications **1**, 100032.

**Brodribb TJ, Holbrook NM**. 2006. Declining hydraulic efficiency as transpiring leaves desiccate: two types of response. Plant, Cell & Environment **29**, 2205–2215.

**Calafiore R, Aliberti A, Ruggieri V, Olivieri F, Rigano MM, Barone A**. 2019. Phenotypic and Molecular Selection of a Superior Solanum pennellii Introgression Sub-Line Suitable for Improving Quality Traits of Cultivated Tomatoes. Frontiers in Plant Science **10**.

**Carins Murphy MR, Jordan GJ, Brodribb TJ**. 2012. Differential leaf expansion can enable hydraulic acclimation to sun and shade: Leaf expansion can enable hydraulic acclimation. Plant, Cell & Environment **35**, 1407–1418.

**Carins Murphy MR, Jordan GJ, Brodribb TJ**. 2014. Acclimation to humidity modifies the link between leaf size and the density of veins and stomata: VPD alters the link between leaf size and anatomy. Plant, Cell & Environment **37**, 124–131.

**Centritto M, Jarvis PG**. 1999. Long-term effects of elevated carbon dioxide concentration and provenance on four clones of Sitka spruce (Picea sitchensis). II. Photosynthetic capacity and nitrogen use efficiency. Tree Physiology **19**, 807–814.

**Chen Y, Han Y, Zhang M, Zhou S, Kong X, Wang W**. 2016. Overexpression of the Wheat Expansin Gene TaEXPA2 Improved Seed Production and Drought Tolerance in Transgenic Tobacco Plants (ZM Yang, Ed.). PLOS ONE **11**, e0153494.

**Chitwood DH, Kumar R, Headland LR, *et al.*** 2013. A Quantitative Genetic Basis for Leaf Morphology in a Set of Precisely Defined Tomato Introgression Lines. The Plant Cell **25**, 2465–2481.

**Condon AG**. 2004. Breeding for high water-use efficiency. Journal of Experimental Botany **55**, 2447–2460.

**Coneva V, Frank MH, Balaguer MA de L, Li M, Sozzani R, Chitwood DH**. 2017. Genetic Architecture and Molecular Networks Underlying Leaf Thickness in Desert-Adapted Tomato *Solanum pennellii*. Plant Physiology **175**, 376–391.

**deVicente MC, Tanksley SD**. 1993. QTL analysis of transgressive segregation in an interspecific tomato cross. Genetics **134**, 585–596.

**Duursma RA, Blackman CJ, Lopéz R, Martin-StPaul NK, Cochard H, Medlyn BE**. 2019. On the minimum leaf conductance: its role in models of plant water use, and ecological and environmental controls. New Phytologist **221**, 693–705.

**Egea I, Albaladejo I, Meco V, Morales B, Sevilla A, Bolarin MC, Flores FB**. 2018. The drought-tolerant Solanum pennellii regulates leaf water loss and induces genes involved in amino acid and ethylene/jasmonate metabolism under dehydration. Scientific Reports **8**, 2791.

**Eggli U, Nyffeler R**. 2009. Living under temporarily arid conditions - succulence as an adaptive strategy. Bradleya **2009**, 13–36.

**Eshed Y, Zamir D**. 1995. An introgression line population of Lycopersicon pennellii in the cultivated tomato enables the identification and fine mapping of yield-associated QTL. Genetics **141**, 1147–1162.

**Fernandez-Moreno J-P, Levy-Samoha D, Malitsky S, Monforte AJ, Orzaez D, Aharoni A, Granell A**. 2017. Uncovering tomato quantitative trait loci and candidate genes for fruit cuticular lipid composition using the Solanum pennellii introgression line population. Journal of Experimental Botany **68**, 2703–2716.

**Flexas J, Cano FJ, Carriquí M, Coopman RE, Mizokami Y, Tholen D, Xiong D**. 2018. CO2 Diffusion Inside Photosynthetic Organs. In: Adams III WW,, In: Terashima I,

eds. Advances in Photosynthesis and Respiration. The Leaf: A Platform for Performing Photosynthesis. Cham: Springer International Publishing, 163–208.

**Flexas J, Diaz-Espejo A, Gago J, Gallé A, Galmés J, Gulías J, Medrano H**. 2014. Photosynthetic limitations in Mediterranean plants: A review. Environmental and Experimental Botany **103**, 12–23.

**Frary A, Nesbitt TC, Frary A, Grandillo S, Van Der Knaap E, Cong B, Liu J, Meller J, Elber R, Alpert KB**. 2000. fw2. 2: a quantitative trait locus key to the evolution of tomato fruit size. Science **289**, 85–88.

**Fullana-Pericàs M, Conesa MÀ, Soler S, Ribas-Carbó M, Granell A, Galmés J**. 2017. Variations of leaf morphology, photosynthetic traits and water-use efficiency in Western-Mediterranean tomato landraces. Photosynthetica **55**, 121–133.

**Galdon-Armero J, Fullana-Pericas M, Mulet PA, Conesa MA, Martin C, Galmes J**. 2018. The ratio of trichomes to stomata is associated with water use efficiency in *Solanum lycopersicum* (tomato). The Plant Journal **96**, 607–619.

**Galmés J, Ochogavía JM, Gago J, Roldán EJ, Cifre J, Conesa MÀ**. 2013. Leaf responses to drought stress in Mediterranean accessions of *Solanum lycopersicum* : anatomical adaptations in relation to gas exchange parameters: Anatomical adaptations to water stress in tomato. Plant, Cell & Environment **36**, 920–935.

**Genty B, Briantais J-M, Baker NR**. 1989. The relationship between the quantum yield of photosynthetic electron transport and quenching of chlorophyll fluorescence. Biochimica et Biophysica Acta (BBA)-General Subjects **990**, 87–92.

**Gibson AC**. 1982. The anatomy of succulence. Crassulacean acid metabolism, 1–17.

**Gong P, Zhang J, Li H, *et al.*** 2010. Transcriptional profiles of drought-responsive genes in modulating transcription signal transduction, and biochemical pathways in tomato. Journal of Experimental Botany **61**, 3563–3575.

**Gornall J, Betts R, Burke E, Clark R, Camp J, Willett K, Wiltshire A**. 2010. Implications of climate change for agricultural productivity in the early twenty-first century. Philosophical Transactions of the Royal Society B: Biological Sciences **365**, 2973–2989.

**Grace OM**. 2019. Succulent plant diversity as natural capital. PLANTS, PEOPLE, PLANET **1**, 336–345.

**Grassi G, Magnani F**. 2005. Stomatal, mesophyll conductance and biochemical limitations to photosynthesis as affected by drought and leaf ontogeny in ash and oak trees. Plant, Cell & Environment **28**, 834–849.

**Han Y, Wang W, Sun J, *et al.*** 2013. Populus euphratica XTH overexpression enhances salinity tolerance by the development of leaf succulence in transgenic tobacco plants. Journal of Experimental Botany **64**, 4225–4238.

**Harley PC, Loreto F, Di Marco G, Sharkey TD**. 1992. Theoretical considerations when estimating the mesophyll conductance to CO2 flux by analysis of the response of photosynthesis to CO2. Plant physiology **98**, 1429–1436.

**Hughes J, Hepworth C, Dutton C, Dunn JA, Hunt L, Stephens J, Waugh R, Cameron DD, Gray JE**. 2017. Reducing Stomatal Density in Barley Improves Drought Tolerance without Impacting on Yield. Plant Physiology **174**, 776–787.

**Iovieno P, Punzo P, Guida G, *et al.*** 2016. Transcriptomic Changes Drive Physiological Responses to Progressive Drought Stress and Rehydration in Tomato. Frontiers in Plant Science **7**.

**Kebede H, Martin B, Nienhuis J, King G**. 1994. Leaf Anatomy of Two Lycopersicon Species with Contrasting Gas Exchange Properties. Crop Science **34**, cropsci1994.0011183X003400010019x.

**Kitajima M, Butler WL**. 1975. Quenching of chlorophyll fluorescence and primary photochemistry in chloroplasts by dibromothymoquinone. Biochimica et Biophysica Acta (BBA) - Bioenergetics **376**, 105–115.

**Koenig D, Jiménez-Gómez JM, Kimura S, Fulop D, Chitwood DH, Headland LR, Kumar R, Covington MF, Devisetty UK, Tat AV**. 2013. Comparative transcriptomics reveals patterns of selection in domesticated and wild tomato. Proceedings of the National Academy of Sciences **110**, E2655–E2662.

**Lana-Costa J, de Oliveira Silva FM, Batista-Silva W, Carolino DC, Senra RL, Medeiros DB, Martins SCV, Gago J, Araújo WL, Nunes-Nesi A**. 2020*b*. High Photosynthetic Rates in a Solanum pennellii Chromosome 2 QTL Is Explained by Biochemical and Photochemical Changes. Frontiers in Plant Science **11**, 794.

**Leng G, Hall J**. 2019. Crop yield sensitivity of global major agricultural countries to droughts and the projected changes in the future. Science of The Total Environment **654**, 811–821.

**Li W-D, Biswas DK, Xu H, *et al.*** 2009. Photosynthetic responses to chromosome doubling in relation to leaf anatomy in Lonicera japonica subjected to water stress. Functional Plant Biology **36**, 783–792.

**Li S, Hamani AKM, Zhang Y, Liang Y, Gao Y, Duan A**. 2021. Coordination of leaf hydraulic, anatomical, and economical traits in tomato seedlings acclimation to long-term drought. BMC Plant Biology **21**, 536.

**Lim SD, Mayer JA, Yim WC, Cushman JC**. 2020. Plant tissue succulence engineering improves water-use efficiency, water-deficit stress attenuation and salinity tolerance in Arabidopsis. The Plant Journal **103**, 1049–1072.

**Lippman ZB, Semel Y, Zamir D**. 2007. An integrated view of quantitative trait variation using tomato interspecific introgression lines. Current Opinion in Genetics & Development **17**, 545–552.

**Long SP, Bernacchi CJ**. 2003. Gas exchange measurements, what can they tell us about the underlying limitations to photosynthesis? Procedures and sources of error. Journal of Experimental Botany **54**, 2393–2401.

**Males J**. 2017. Secrets of succulence. Journal of Experimental Botany **68**, 2121–2134.

**Melis A, Spangfort M, Andersson B**. 1987. Light-absorption and electron-transport balance between photosystem II and photosystem I in spinach chloroplasts. Photochemistry and Photobiology **45**, 129–136.

**Mishra KB, Iannacone R, Petrozza A, Mishra A, Armentano N, La Vecchia G, Trtílek M, Cellini F, Nedbal L**. 2012. Engineered drought tolerance in tomato plants is reflected in chlorophyll fluorescence emission. Plant Science **182**, 79–86.

**Muir CD, Conesa MÀ, Roldán EJ, Molins A, Galmés J**. 2017. Weak coordination between leaf structure and function among closely related tomato species. New Phytologist **213**, 1642–1653.

**Niinemets Ü, Díaz-Espejo A, Flexas J, Galmés J, Warren CR**. 2009. Role of mesophyll diffusion conductance in constraining potential photosynthetic productivity in the field. Journal of experimental botany **60**, 2249–2270.

**Nobel PS**. 2006. Parenchyma–Chlorenchyma Water Movement during Drought for the Hemiepiphytic Cactus Hylocereus undatus. Annals of Botany **97**, 469–474.

**Ogburn RM, Edwards EJ**. 2010. The Ecological Water-Use Strategies of Succulent Plants. Advances in Botanical Research. Elsevier, 179–225.

**Ogburn RM, Edwards EJ**. 2012. Quantifying succulence: a rapid, physiologically meaningful metric of plant water storage: Quantifying succulence. Plant, Cell & Environment **35**, 1533–1542.

**Pailles Y, Awlia M, Julkowska M, Passone L, Zemmouri K, Negrão S, Schmöckel SM, Tester M**. 2020. Diverse Traits Contribute to Salinity Tolerance of Wild Tomato Seedlings from the Galapagos Islands1 [OPEN]. Plant Physiology **182**, 534–546.

**Paterson AH, DeVerna JW, Lanini B, Tanksley SD**. 1990. Fine mapping of quantitative trait loci using selected overlapping recombinant chromosomes, in an interspecies cross of tomato. Genetics **124**, 735–742.

**Peguero-Pina JJ, Sisó S, Flexas J, Galmés J, García-Nogales A, Niinemets Ü, Sancho-Knapik D, Saz MÁ, Gil-Pelegrín E**. 2017. Cell-level anatomical characteristics explain high mesophyll conductance and photosynthetic capacity in sclerophyllous Mediterranean oaks. New Phytologist **214**, 585–596.

**Poorter H, Niinemets Ü, Poorter L, Wright IJ, Villar R**. 2009. Causes and consequences of variation in leaf mass per area (LMA): a meta-analysis. New Phytologist **182**, 565–588.

**Poorter H, Niklas KJ, Reich PB, Oleksyn J, Poot P, Mommer L**. 2012. Biomass allocation to leaves, stems and roots: meta-analyses of interspecific variation and environmental control. New Phytologist **193**, 30–50.

**Ren T, Weraduwage SM, Sharkey TD**. 2019. Prospects for enhancing leaf photosynthetic capacity by manipulating mesophyll cell morphology. Journal of Experimental Botany **70**, 1153–1165.

**Rick CM**. 1973. Potential Genetic Resources in Tomato Species: Clues from Observations in Native Habitats. In: Srb AM, ed. Basic Life Sciences. Genes, Enzymes, and Populations. Boston, MA: Springer US, 255–269.

**Ripley BS, Abraham T, Klak C, Cramer MD**. 2013. How succulent leaves of Aizoaceae avoid mesophyll conductance limitations of photosynthesis and survive drought. Journal of Experimental Botany **64**, 5485–5496.

**Rodeghiero M, Niinemets Ü, Cescatti A**. 2007. Major diffusion leaks of clamp-on leaf cuvettes still unaccounted: how erroneous are the estimates of Farquhar et al. model parameters? Plant, cell & environment **30**, 1006–1022.

**Sack L, Scoffoni C, McKown AD, Frole K, Rawls M, Havran JC, Tran H, Tran T**. 2012. Developmentally based scaling of leaf venation architecture explains global ecological patterns. Nature Communications **3**, 837.

**Tardieu F, Simonneau T, Muller B**. 2018. The Physiological Basis of Drought Tolerance in Crop Plants: A Scenario-Dependent Probabilistic Approach. Annual Review of Plant Biology **69**, 733–759.

**Terashima I, Hanba YT, Tholen D, Niinemets Ü**. 2011. Leaf functional anatomy in relation to photosynthesis. Plant physiology **155**, 108–116.

**Tomás M, Flexas J, Copolovici L, Galmés J, Hallik L, Medrano H, Ribas-Carbó M, Tosens T, Vislap V, Niinemets Ü**. 2013. Importance of leaf anatomy in determining mesophyll diffusion conductance to CO2 across species: quantitative limitations and scaling up by models. Journal of Experimental Botany **64**, 2269–2281.

**Trueba S, Pan R, Scoffoni C, John GP, Davis SD, Sack L**. 2019. Thresholds for leaf damage due to dehydration: declines of hydraulic function, stomatal conductance and cellular integrity precede those for photochemistry. New Phytologist **223**, 134–149.

**Tyree MT, Ewers FW**. 1991. The hydraulic architecture of trees and other woody plants. New Phytologist **119**, 345–360.

**Tyree MT, Hammel HT**. 1972. The Measurement of the Turgor Pressure and the Water Relations of Plants by the Pressure-bomb Technique. Journal of Experimental Botany **23**, 267–282.

**Van Oosten MJ, Costa A, Punzo P, Landi S, Ruggiero A, Batelli G, Grillo S**. 2016. Genetics of Drought Stress Tolerance in Crop Plants. In: Hossain MA,, In: Wani SH,, In: Bhattacharjee S,, In: Burritt DJ,, In: Tran L-SP, eds. Drought Stress Tolerance in Plants, Vol 2. Cham: Springer International Publishing, 39–70.

**Vile D, Garnier É, Shipley B, *et al.*** 2005. Specific Leaf Area and Dry Matter Content Estimate Thickness in Laminar Leaves. Annals of Botany **96**, 1129–1136.

**Willert DJ von, Eller BM, Werger MJA, Brinckmann E, Ihlenfeldt H-D, Birks HJB, Wiens JA**. 1992. Life Strategies of Succulents in Deserts: With Special Reference to the Namib Desert. CUP Archive.

**Zhou R, Wu Z, Wang X, Rosenqvist E, Wang Y, Zhao T, Ottosen C-O**. 2018. Evaluation of temperature stress tolerance in cultivated and wild tomatoes using photosynthesis and chlorophyll fluorescence. Horticulture, Environment, and Biotechnology **59**, 499–509.

TABLES

**Table 1:** Photosynthetic characterization of M82, IL 2-5, IL 4-3, and IL 2-5/4-3 grown under control conditions. General photosynthetic limitations associated with stomatal, mesophilic, and biochemical factors are also shown below. Data are the mean and standard error of five replicates. Significant differences according to ANOVA are shown in p-values in bold. Different letters indicate significant differences according to Tukey's test ($p < 0.05$). Abbreviations: net photosynthesis ($A$); stomatal conductance ($g_s$); mesophyll conductance to

$CO_2$ estimated according to the Harley (gm), transpiration ($E$); chloroplastic $CO_2$ concentration ($C_c$); substomatal $CO_2$ concentration ($C_i$); maximum carboxylation capacity ($V_{cmax}$); maximum capacity for electron transport rate ($J_{max}$); use of triose phosphate ($TPU$); dark respiration ($R_{dark}$).

| Parameters | M82 | IL 2-5 | IL 4-3 | IL 2-5/4-3 | *p* |
|---|---|---|---|---|---|
| $A$ (µmol $CO_2$ $m^{-2}$ $s^{-1}$) | 22 ± 1.6 | 23.05 ± 0.64 | 23.56 ± 1.15 | 25.22 ± 0.89 | 0.28 |
| $g_s$ (mol $H_2O$ $m^{-2}$ $s^{-1}$) | 0.57 ± 0.05 | 0.58 ± 0.08 | 0.54 ± 0.04 | 0.52 ± 0.01 | 0.87 |
| $g_m$ (mol $CO_2$ $m^{-2}$ $s^{-1}$) | 0.15 ± 0.017 | 0.14 ± 0.008 | 0.16 ± 0.01 | 0.17 ± 0.01 | 0.19 |
| $g_m/g_s$ (mol $CO_2$ $mol^{-1}$ $CO_2$) | 0.48 ± 0.05 | 0.47 ± 0.07 | 0.54 ± 0.05 | 0.59 ± 0.02 | 0.22 |
| $E$ (mmol $H_2O$ $m^{-2}$ $s^{-1}$) | 4.23 ± 0.46 | 4.62 ± 0.34 | 4.71 ± 0.35 | 4.33 ± 0.31 | 0.68 |
| $C_c/C_i$ (µmol $CO_2$ µmol$^{-1}$ $CO_2$) | 0.53 ± 0.018 a | 0.46 ± 0.014 b | 0.52 ± 0.012 ab | 0.51 ± 0.01 ab | **0.02** |
| $R_{dark}$ (µmol $CO_2$ $m^{-2}$ $s^{-1}$) | 1.20 ± 0.05 b | 1.41 ± 0.04 b | 1.32 ± 0.09 b | 1.79 ± 0.09 a | **0.001** |
| $V_{cmax\_Cc}$ (µmol $CO_2$ $m^{-2}$ $s^{-1}$) | 143.5 ± 6.39 b | 180.2 ± 2.97 a | 171.2 ± 5.54 a | 182.9 ± 6.27 a | **0.0004** |
| $J_{max\_Cc}$ (µmol $CO_2$ $m^{-2}$ $s^{-1}$) | 181.3 ± 6.56 b | 213.9 ± 4.38 a | 207.3 ± 2.31 a | 228 ± 6.66 a | **0.0001** |
| $TPU_{\_Cc}$ (µmol $CO_2$ $m^{-2}$ $s^{-1}$) | 10.5 ± 0.44 c | 12.3 ± 0.47 b | 12 ± 0.29 b | 13.8 ± 0.58 a | **0.001** |
| *ls* | 0.19 ± 0.01 | 0.19 ± 0.02 | 0.21 ± 0.014 | 0.22 ± 0.003 | 0.34 |
| *l*m | 0.46 ± 0.03 | 0.50 ± 0.02 | 0.43 ± 0.015 | 0.44 ± 0.01 | 0.09 |
| *l*b | 0.33 ± 0.02 | 0.29 ± 0.003 | 0.35 ± 0.01 | 0.32 ± 0.008 | 0.18 |

**Table 2**: Hydraulic parameters in apical leaflets of the fifth leaf in well-watered plants. The significance of the ANOVA is highlighted in bold. Lowercase letters compare means that differ between genotypes according to the Tukey test ($p < 0.05$). Data are the mean and standard error of seven replicates. Abbreviations: saturated water content based on mass (SWC); leaf hydraulic conductance ($K_{leaf}$); minimum leaf conductance ($g_{min}$).

| Parameters | M82 | IL2-5 | IL4-3 | IL2-5/4-3 | *P* |
|---|---|---|---|---|---|
| SWC (g $g^{-1}$) | 9.6 ± 0.27 b | 9.4 ± 0.32 b | 10.9 ± 0.21 a | 9.7 ± 0.16 b | **0.0005** |
| Volume ($cm^3$) | 2.66 ± 0.21 c | 3 ± 0.28 bc | 4.24 ± 0.42 a | 3.5 ± 0.25 ab | **0.0003** |
| Leaf density (g $cm^3$) | 0.70 ± 0.03 a | 0.59 ± 0.03 ab | 0.58 ± 0.02 b | 0.57 ± 0.01 b | **0.03** |
| $K_{leaf}$ (mmol $H_2O$ $m^{-2}$ $s^{-1}$ MPa) | 7.8 ± 0.8 ab | 7.7 ± 0.6 ab | 7.2 ± 0.2 b | 9.8 ± 0.4 a | **0.03** |
| $g_{min}$ (mmol $H_2O$ $m^{-2}$ $s^{-1}$ MPa) | 7.5 ± 0.37 | 7.3 ± 0.43 | 8.3 ± 0.44 | 6.9 ± 0.31 | 0.17 |

FIGURES LEGENDS

**Figure 1:** IL2-5/4-3 has greater leaf thickness compared to cv. M82. (**A**) Representative images of cross-sections of M82 and IL 2-5/4-3 leaflets of the fifth leaf at 93 DAG. (**B**) Leaf thickness, (**C**) adaxial and (**D**) abaxial epidermis, (**E**) palisade and, (**F**) spongy parenchyma. Columns and bars represent the mean and standard error of the mean (n = 5). Significant differences between genotypes are represented by the *p*-value according to the t-test ($p < 0.05$). Abbreviations: palisade parenchyma (PP); spongy parenchyma (SP); epidermis (Ep); intercellular airspaces (IAS).

**Figure 2:** Il2-5/4-3 can maintain gas exchange for longer and prevent photoinhibition and chlorophyll degradation under drought. (**A**) Representative images of M82 and IL2-3 5/4-3 after 10 days (82-DAG) of water deficit and three days (85-DAG) after the 4 resumption of irrigation (recovery). (**B**) Net photosynthesis, (**C**) stomatal conductance, (**D**) transpiration, (**E**) PSII maximum quantum yield, (**F**) SPAD chlorophyll index performed in apical leaflets of the fifth leaf, and (**G**) pre-dawn water potential quantified in fully expanded fourth leaf leaflets from base to apex. The light blue band represents the plant's rehydration period (started on day 10 after the start of the drought treatment (DAT)). Asterisks indicate significant differences between genotypes in the dry condition in each DAT isolated according to the Tukey test ($p < 0.05$). Values represent the mean and standard error of the mean (n = 5).

**Figure 3:** *S. pennelli* ILs can delay the decrease in gas exchange in response to drought and improve the ability to recover from stress. (**A**) net photosynthesis, (**B**) stomatal conductance, (**C**) transpiration, (**D**) electron transport rate, (**E**) water potential and (F) pre-dawn relative water content, (**G**) water potential, and (**H**) midday relative water content. The gas exchange parameters were performed on apical leaflets of the sixth leaf. The other parameters were measured on leaflets of the fifth and fourth leaf. Asterisks indicate significant differences between genotypes in the dry condition in each DAT isolated according to the Tukey test ($p < 0.05$). Values represent the mean and standard error of the mean (n = 6).

**Figure 4:** Dry mass and growth parameters of M82, IL2-5, IL4-3, and IL2-5/4-3 were measured 63 days after germination (DAG). Values represent means and standard error (n = 6). Uppercase letters compare control treatments, and lowercase letters compare treatments that experienced 12 days of drought according to Tukey's test ($p < 0.05$). Asterisks denote statistical differences between the drought and control treatments within each isolated genotype according to Šídák's multiple comparisons test ($p < 0.05$). Abbreviations: saturated water content (SWC); leaf mass per area (LMA).

**Figure 5:** The anatomical changes in the ILs are accompanied by an expressive increase in leaf succulence. (**A**) Representative images of leaf morphology traits of plants in control conditions and (**B**) acclimatized to drought (60% of field capacity) for 40 days. (**C**) Leaf thickness, (**D** and **E**) adaxial and abaxial stomatal density, (F) vein density, (**G**) stomatal pore area index (calculated as (guard cell length)2 × stomatal density for the adaxial and abaxial epidermes and then added up), (**H**) stomatal index (the proportion of stomatal to total cells in the epidermis, expressed as percentage of total cells), (**I**) intercellular airspace, and (**J**)

saturated water content. Analyzes were performed on apical leaflets of the seventh fully developed leaf under moderate drought conditions at 93 DAG (n = 6). Stomata in the adaxial and abaxial epidermis are highlighted. Uppercase letters compare control treatments and lowercase letters compare drought treatments according to Tukey's test ($p < 0.05$). Asterisks denote statistical differences between the drought and control treatments within each isolated genotype according to Šídák's multiple comparisons test ($p < 0.05$).

**Figure 6:** Increased thickness and succulence can affect the diameter and number of vessels in the xyllem. Xylem traits measured on the midrib. Values represent the mean and standard error of (n = 6). Analyzes were performed on apical leaflets of the seventh fully developed leaf under moderate drought conditions at 93 DAG. Uppercase letters compare control treatments and lowercase letters compare drought treatments according to Tukey's test ($p < 0.05$). Asterisks denote statistical differences between the drought and control treatments within each isolated genotype according to Šídák's multiple comparisons test ($p < 0.05$). Abbreviations: theoretical hydraulic conductance (Kt).

**Figure 7:** (**A**) Representative images of fruit production in plants of the control treatment (well-irrigated) and acclimatized to drought (60% of field capacity) for 40 days. (**B**, **C** and **D**) Effects of drought in fruit productivity measured at 93 days after germination (DAG). Values represent the means and standard error (n = 6). Uppercase letters compare control treatments and lowercase letters compare drought treatments according to Tukey's test ($p < 0.05$). Asterisks denote statistical differences between the drought and control treatments within each isolated genotype according to Šídák's multiple comparisons test ($p < 0.05$).

**Figure 8:** Principal Component Analysis (PCA) biplot of M82, IL2-5, IL4-3 and IL2-5/4-3 (n = 4). PC1 (48.53%) and PC2 (16.18%) explain most of the variance found in 15 traits related to physiology, leaf anatomy, and productivity of plants grown under control and drought conditions. The length and direction of the arrows indicate the contribution of traits on the two PCs shown. The angle between the vectors determines the degree of correlation between traits. Aligned vectors indicate a high positive correlation between traits. Abbreviations: saturated water content (SWC); leaf mass per area (LMA); intercellular air space (IAS); maximum electron transport rate (*ETR*); relative water content (RWC); harvest index (H index); net photosynthesis (*A*); diameter of midrib vessels (VD); stomatal density (SD).

**Figure 9:** Photosynthesis and electron transport rate (*ETR*) response curves to chloroplast $CO_2$ concentrations ($A/C_c$) and photon flux density ($A$/PPFD). (**A**) $A/C_c$, (**B**) $ETR/C_c$, (**C**) $A$/PPFD and (**D**) $ETR$/PPFD. Data show the mean and standard error of the mean of five replicates. The curves were measured in fully expanded fifth leaf apical leaflets from base to apex. The evaluations were carried out at 46 DAG. Asterisks denote statistical differences between the genotype according to Tukey's test ($p < 0.05$)

FIGURES

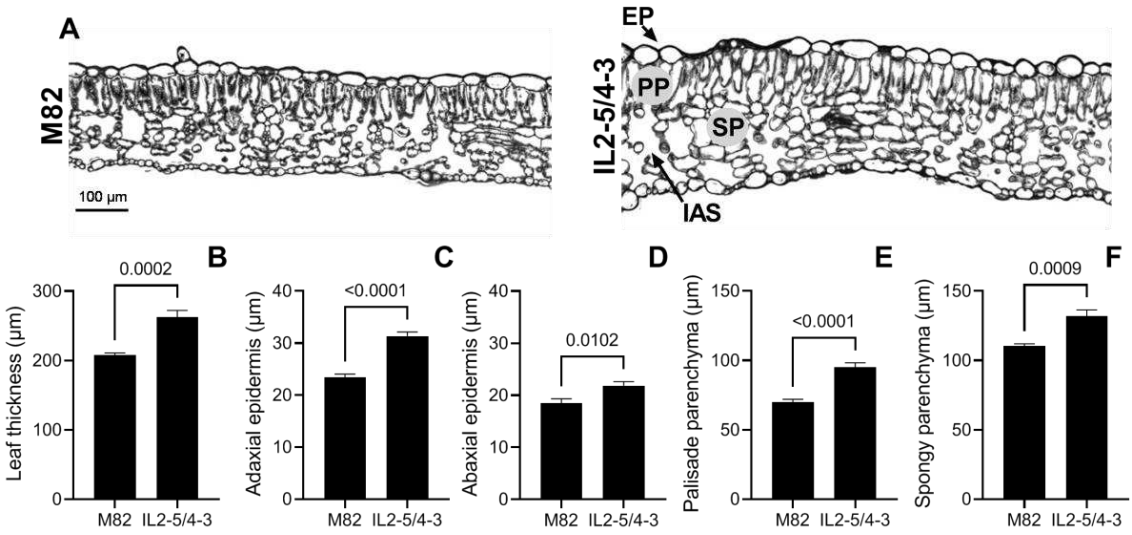


**Figure 1:** IL2-5/4-3 has greater leaf thickness compared to cv. M82. (**A**) Representative images of cross-sections of M82 and IL 2-5/4-3 leaflets of the fifth leaf at 93 DAG. (**B**) Leaf thickness, (**C**) adaxial and (**D**) abaxial epidermis, (**E**) palisade and, (**F**) spongy parenchyma. Columns and bars represent the mean and standard error of the mean (n = 5). Significant differences between genotypes are represented by the *p*-value according to the t-test ($p < 0.05$). Abbreviations: palisade parenchyma (PP); spongy parenchyma (SP); epidermis (Ep); intercellular airspaces (IAS).

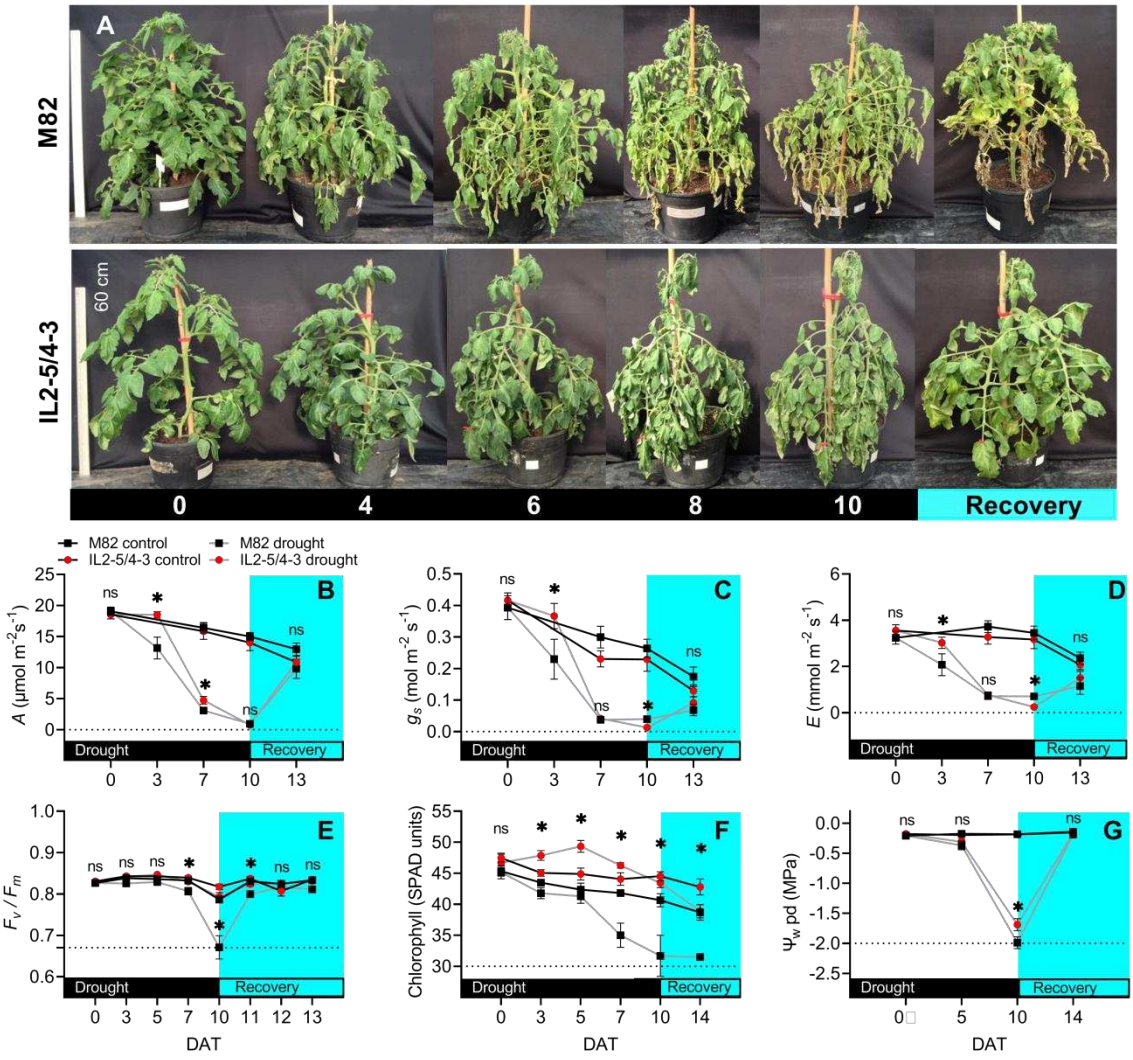


**Figure 2:** Il2-5/4-3 can maintain gas exchange for longer and prevent photoinhibition and chlorophyll degradation under drought. (**A**) Representative images of M82 and IL2-3 5/4-3 after 10 days (82-DAG) of water deficit and three days (85-DAG) after the 4 resumption of irrigation (recovery). (**B**) Net photosynthesis, (**C**) stomatal conductance, (**D**) transpiration, (**E**) PSII maximum quantum yield, (**F**) SPAD chlorophyll index performed in apical leaflets of the fifth leaf, and (**G**) pre-dawn water potential quantified in fully expanded fourth leaf leaflets from base to apex. The light blue band represents the plant's rehydration period (started on day 10 after the start of the drought treatment (DAT)). Asterisks indicate significant differences between genotypes in the dry condition in each DAT isolated according to the Tukey test ($p < 0.05$). Values represent the mean and standard error of the mean ($n = 5$).

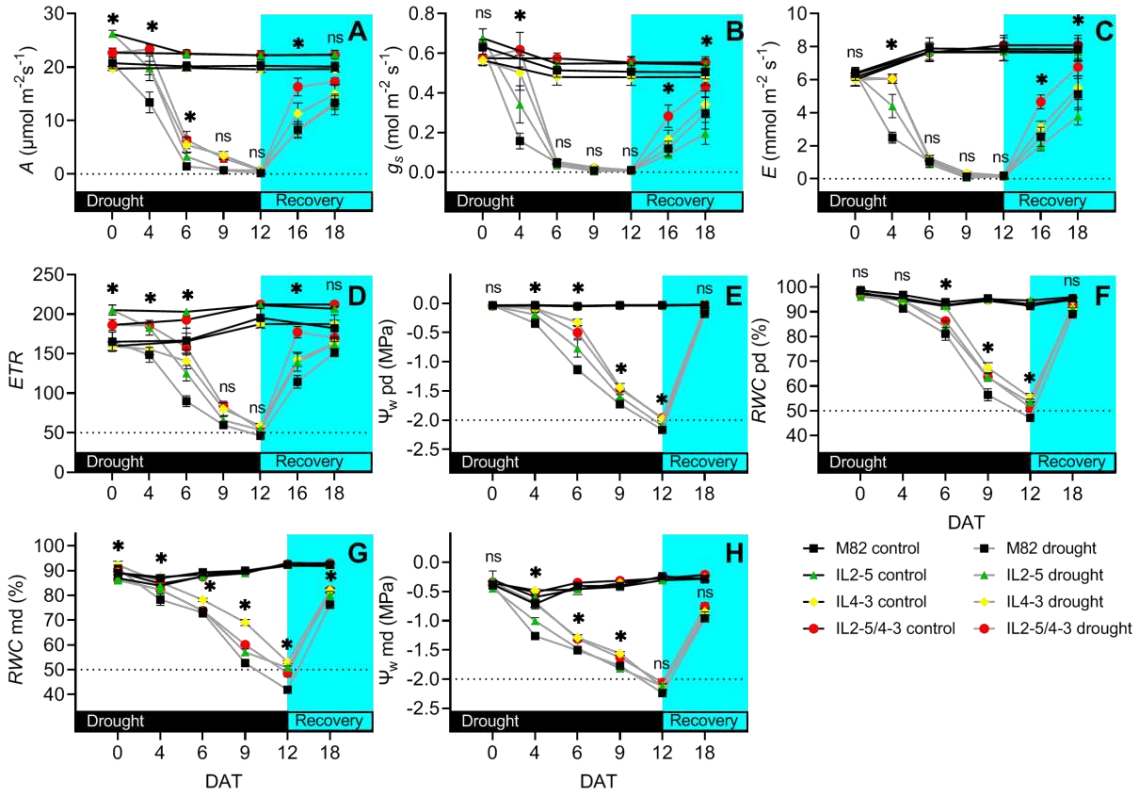


**Figure 3:** *S. pennelli* ILs can delay the decrease in gas exchange in response to drought and improve the ability to recover from stress. (**A**) net photosynthesis, (**B**) stomatal conductance, (**C**) transpiration, (**D**) electron transport rate, (**E**) water potential and (F) pre-dawn relative water content, (**G**) water potential, and (**H**) midday relative water content. The gas exchange parameters were performed on apical leaflets of the sixth leaf. The other parameters were measured on leaflets of the fifth and fourth leaf. Asterisks indicate significant differences between genotypes in the dry condition in each DAT isolated according to the Tukey test ($p < 0.05$). Values represent the mean and standard error of the mean ($n = 6$).

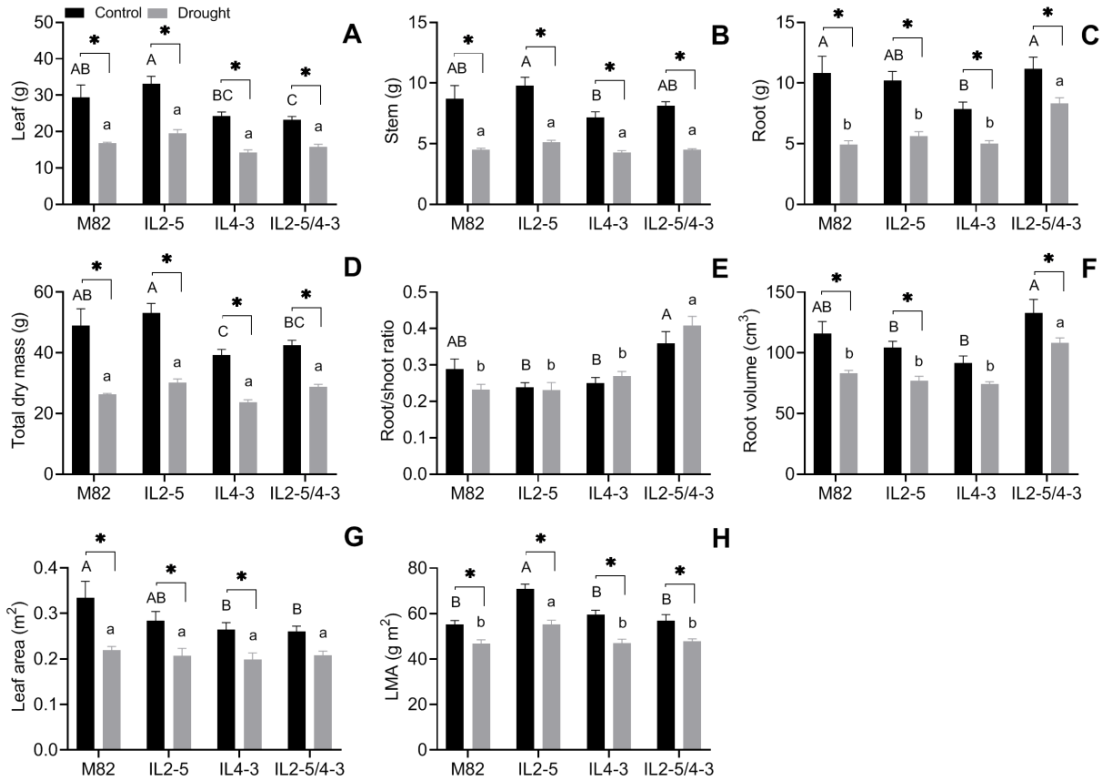


**Figure 4:** Dry mass and growth parameters of M82, IL2-5, IL4-3, and IL2-5/4-3 were measured 63 days after germination (DAG). Values represent means and standard error (n = 6). Uppercase letters compare control treatments, and lowercase letters compare treatments that experienced 12 days of drought according to Tukey's test ($p < 0.05$). Asterisks denote statistical differences between the drought and control treatments within each isolated genotype according to Šídák's multiple comparisons test ($p < 0.05$). Abbreviations: saturated water content (SWC); leaf mass per area (LMA).

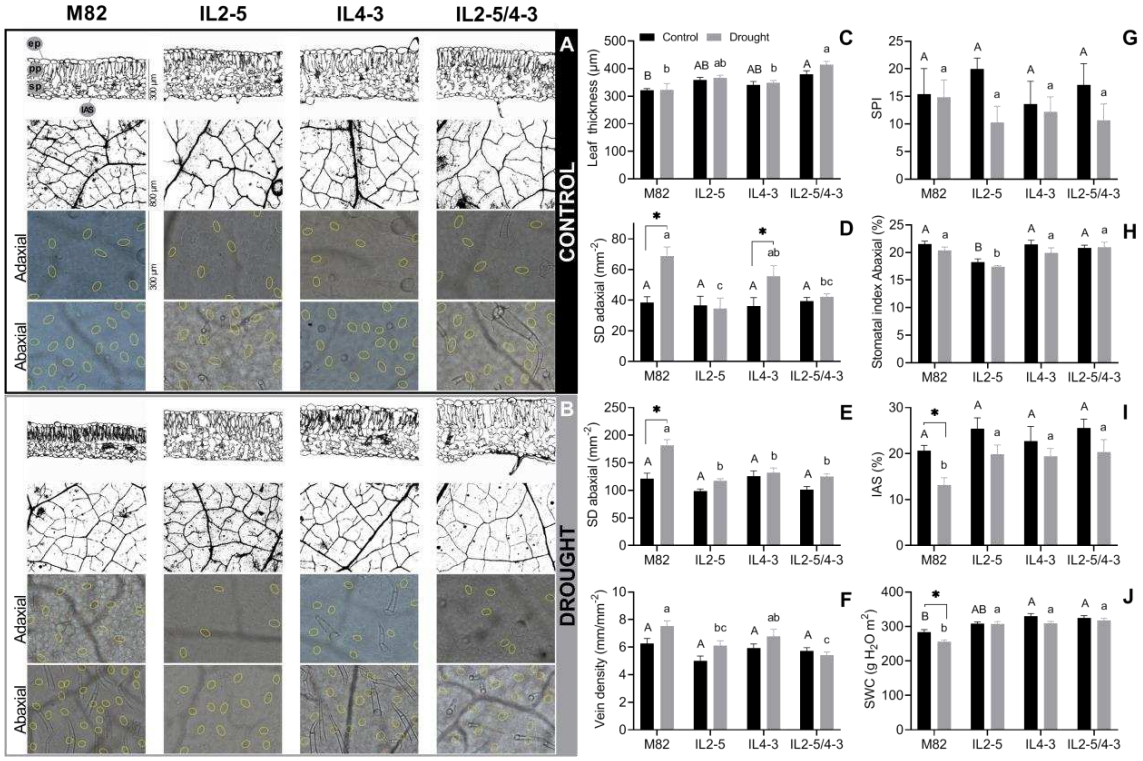


**Figure 5:** The anatomical changes in the ILs are accompanied by an expressive increase in leaf succulence. (**A**) Representative images of leaf morphology traits of plants in control conditions and (**B**) acclimatized to drought (60% of field capacity) for 40 days. (**C**) Leaf thickness, (**D** and **E**) adaxial and abaxial stomatal density, (F) vein density, (**G**) stomatal pore area index (calculated as (guard cell length)2 × stomatal density for the adaxial and abaxial epidermes and then added up), (**H**) stomatal index (the proportion of stomatal to total cells in the epidermis, expressed as percentage of total cells), (**I**) intercellular airspace, and (**J**) saturated water content. Analyzes were performed on apical leaflets of the seventh fully developed leaf under moderate drought conditions at 93 DAG (n = 6). Stomata in the adaxial and abaxial epidermis are highlighted. Uppercase letters compare control treatments and lowercase letters compare drought treatments according to Tukey's test ($p < 0.05$). Asterisks denote statistical differences between the drought and control treatments within each isolated genotype according to Šídák's multiple comparisons test ($p < 0.05$).

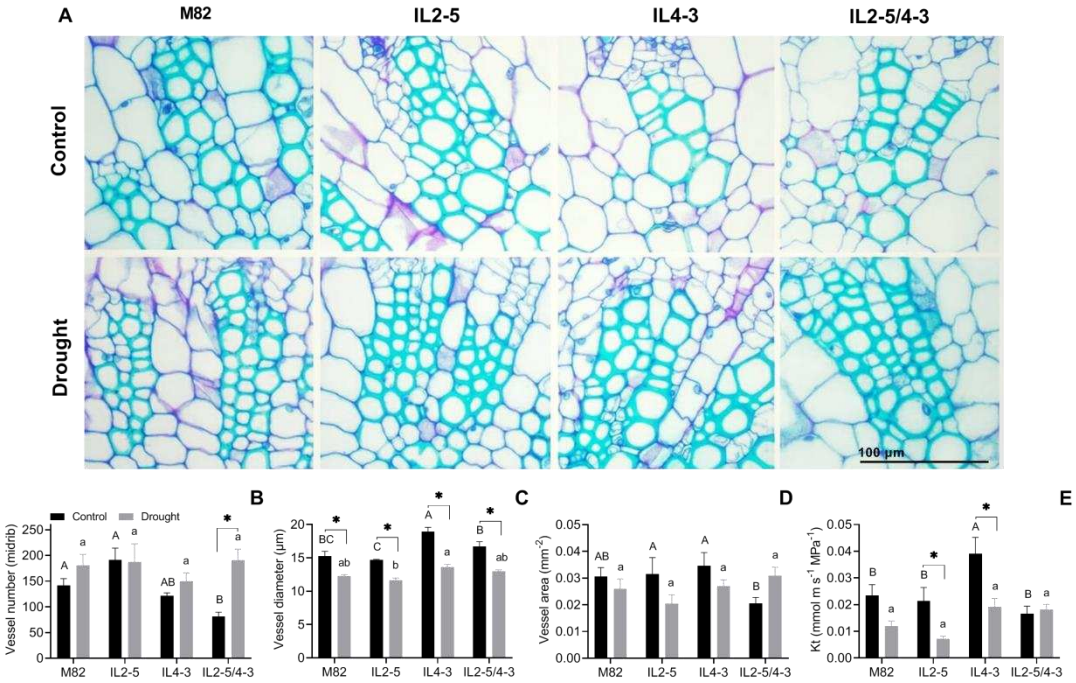


**Figure 6:** Increased thickness and succulence can affect the diameter and number of vessels in the xyllem. Xylem traits measured on the midrib. Values represent the mean and standard error of (n = 6). Analyzes were performed on apical leaflets of the seventh fully developed leaf under moderate drought conditions at 93 DAG. Uppercase letters compare control treatments and lowercase letters compare drought treatments according to Tukey's test ($p < 0.05$). Asterisks denote statistical differences between the drought and control treatments within each isolated genotype according to Šídák's multiple comparisons test ($p < 0.05$). Abbreviations: theoretical hydraulic conductance (Kt).

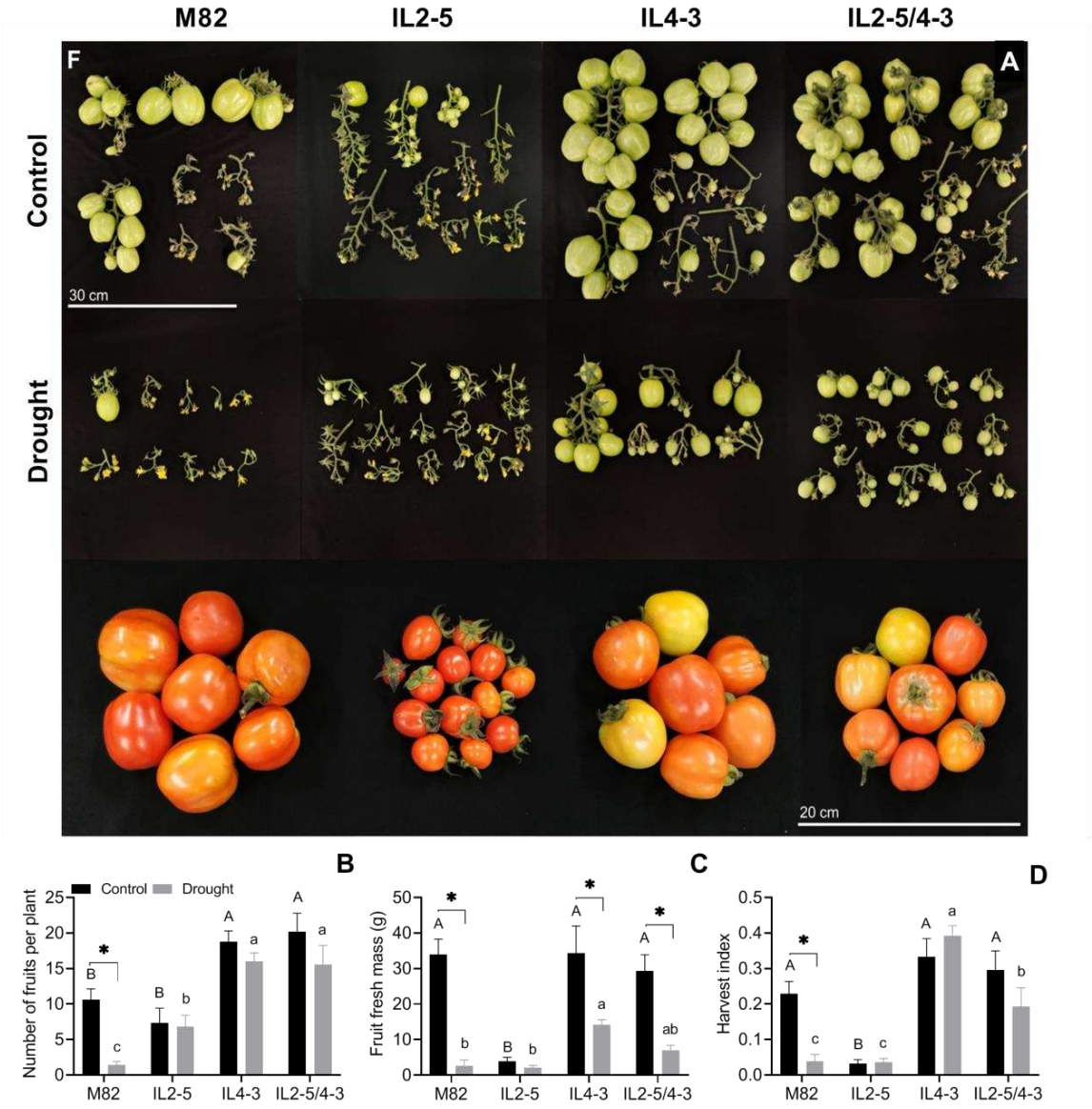


**Figure 7:** (**A**) Representative images of fruit production in plants of the control treatment (well-irrigated) and acclimatized to drought (60% of field capacity) for 40 days. (**B**, **C** and **D**) Effects of drought in fruit productivity measured at 93 days after germination (DAG). Values represent the means and standard error (n = 6). Uppercase letters compare control treatments and lowercase letters compare drought treatments according to Tukey's test ($p < 0.05$). Asterisks denote statistical differences between the drought and control treatments within each isolated genotype according to Šídák's multiple comparisons test ($p < 0.05$).

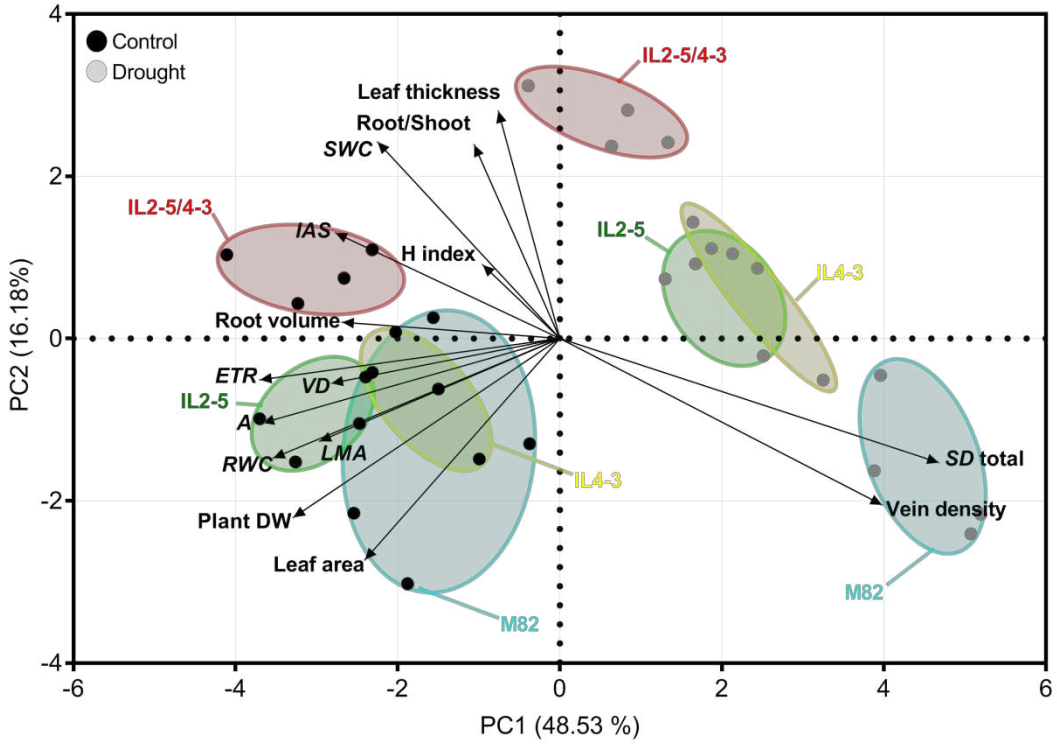


**Figure 8:** Principal Component Analysis (PCA) biplot of M82, IL2-5, IL4-3 and IL2-5/4-3 (n = 4). PC1 (48.53%) and PC2 (16.18%) explain most of the variance found in 15 traits related to physiology, leaf anatomy, and productivity of plants grown under control and drought conditions. The length and direction of the arrows indicate the contribution of traits on the two PCs shown. The angle between the vectors determines the degree of correlation between traits. Aligned vectors indicate a high positive correlation between traits. Abbreviations: saturated water content (SWC); leaf mass per area (LMA); intercellular air space (IAS); maximum electron transport rate (*ETR*); relative water content (RWC); harvest index (H index); net photosynthesis (*A*); diameter of midrib vessels (VD); stomatal density (SD).

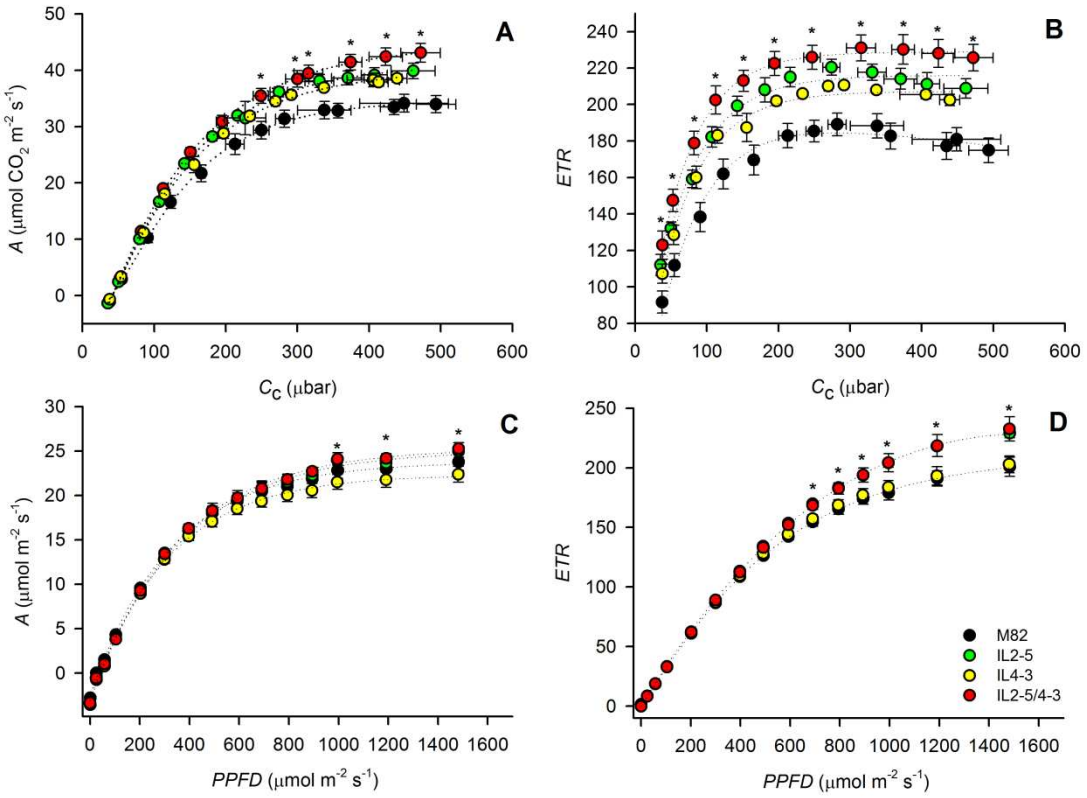


**Figure 9:** Photosynthesis and electron transport rate (*ETR*) response curves to chloroplast $CO_2$ concentrations ($A/C_c$) and photon flux density ($A$/PPFD). (**A**) $A/C_c$, (**B**) $ETR/C_c$, (**C**) $A$/PPFD and (**D**) $ETR$/PPFD. Data show the mean and standard error of the mean of five replicates. The curves were measured in fully expanded fifth leaf apical leaflets from base to apex. The evaluations were carried out at 46 DAG. Asterisks denote statistical differences between the genotype according to Tukey's test ($p < 0.05$)

SUPPLEMENTARY MATERIAL

# Supplementary Materials for

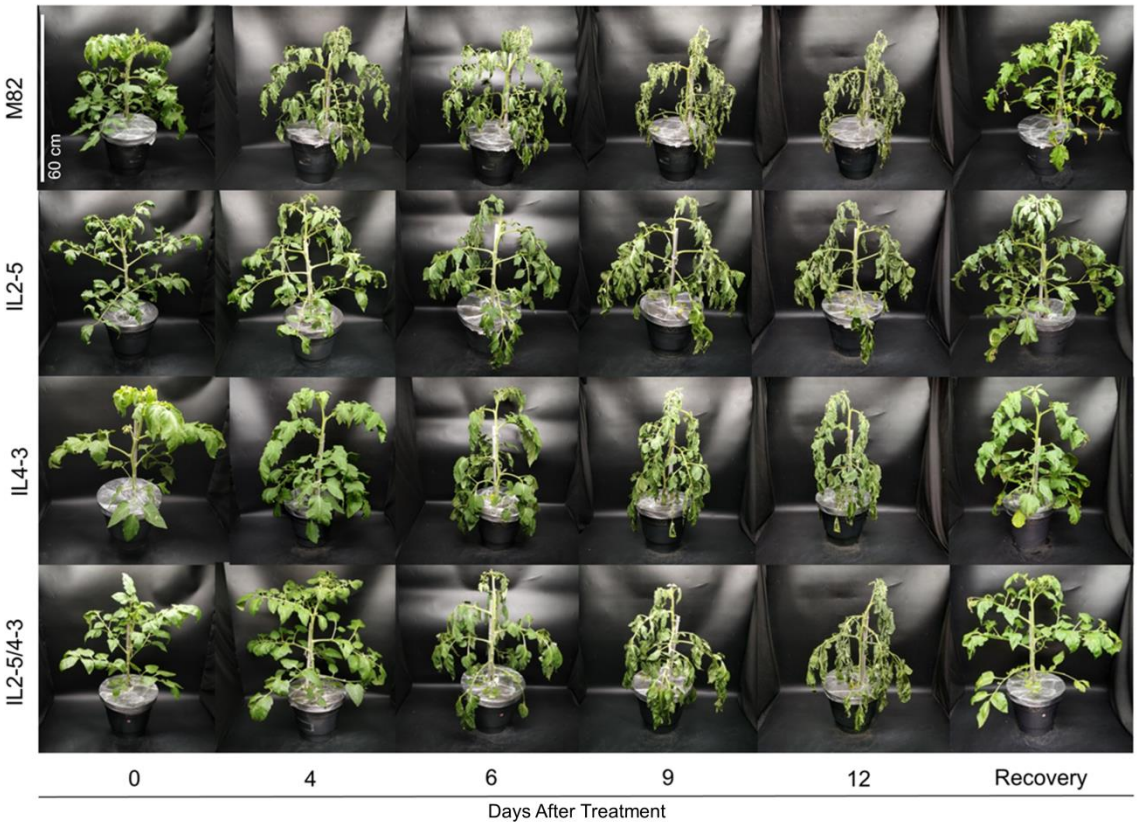


Figure S1: Visible drought symptoms observed in the ILs genotypes over 12 days of drought followed by rehydration. The lines IL2-5, IL4-3 and IL2-5/4-3 showed a significant delay in leaf wilting even after four days of irrigation suspension. The drought treatment was started 45 days after plant germination (DAG).

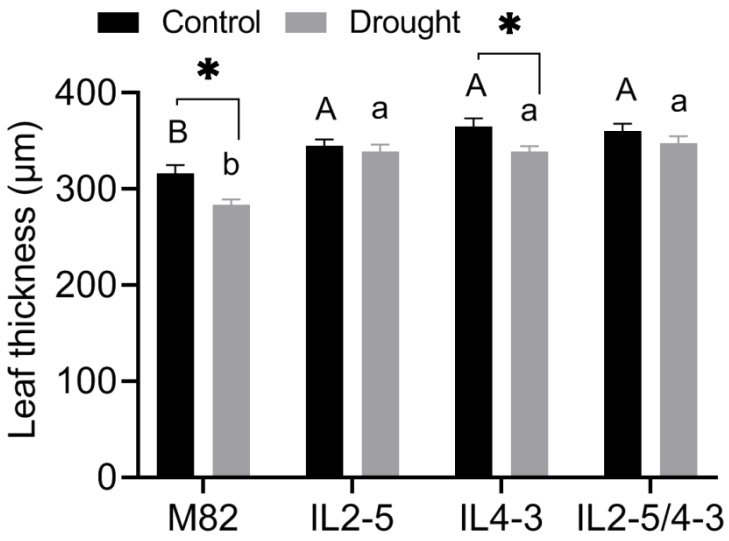


Figure S2: Leaf thickness estimated by Vile et al. (2005). Parameter was estimated using n = 30 leaflets taken from the fourth and fifth leaf of six replicates. Uppercase letters compare control treatments and lowercase letters compare drought treatments according to Tukey's test ($p < 0.05$). Asterisks denote statistical differences between the drought and control treatments within each isolated genotype according to Šídák's multiple comparisons test ($p < 0.05$).

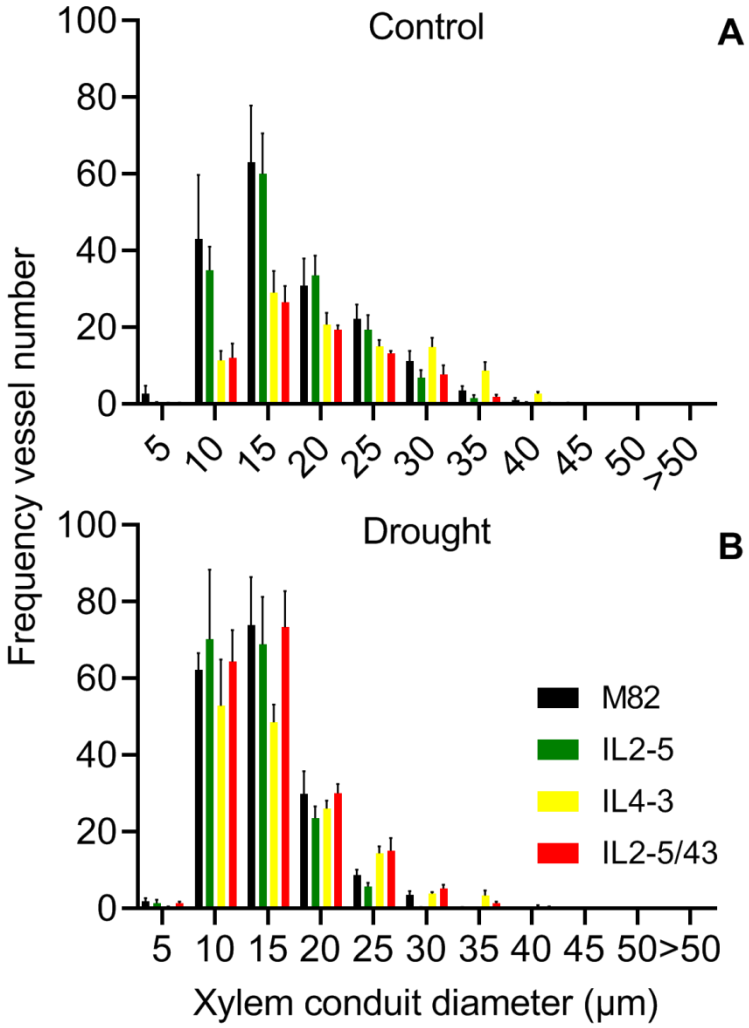


Figure S3: Frequency diameter class vessel in the M82, IL2-5, IL4-3 and IL2-5/4-3 in (**A**) control and (**B**) drought conditions.

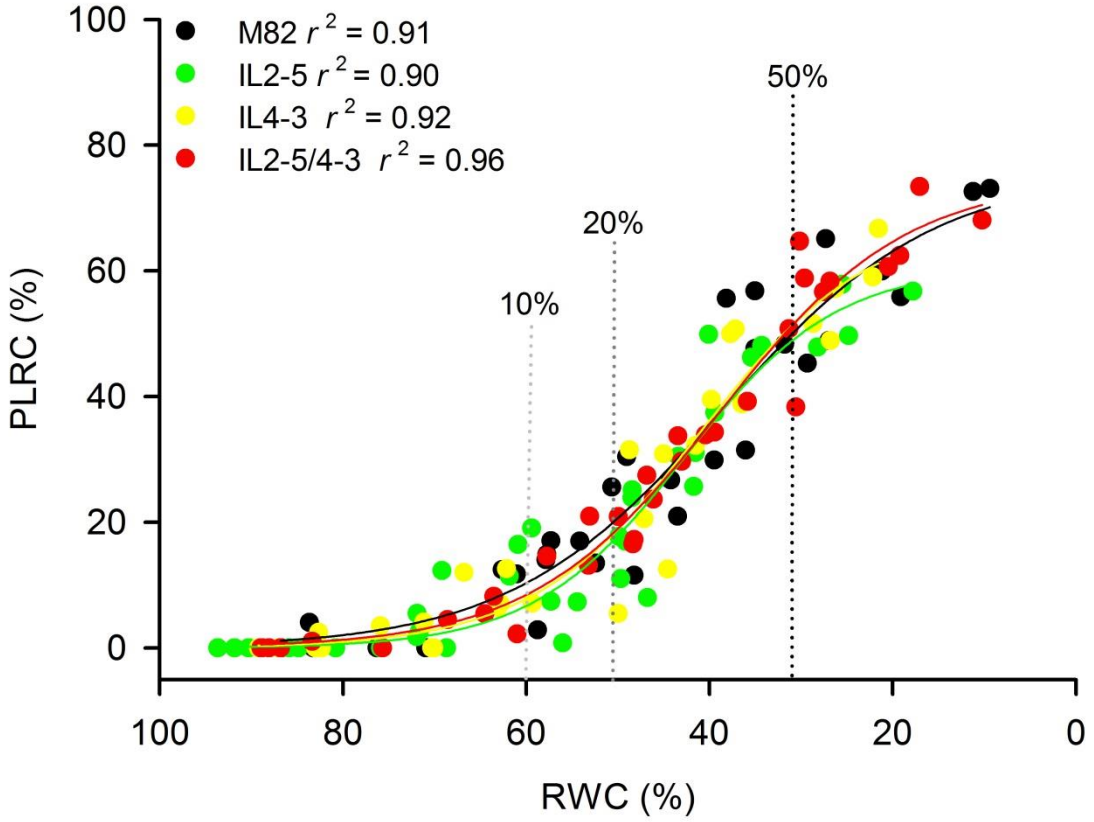


Figure S4: Percentage loss of rehydration capacity (PLRC) in response to the decrease in relative water content (RWC) for the four genotypes studied. The dashed lines indicate the RWC associated with losses of rehydration capacity of 10%, 20% and, 50% of cv. M82.

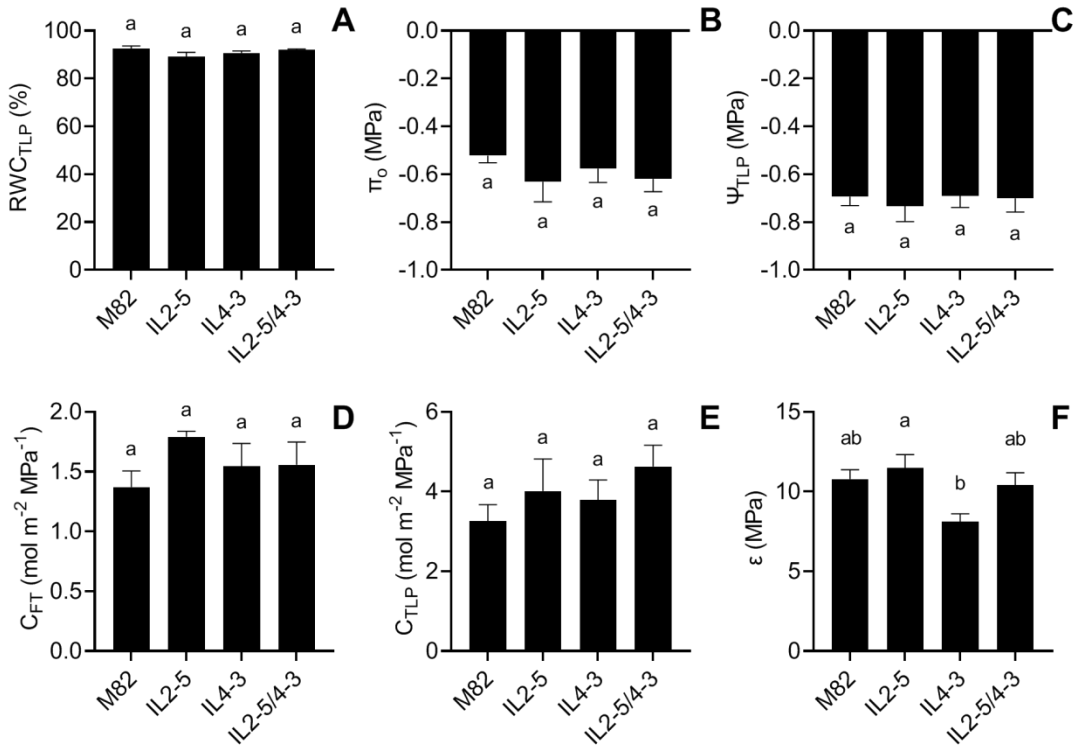


Figure S5: (**A**) Relative water content, (**B**) osmotic potential in full turgor, (**C**) water potential (interception method) at the turgor loss point, (**D**) capacitance in total turgor and (**E**) turgor loss point, (**F**) modulus of elasticity. The values observed in each genotype are represented by the mean and standard error of four replicates. Letters indicate significant differences between genotypes according to ANOVA and Tukey tests ($p < 0.05$).

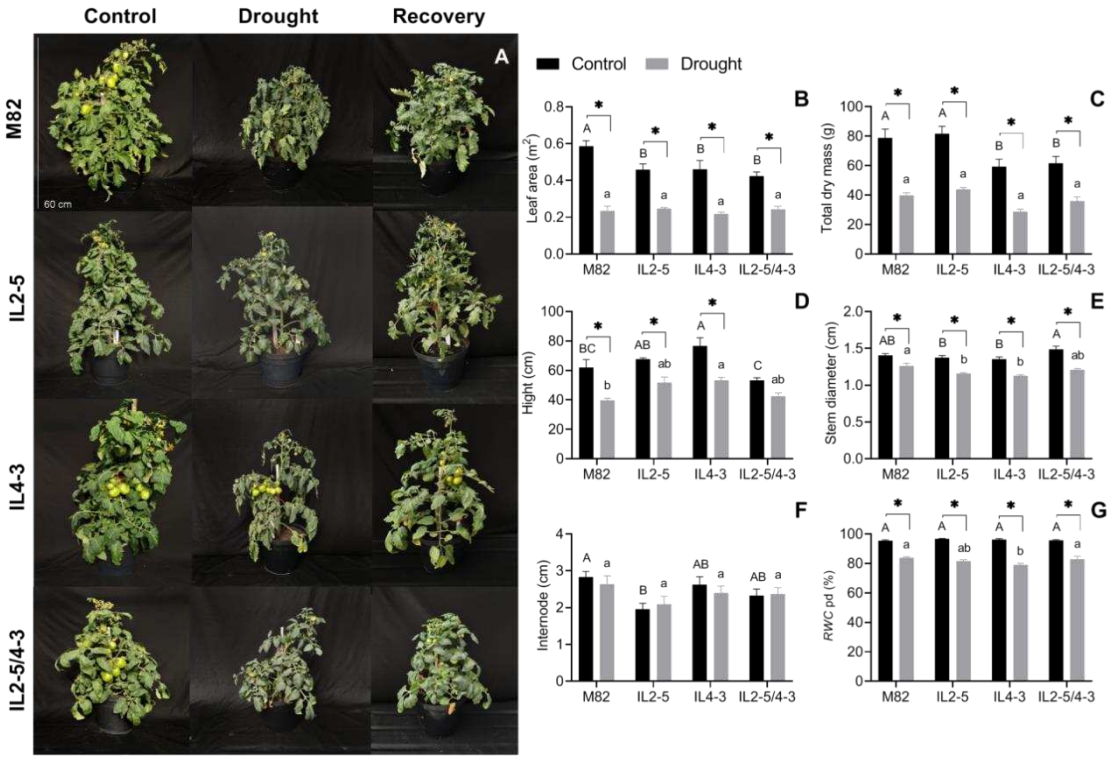


Figure S6: (**A**) Figure shows the plants of the control treatment (well-irrigated), acclimatized to drought (60% of field capacity) for 40 days (drought) and plants acclimatized to drought after rehydration (recovery). (**B**, **C**, **D**, **E** and **F**) Growth parameters of tomato plants M82, IL 2-5, IL 4-3, and IL 2-5/4-3 were measured at 93 days after germination (DAG). (**G**) RWC pd performed at 76 DAG on apical leaflets of the sixth fully expanded leaf from the apex to the base of the plant. Values represent the means and standard error (n = 6). Uppercase letters compare control treatments and lowercase letters compare drought treatments according to Tukey's test ($p < 0.05$). Asterisks denote statistical differences between the drought and control treatments within each isolated genotype according to Šídák's multiple comparisons test ($p < 0.05$).

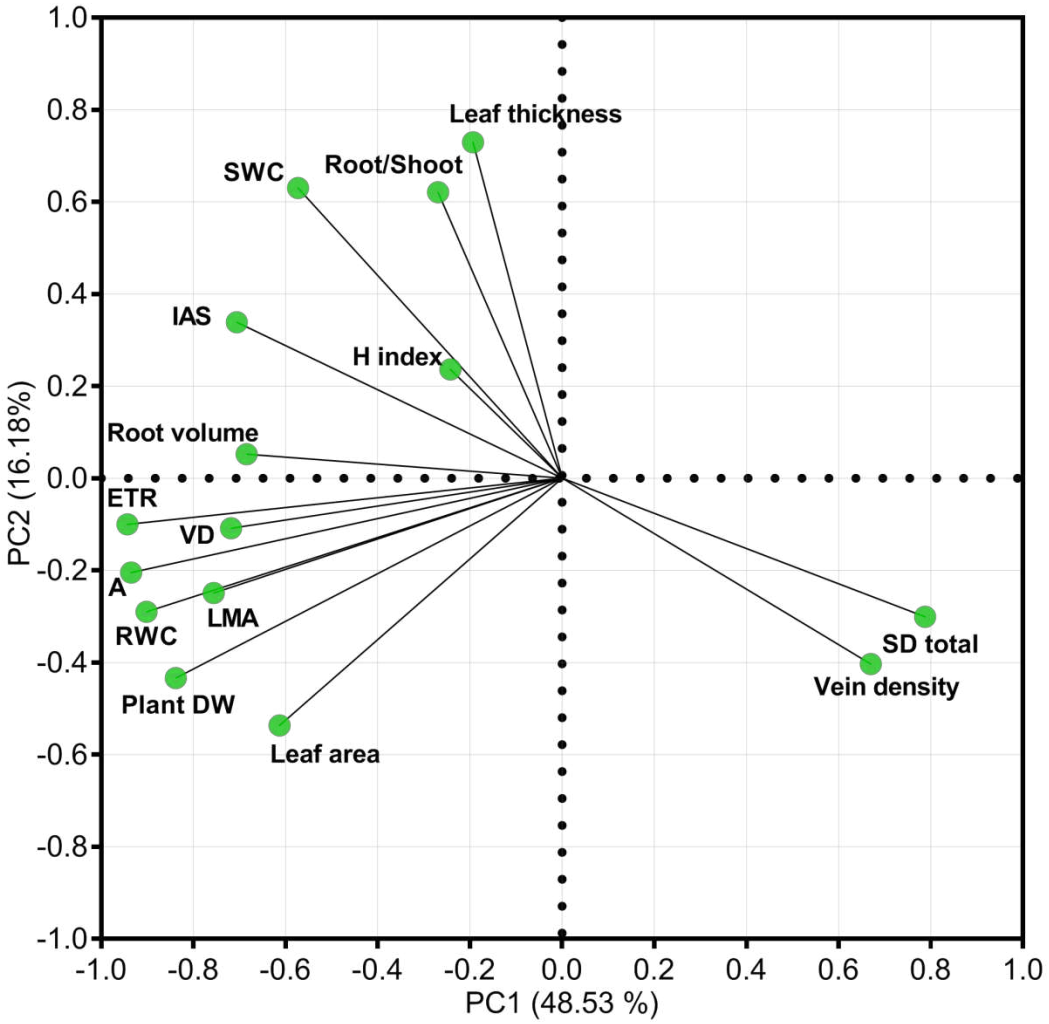


Fig S7: Correlation between the evaluated traits and the first two principal components PC1 and PC2. Abbreviations: saturated water content (SWC); leaf mass per area (LMA); intercellular air space (IAS); maximum electron transport rate (*ETR*); relative water content (RWC); harvest index (H index); net photosynthesis (*A*); diameter of midrib vessels (VD); stomatal density (SD).

Table S1: Principal components selected based on Eigenvalues > 1

| PC summary | Eigenvalue | Proportion of variance | Cumulative proportion of variance |
|---|---|---|---|
| PC1 | 7.28 | 48.53% | 48.53% |
| PC2 | 2.43 | 16.18% | 64.71% |
| PC3 | 1.67 | 11.11% | 75.82% |
| PC4 | 1.08 | 7.23% | 83.05% |

Table S2: Correlation estimate between the four PCAs and the evaluated traits.

| Loadings | | | | |
|---|---|---|---|---|
| Traits | PC1 | PC2 | PC3 | PC4 |
| *A* | -0.94 | -0.21 | 0.06 | -0.03 |
| *ETR* | -0.94 | -0.10 | -0.02 | 0.02 |
| Leaf thickness | -0.19 | 0.73 | -0.16 | 0.35 |
| SWC | -0.57 | 0.63 | -0.09 | -0.35 |
| *IAS* | -0.71 | 0.34 | -0.20 | -0.08 |
| Vein density | 0.67 | -0.40 | 0.38 | -0.08 |
| $S_d$ total | 0.79 | -0.30 | 0.32 | 0.07 |
| Vessel diameter | -0.72 | -0.11 | 0.30 | -0.44 |
| LMA | -0.76 | -0.25 | -0.42 | -0.07 |
| RWC | -0.90 | -0.29 | 0.11 | -0.16 |
| Leaf área | -0.61 | -0.54 | 0.16 | 0.29 |
| Root/shoot | -0.27 | 0.62 | 0.54 | 0.33 |
| Root volume | -0.68 | 0.05 | 0.46 | 0.43 |
| Plant DW | -0.84 | -0.43 | -0.05 | 0.27 |
| Harvest index | -0.24 | 0.24 | 0.73 | -0.37 |

Table S3: Contribution of traits on the fourth PCA. Values were obtained from a matrix of 15 traits x 32 individuals. The traits with the highest correlation on each PCA axis are highlighted in bold.

| Traits contribuition | | | | |
|---|---|---|---|---|
| Traits | PC1 | PC2 | PC3 | PC4 |
| A | 12.02 | 1.73 | 0.22 | 0.10 |
| ETR | 12.23 | 0.42 | 0.03 | 0.06 |
| Leaf thickness | 0.51 | 21.90 | 1.54 | 11.26 |
| SWC | 4.51 | 16.34 | 0.47 | 11.33 |
| IAS | 6.85 | 4.72 | 2.41 | 0.62 |
| Vein density | 6.16 | 6.71 | 8.65 | 0.63 |
| $S_d$ total | 8.51 | 3.73 | 6.25 | 0.40 |
| Vessel diameter | 7.09 | 0.49 | 5.48 | 17.99 |
| LMA | 7.86 | 2.56 | 10.76 | 0.40 |
| RWC | 11.18 | 3.47 | 0.71 | 2.31 |
| Leaf área | 5.17 | 11.88 | 1.60 | 7.82 |
| Root/shoot | 1.00 | 15.87 | 17.18 | 10.10 |
| Root volume | 6.44 | 0.11 | 12.97 | 17.38 |
| Plant DW | 9.66 | 7.76 | 0.13 | 6.86 |
| Harvest index | 0.81 | 2.29 | 31.61 | 12.76 |

Table S4: Mean values for photosynthetic parameters of M82, IL2-5, IL4-3 and IL2-5/4-3 calculated from the light curve. Abbreviations: maximum photosynthetic rate ($A_{max}$) and photosynthetic rate in saturating light ($A_{sat}$); luminous compensation point (LCP); luminous saturation point (LSP). Significant differences according to ANOVA are shown in *p*-values in bold.

| Parameters | M82 | IL 2-5 | IL 4-3 | IL 2-5/4-3 | *P* |
|---|---|---|---|---|---|
| $A_{max}$ (µmol $CO_2$ $m^{-2}$ $s^{-1}$) | 28.6 ± 1 | 32.1 ± 0.7 | 27.7 ± 1.3 | 32.3 ± 2.2 | 0.05 |
| $A_{sat}$ (µmol $CO_2$ $m^{-2}$ $s^{-1}$) | 23.1 ± 0.9 | 24.2 ± 0.7 | 21.8 ± 0.8 | 24.5 ± 0.6 | 0.13 |
| *LCP* | 33.7 ± 3 | 43.3 ± 3.7 | 41.1 ± 4.5 | 40.4 ± 2.7 | 0.08 |
| *LSP* | 610 ± 20 | 681 ± 35 | 602 ± 21 | 658 ± 49 | 0.28 |

CHAPTER II

Preprint: https://doi.org/10.1101/2021.12.16.473023

**Auxin-driven ecophysiological diversification of leaves in domesticated tomato**

Juliene d. R. Moreira[1]; Bruno L. Rosa[1]; Bruno S. Lira[2]; Joni E. Lima[3]; Ludmila N. Souza[1]; Wagner C. Otoni[1]; Antonio Figueira[4]; Luciano Freschi[2]; Tetsu Sakamoto[5]; Lázaro E. P. Peres[6]; Magdalena Rossi[2]; Agustin Zsögön[1]

[1]*Departamento de Biologia Vegetal, Universidade Federal de Viçosa, 36570-900, Viçosa, MG, Brazil*

[2]*Departamento de Botânica, Instituto de Biociências, Universidade de São Paulo, 05508-090, São Paulo, SP, Brazil*

[3]*Universidade Federal de Minas Gerais*

[4]*CENA, USP*

*5Universidade Federal do Rio Grande do Norte*

[6]*Laboratory of Hormonal Control of Plant Development. Departamento de Ciências Biológicas (LCB), Escola Superior de Agricultura "Luiz de Queiroz", Universidade de São Paulo, CP 09, 13418-900, Piracicaba, SP, Brazil*

**Corresponding author**

Agustin Zsögön
Universidade Federal de Viçosa, Brazil
Phone: +55 31 3899 2592
Fax: +55 31 3899 4139
Email: agustin.zsogon@ufv.br

**One sentence summary:** distribution of tomato heterobaric and homobaric leaves is controlled by variation in an auxin-related transcription factor

SUMMARY

The study of crop diversification has focussed mainly on the genetic changes underlying traits favoured by humans. However, the passage from natural habitats to agronomic settings probably operated changes beyond those comprising the classical domestication syndrome. A deeper understanding of these traits and their genetic signature would be valuable to inform conventional crop breeding and *de novo* domestication of crop wild relatives. Here, we show that domesticated tomatoes diversified into heterobaric and homobaric leaf types. Homobaric leaves lack bundle sheath extensions (BSEs), which causes a reduction in leaf vein density, leaf hydraulic conductance and photosynthetic assimilation rate. BSEs development is controlled by a single, non-synonymous nucleotide change in the *OBSCURAVENOSA* (*OBV*) gene, which exists as a rare balanced polymorphism in the natural range of wild tomatoes but has increased in frequency in domesticated tomatoes. The mutation disrupts a C2H2 zinc finger motif in the OBV protein, resulting in the absence of BSEs in leaves. We show that this and other pleiotropic effects, including changes in leaf insertion angle, leaf margin serration, minor vein density and fruit shape, are controlled by OBV via changes in auxin signalling. Notably, loss of function of the transcriptional regulator AUXIN RESPONSE FACTOR (ARF4) also results in defective BSE development. Our findings reveal a novel genetic module controlling leaf development and have ecophysiological implications for the transition from wild to domesticated crop species.

Crop domestication was driven by artificial selection to create a loose suite of traits known as the 'domestication syndrome' (*1*). Considerable effort has been devoted to unveiling the genetic basis of these traits. However, the passage from natural ecosystems to increasingly sophisticated, human-managed ones created new drivers for crop evolution that may have had impact beyond the domestication syndrome (*2*). These drivers include geographic expansion beyond the crops' centre of origin, natural selection under cultivation in a highly modulated environment, and indirect selection due to constraints caused by developmental trait correlations and physiological trade-offs (*3*). The extent and breadth of the genetic signature created by these processes in crops is not yet known. Identifying these variants and characterizing their consequences to plant development and function would lead to a more integrated understanding of crop ecology and provide valuable support to crop breeding and to the effort of creating new crops with *de novo* domestication pipelines (*4*, *5*).

Leaf functional traits are key for resource acquisition and thus strongly constrained by developmental co-variation (*6*). For instance, high photosynthetic capacity requires high transpiration capacity, which in turn depends on water transport capacity (*7*). This trait is a fundamental driver of leaf diversity, as it is linked with leaf shape, longevity and venation architecture (*8*). Notably, many angiosperm species have translucent leaf veins due to the presence of bundle sheath extensions (BSEs), compact columns of chlorophyll-less cells that link the veins to the leaf epidermis (*9*, *10*) (Fig. 1A). BSEs have considerable functional impact, as they can divide the leaf mesophyll into compartments, resulting in patchy stomatal opening and non-uniform photosynthesis (*11*). Leaves harbouring such compartments created by BSEs are called heterobaric, as opposed to homobaric ones, where the leaf lamina is topologically continuous. The effect of BSEs on leaf compartmentalization can be demonstrated by water infiltration in the lamina (Fig. S2). The distribution of these leaf functional types in natural ecosystems is highly skewed: in a climax forest, most species from the upper strata are heterobaric, whereas those dwelling in the understorey are homobaric (*12*). Likewise, some crops (*e.g.* soybean, sunflower) are heterobaric, whereas others (*e.g.* coffee, cocoa) are homobaric (*13*). What determines the distribution of these leaf functional types in natural and agricultural environments? Identifying the genetic basis of BSEs development would provide a stepping stone to answer this question.

We previously reported that the tomato monogenic recessive mutant *obscuravenosa* (*obv*) lacks BSEs in leaves, leading to reduced water transport capacity: both stomatal conductance ($g_s$) and hydraulic conductance ($K_{leaf}$) are lower in the mutant compared to wild-

type (WT) plants (*14*). However, the underlying genetic lesion in *obv* is unknown. Analysis of *S. pennellii* introgression lines (ILs) in tomato showed that *OBV* resides on a chromosome 5 interval defined by the bin d-5E (Fig. 1B and C), which contains 37 genes (Table S1) (*15*). A genome wide association study (GWAS) revealed a significant single nucleotide polymorphism (SNP) in Solyc05g054030 (Fig. 1D and fig. S1). The SNP is an A→G nucleotide change in the third exon of the gene coding sequence (CDS), resulting in a predicted histidine to arginine substitution on position 135 (H135R) of the protein (Fig. 1E), which is present in different tomato cultivars harbouring the *obv* mutation (Table S2). This genetic identity for *obv* was reported recently (Lu et al., 2021). Combining genomic and passport information we analysed the geographic distribution of the mutation in the natural range of tomato wild relatives, including the ancestral species *S. pimpinellifolium* and found a sympatric cluster of mutant accessions in the lowlands of Ecuador and northern Peru (Fig. 1F). Nucleotide diversity analysis on 360 wild and domesticated tomato accessions (available on solgenomics.net) showed that *OBV* resides within a tomato domestication sweep (Fig. 1G) (*16*). We also found that the mutation increases in frequency between accessions along the wild-domesticated continuum (Fig. 1H).

In order to confirm the genetic identity of *OBV*, we transformed the *obv* mutant in tomato cv. Micro-Tom (MT) (Figure 2A) with an overexpression (OE) vector for the CDS of Solyc05g054030. We observed correct BSE development leading to translucent veins in all *obv* plants harboring the construct (Fig. 2B, and fig. S2). To assess whether the defect in BSE development in *obv* is indeed caused by a single, non-synonymous nucleotide change we next constructed another OE vector with the *OBV* CDS but containing the A404G SNP and transformed it into the *obv* mutant. All transgenics expressed the transgene, but none reverted the dark-vein mutant phenotype lacking BSEs (Fig. 2C and fig. S3). We further confirmed that the *obv* mutant could be phenocopied by knocking down Solyc05g054030 expression with an RNA interference (RNAi) construct (Fig. 2D). We further crossed two cultivars lacking BSEs (M82 and VFN8) with either the *obv* mutant in the MT background or the *obv* mutant harbouring the *OBV*-OE transgene. Hybrid plants derived from the former cross lacked BSEs leading to dark veins, but those derived from the latter showed phenotypic reversion, displaying transduced veins and BSEs (Fig. 2E and fig. S4). These results demonstrated that Solyc05g054030 is *OBV*, the gene responsible for BSE development in tomato leaves, and that a single amino acid change causes de *obv* mutation, which is responsible for the switch from heterobaric to homobaric leaves in tomato (*14*).

To better understand the nature of the genetic change underlying the *obv* mutation, we conducted *in silico* analyses of the gene and protein sequences of *OBV* (Fig. 2F). The complete sequence of the *OBV* gene encodes a 381 amino acid protein containing three $Cys_2$-$Hys_2$ (C2H2) Zn finger domains, which are associated with DNA-binding capability (*17*), an ethylene-responsive element binding factor-associated amphiphilic repression (EAR) domain, defined by the LxLxL motif and associated with transcriptional repression (*18*), and a carboxy-terminal coiled coil domain, which may function as molecular spacer or macromolecular scaffold (*19*). Gene ontology (GO) terms associated with this protein are nucleic acid binding (GO:0003676) and metal ion binding (GO:0046872) (Table S2). Using 324 protein sequences of the *OBV* orthologous group from 39 plant species (Table S3) we pinpointed the H135R amino acid change of the *obv* mutant to a highly conserved motif of the second Zn finger domain (Fig. 2G). Protein modelling showed that the C2H2 motif is contained within a ββα structure, forming a functional unit internally stabilized by chelation of a single zinc ion (Fig. 2F). This suggests that the *obv* mutation leads to complete loss of protein function via disruption of its tertiary structure. Targeted phylogenetic analysis in relevant crop and model species revealed an ancient evolutionary origin of the *OBV* gene with great expansion due to duplication events (Fig. 2G and fig. S6). Protein sequence alignment of the Zn finger motif that contains the *obv* mutation in tomato showed that even the most phylogenetically distant species showed high sequence identity across the domain, suggesting a conserved protein function (Fig. 2G). The closest *Arabidopsis* orthologs (*INDETERMINATE DOMAIN 14*, *15* and *16*), encode proteins involved in shoot gravitropism and regulation of auxin biosynthesis and transport (Table S4 and fig. S6) (*20*).

We next characterized the expression profile of *OBV*, the gene is highly expressed in meristems leaf primordia, expanding and mature leaves and flowers (fig. S7A and B). Changing *OBV* expression levels led to changes on leaf insertion angle, leaf margin serration and fruit shape (fig. S7C-E), which hinted at a potential role for auxin as a mediator of BSE development. Auxins, like other plant hormones, exert their effect through alterations in metabolism, transport, and sensitivity (*21*). We found no differences either in auxin content fig. S9A) nor in polar auxin transport (fig. S9B) between wild type, *obv* mutant and *OBV*-OE lines in leaf primordia. However, GUS expression driven by the *DR5* auxin-induced promoter was increased in the *obv* mutant (Fig. 3A) but decreased in the $OBV^{OE}$ lines (fig. S10). Exogenous auxin also led to higher inhibition of hypocotyl elongation and stimulation of *in vitro* rhizogenesis from explants in *obv*, compared to WT or $OBV^{OE}$ lines (fig. S11). Taken together, the results suggested that *OBV* could be responsible for alterations in auxin

signalling. Thus, we next assessed the expression profiles of *AUXIN RESPONSE FACTOR* (*ARFs*) and *AUXIN/INDOLE-3-ACETIC ACID* (*Aux/IAAs*) transcriptional regulators, which are components of auxin signal transduction (*22*). We found consistent upregulation of some *ARFs* (*ARF3*, *9B*, *10B*, *19* and *AUX/IAA4* and *14*) and downregulation of some *Aux/IAAs* (*Aux/IAA1A*, *1B*, *2*, *3*, *11*, *13*, *26* and *35*) in $OBV^{OE}$ lines compared to WT (Fig. 3B). Regarding *obv* the strongest differences were found for *ARF4* and *Aux/IAA15*, both of which were strongly upregulated in the mutant compared to WT (Fig. 3B).

*ARF4* was the auxin responsive factor expression in *obv* compared to WT genotype; thus, we focussed on the potential role of *ARF4* in BSE development using a CRISPR/Cas9-generated knockout mutant (*arf4*-CR) and a transcriptionally silenced line harbouring an *ARF4*-antisense (*ARF4*-as) transgene (*23*). We confirmed the lack of BSEs and the associated dark vein phenotype in leaves of both *arf4-CR* and *ARF4*-as plants (Fig. 3C and fig S11). Further, *OBV* expression was increased in *arf4* and *ARF4-as* leaves (Fig. 3D) and *ARF4* expression was increased in the *obv* mutant but not in the $OBV^{OE}$ lines (Fig. 3 E). Taken together, these results suggest that *OBV* controls BSE development via interaction with the auxin signalling machinery.

Lastly, we analysed the functional consequences of allelic variation in *OBV*. We first determined that leaf vein density (vein length per leaf area, VLA) was reduced in *obv* plants (Fig 4A and B). Vein architecture plays a key role in carbon assimilation rate and water distribution within the leaf (*24*). $K_{leaf}$ is a measure of how efficiently water is transported through the leaf: We found that the *obv* mutant had reduced $K_{leaf}$, which was restored to wild-type levels in $OBV^{OE}$ transgenic lines (Fig. 4C and D). A regression analysis between VLA and $K_{leaf}$ showed a strong positive correlation ($r$=0.811, $p$<0.001) between the variables, with a coefficient of determination ($R^2$) of 0.657 (Fig. 4E). This suggests that variation in VLA caused by *OBV* is a major determinant of variation in $K_{leaf}$. Interestingly, an auxin biosynthesis mutant with reduced VLA showed reduced $K_{leaf}$ and photosynthetic rate in pea (*Pisum sativum*) (*25*). Net assimilation of $CO_2$ ($A_n$)-chloroplastic $CO_2$ concentration curves ($C_c$) (Fig. 4E) revealed no difference in maximum Rubisco carboxylation rate ($V_{cmax}$) (Table S6) between genotypes, however, the maximum rate of light-saturated net $CO_2$ assimilation ($A_{max}$) was lower in the *obv* mutant (Fig. 4F and Table S7). This suggests that the presence of BSEs overrides diffusive limitations to photosynthesis through their effect on the water transport capacity of the plants (*26*, *27*).

Leaf BSEs fulfils significant roles in leaf function with large ecophysiological impact. Firstly, by connecting the vascular bundles to the leaf epidermis, BSEs minimize the extra-

xylematic path length and favor a greater hydraulic integration in the leaf lamina. The stomata of heterobaric leaves may therefore operate closer to the point of embolism, while responding faster to sudden changes in xylem water potential (*28*). This could at least partially explain the distribution of heterobaric wild tomato accessions in more arid habitats with erratic rainfall patterns (*29*). Secondly, photosynthetic assimilation rates are higher in heterobaric leaves due to the optimization of light transmission within the leaf lamina. BSEs can function as 'transparent windows' that enrich neighbouring mesophyll cells, or, in the case of $C_4$ plants, the bundle sheath itself, with high levels of photosynthetically active radiation (400-700 nm) (*30*, *31*). Lastly, the presence of BSEs increases the plasticity of minor vein density in response to growth light intensity, adjusting water supply and photosynthetic rate to specific environmental conditions (*32*). The sum of these effects on leaf function suggests that the presence of BSEs has adaptive value. This raises the question of what the main driver for the loss of BSEs in domesticated tomato cultivars could be. One possible explanation it that the heterobaric/homobaric ecological distribution logic was broken down by the passage to an agricultural setting and, in this case, the homobaric phenotype is functionally more advantageous due a trade-off with the structural and functional costs of BSEs (*33*). Furthermore, since the *obv* mutation increases sensitivity to auxin, we cannot exclude the selection of a favorable pleiotropic effect of this hormone on plant development and productivity (*34*).

In this report we have identified an allelic variant in *OBV*, a gene controlling the development of BSEs, which impacts leaf anatomy and function in tomato and other important crop species. We show that the OBV protein is highly conserved among angiosperms and that it is a key determinant of leaf functional type. BSE development is strongly linked to auxin signalling, involving *ARF4*, whose loss of function also impairs BSE formation. Our findings represent an entry point to unravel leaf functional design through a gene-focused approach and provide a molecular anchor for the analysis of phenotypic co-variation in leaf anatomical and physiological traits. They also suggest that leaf functional type results from a trade-off probably conditioned by environmental factors. The conservation of *OBV* in angiosperms could be leveraged to explore its roles in other plant major crop species and potentially tailor different leaf types to specific agronomic settings. For instance, BSEs were recently shown to provide a pathway for P uptake following foliar fertilization in spring barley (*Hordeum vulgare*) (*35*). Thus, our discovery of a simple genetic switch between leaf functional types could have important ecological implications and agricultural applications.

FIGURES

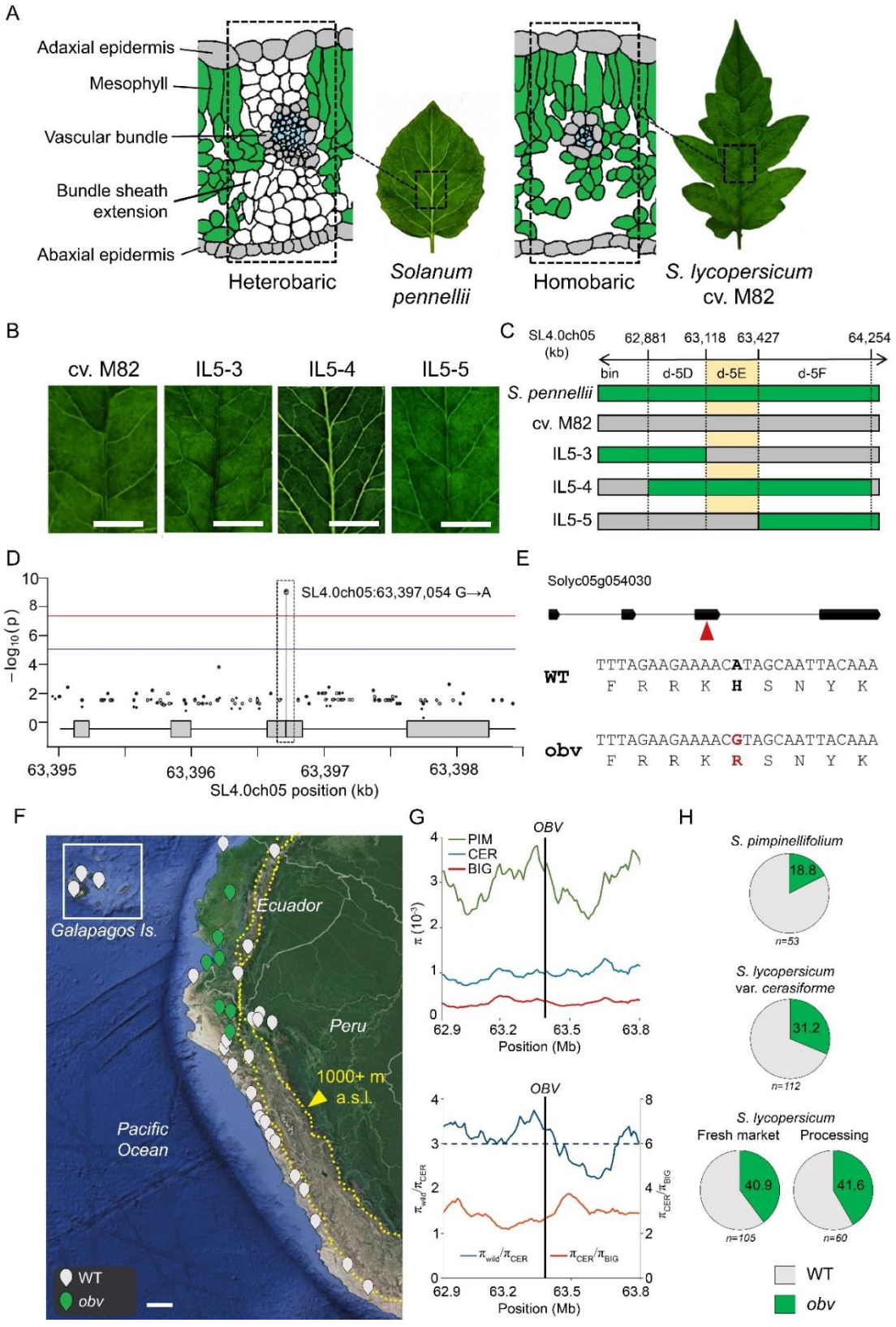
A
Adaxial epidermis
Mesophyll
Vascular bundle
Bundle sheath extension
Abaxial epidermis
Heterobaric
Solanum pennellii
Homobaric
S. lycopersicum cv. M82
B
cv. M82
IL5-3
IL5-4
IL5-5
C
SL4.0ch05 (kb)
62,881
63,118
63,427
64,254
bin
d-5D
d-5E
d-5F
S. pennellii
cv. M82
IL5-3
IL5-4
IL5-5
D
SL4.0ch05:63,397,054 G→A
−log10(p)
63,395
63,396
63,397
63,398
SL4.0ch05 position (kb)
E
Solyc05g054030
WT
TTTAGAAGAAAACATAGCAATTACAAA
F R R K H S N Y K
obv
TTTAGAAGAAAACGTAGCAATTACAAA
F R R K R S N Y K
F
Galapagos Is.
Ecuador
Peru
1000+ m a.s.l.
Pacific Ocean
WT
obv
G
PIM
CER
BIG
OBV
π (10⁻³)
Position (Mb)
H
S. pimpinellifolium
18.8
n=53
S. lycopersicum var. cerasiforme
31.2
n=112
S. lycopersicum
Fresh market
Processing
40.9
41.6
n=105
n=60
WT
obv

**Figure 1 – Mapping and identification of a candidate gene for the *obscuravenosa* (*obv*) mutation.** (**A**) Schematic cross-sectional comparison of heterobaric and homobaric leaves. In the former (*e.g.* the tomato wild relative *Solanum pennellii*) the bundle sheath extensions (BSEs) are visible as a translucent network of veins, whereas leaves of the latter (*e.g.* cultivars of tomato, *S. lycopersicum*, harbouring the *obv* mutation, such as cv. M82) the leaf lamina appears uniformly green. (**B**) Leaf phenotype of tomato cv. M82 and the *S. pennellii* introgression lines 5-3, 5-4 and 5-5. Scale bars, 1 cm. (**C**) Bin-mapping of the genomic region containing the *obv* mutation using ILs sequences. (**D**) Association plot of the GWAS for the *obv* phenotype: the x-axis represents the chromosome region where Solyc05g054030 is located, and the y-axis represents the negative $\log_{10}$ of *p*-values per SNP derived from the association analysis. The red horizontal line represents the Bonferroni-corrected genome-wide significance threshold ($p$=1.554$^{-08}$). The boxes represent the open reading frame of Solyc05g054030. The SNP (an A-to-G transition) located in the third exon of this gene is strongly associated with the *obv* phenotype. (**E**) Gene structure of Solyc05g054030 showing exons (boxes) and introns (lines) and the position of the SNP (red arrowhead) in the third exon and DNA and protein sequence of the region around the SNP, showing that it represents a non-synonymous mutation leading to the substitution of a histidine (H) in the wild-type (WT) for an arginine (R) residue in the *obv* mutant. (**F**) Geographic distribution of accessions of wild tomatoes on the Pacific coast of Peru, Ecuador and the Galapagos Islands (inset) harbouring either the WT or mutant *obv* allele. Scale bar, 100 km. (**G**) Nucleotide diversity ($\pi$) of the ancestral wild species *S. pimpinellifolium* (PIN), *S. lycopersicum* var. *cerasiforme* (CER) and big-fruit cultivars (BIG) of domesticated tomato. The horizontal lines indicates genome-wide top 5% cutoff ratio for domestication sweeps. (**H**) Frequency analysis showing the incidence of the *obv* mutation in four different categories of tomato accessions.

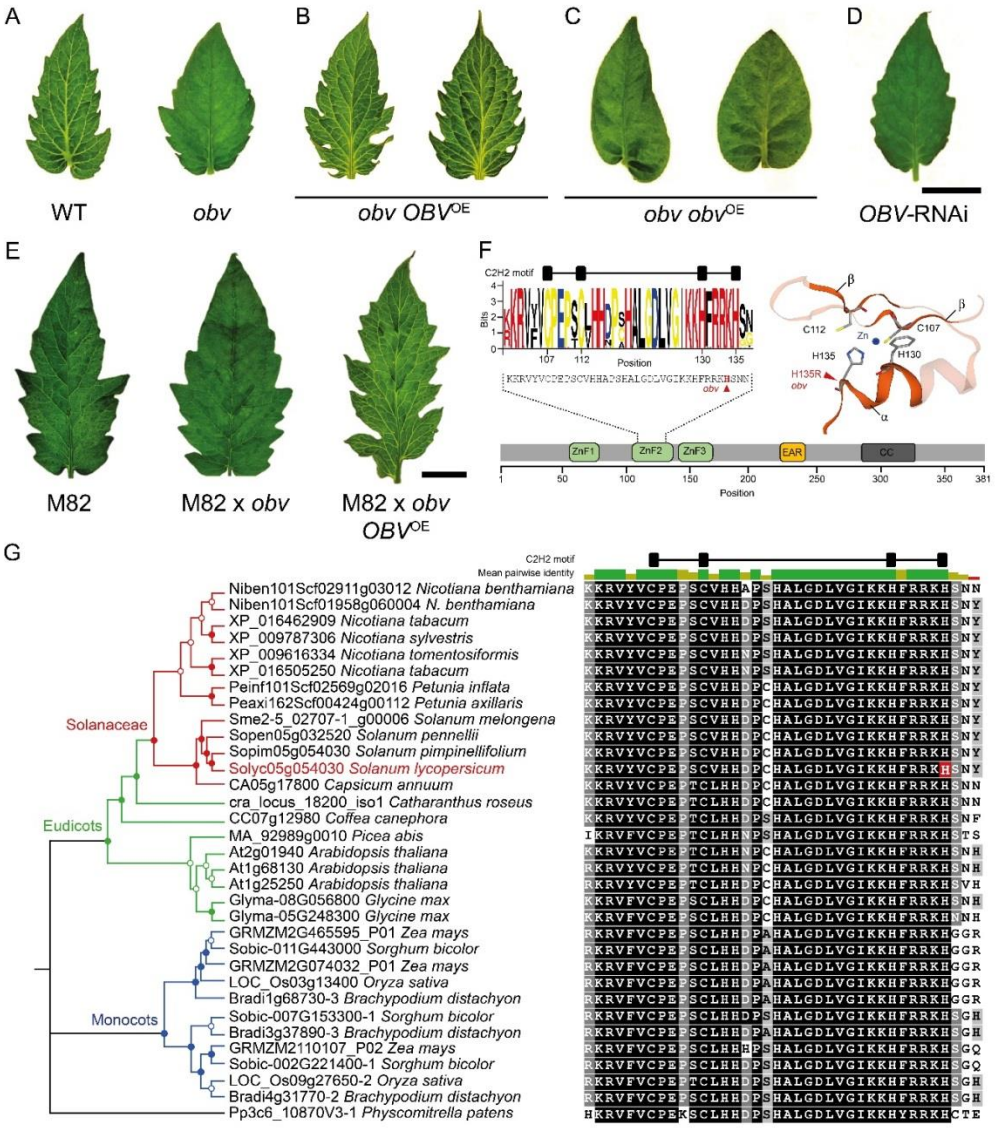


**Figure 2 – Complementation of the *obv* mutant and protein sequence analysis.** (**A**) Representative terminal leaflets of tomato cultivar Micro-Tom (MT) harbouring the wild-type (WT) *OBV* allele and the *obscuravenosa* (*obv*) mutant, (**B** and **C**) independent transgenic *obv* mutants overexpressing (OE) either (**B**) the WT *OBV* allele or (**C**) the mutant *obv* allele, and (**D**) an RNA interference knockdown *OBV* line in WT background. (**E**) Representative terminal leaflets of tomato cv. M82 (an *obv* mutant), an $F_1$ hybrid derived from the cross between M82 and MT-*obv* and an $F_1$ hybrid of M82 and transgenic MT-*obv* harbouring the *OBV* overexpression transgene. Scale bars, 1 cm. (**F**) Schematic representation of the *OBV* protein showing conserved domains: ZnF (zinc finger), EAR (ethylene-responsive element binding factor-associated amphiphilic repression) and CC (coiled coil). The sequence of the second ZnF motif (ZnF2) is described as logo plot of residue conservation, with consensus sequence in the bottom. The relative sizes of letters indicate their frequency in an orthologous group of 324 proteins from 39 plant species. The total height of the letters depicts the information content of the position in bits. Right, 3D model of ZnF2 showing the relative positional arrangement of the C2H2 residues and the Zn ion ligand. (**G**) Left, maximum likelihood protein sequence tree of the *OBV* gene in selected model and crop species. Symbols on nodes represent bootstrap support values: full circles >0.75, open circles <0.75. Right, partial protein sequence alignment focussed on the second ZnF and showing the histidine (H) residue affected by the *obv* mutation in tomato (red). Shading indicates similarity to consensus (according to Blosum62 score matrix with a threshold of 1): black 100%; dark grey 80-99%; light grey 60-79%; white <60%. The bar on the top indicates the mean pairwise identity over all pairs in the column: green 100%; brown 30-99%, red <30%.

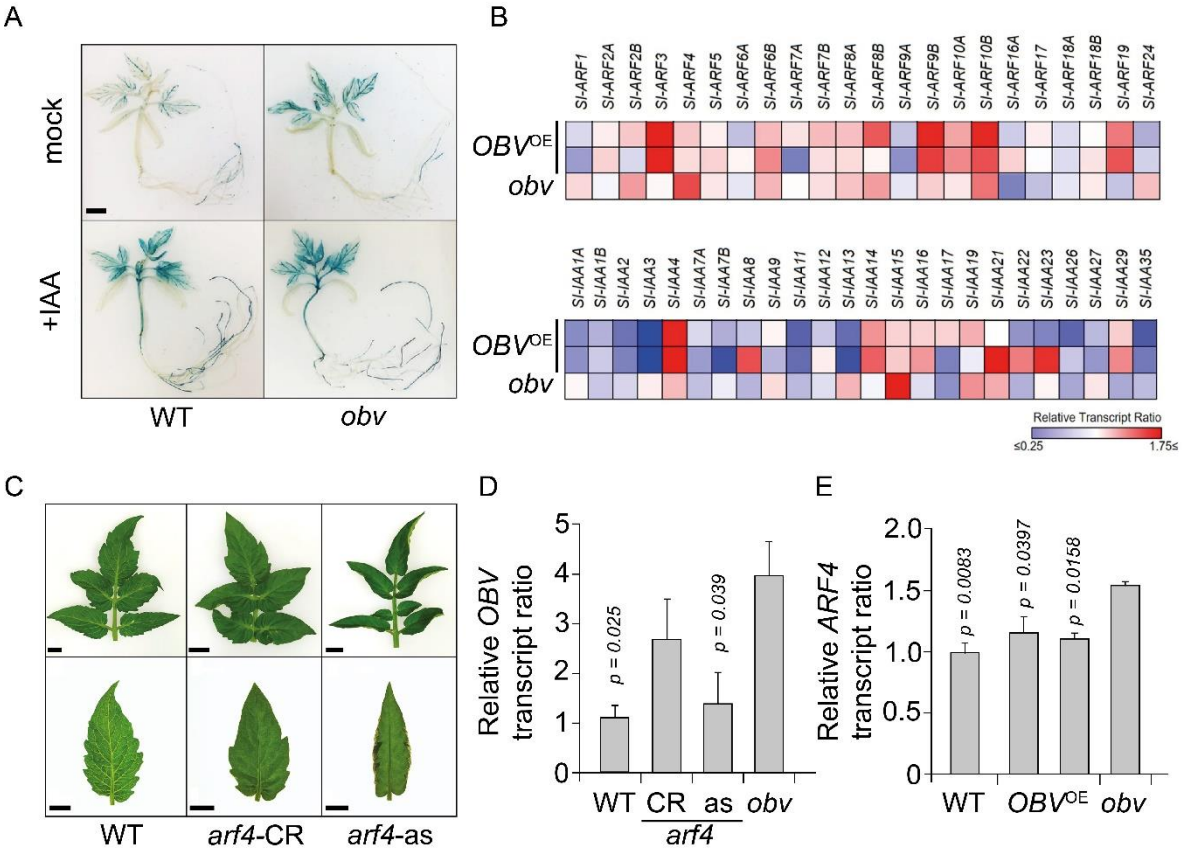


**Figure 3 – Interaction between *OBV* and auxin signalling in the control of leaf functional type.** (**A**) Histochemical GUS analysis in transgenic lines harbouring a homozygous *DR5*::*GUS* construct in either wild type (WT) Micro-Tom or *obv* mutant background. Seedlings were either pre-treated (+IAA) or not (mock) with 20 µM of indol-3-acetic acid. Scale bar = 1 cm. (**B**) Transcriptional profile of *AUXIN RESPONSE FACTOR* (*ARF*) and *AUXIN/INDOLE-3-ACETIC* (*Aux/IAA*) genes from leaf primordia. Heat map represents the transcript profiles in two *OBV* overexpression (OE) homozygous transgenic lines and the *obv* mutant. Values represent means of four biological replicates normalized against the corresponding WT sample. Statistically significant increases (red) or decreases (blue) in comparison with the MT are represented by colored squares ($p$ <0.05). (**C**) Representative leaves and terminal leaflets of MT, a CRISPR *ARF4* mutant (*arf4*-CR) and an antisense *ARF4* knockdown line (*arf4*-as). Scale bars = 1 cm. (**D**) Relative *OBV* mRNA levels in young leaves of MT, *arf4*-CR, *arf4*-as and *obv*. $p$-values show significant differences to the *obv* mutant. (**E**) Relative *ARF4* mRNA levels in young leaves of MT, homozygous transgenic lines overexpressing (OE) *OBV* and the *obv* mutant. $p$-values show significant differences to the *obv* mutant.

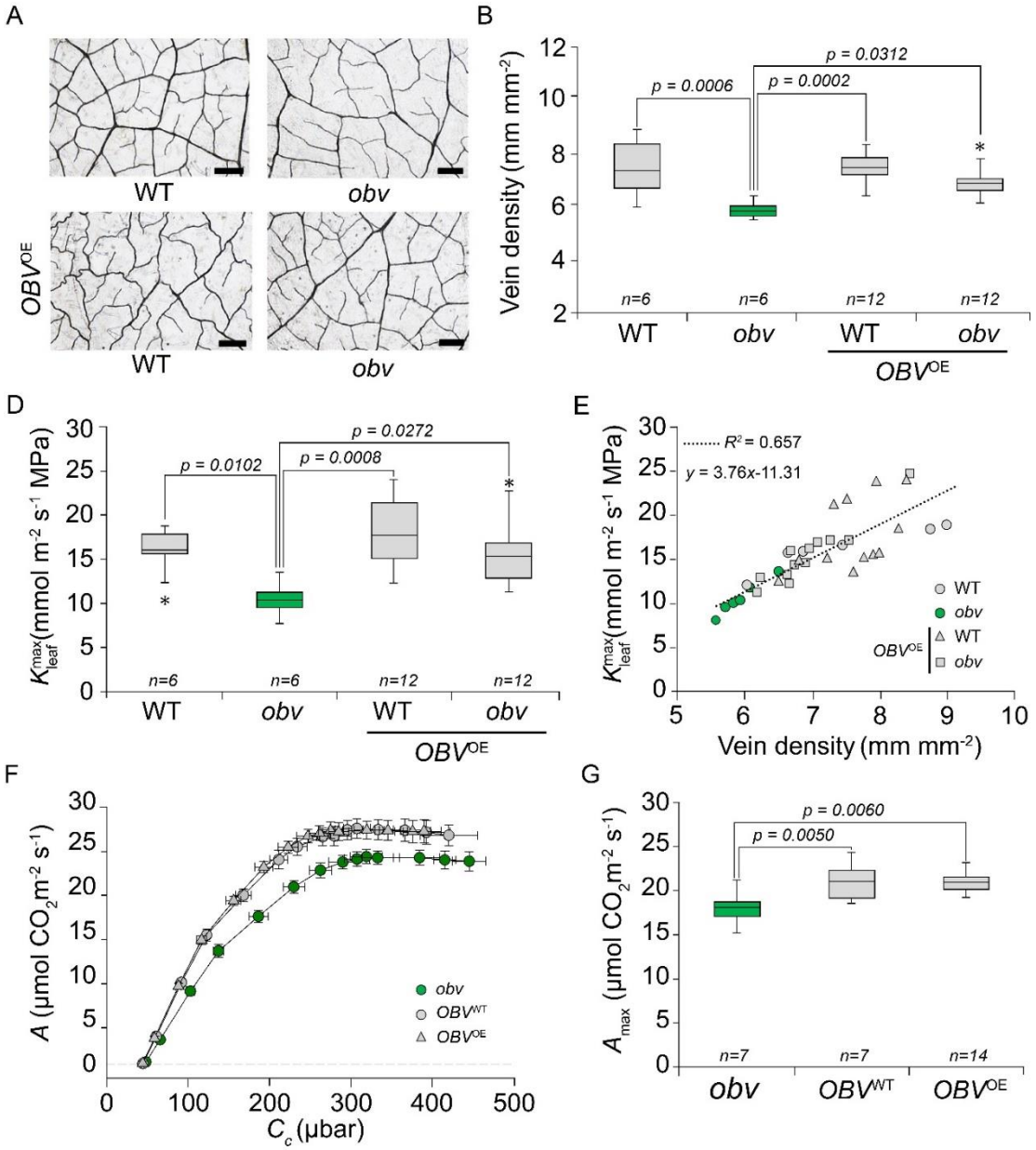


**Figure 4 - *OBV* controls vein development and leaf hydraulic conductance for hydrated leaves ($K_{leaf}^{max}$).** (**A**) Representative micrographs of cleared terminal leaflets of wild-type (WT) tomato cv. Micro-Tom (MT), the *obscuravenosa* (*obv*) mutant, and two independent *OBV* overexpression (OE) lines sections in either WT or *obv* background. Scale bars, 100 µm. (**B**) Leaf vein density in WT, *obv* and the transgenic lines. (**C**) values for tomato cv. M82 (*obv* mutant), a cv. M82 line harbouring the wild-type *OBV* allele introgressed by conventional breeding and a transgenic *OBV*-OE line; and (**D**) in WT, *obv* and the transgenic lines. (**E**) Regression analysis of $K_{leaf}^{max}$ and vein density for WT, *obv* and the transgenic lines. Each point corresponds to an individual measurement on a different plant. (**F**) Net photosynthetic assimilation ($A_n$) response curve to $CO_2$ concentration in the chloroplasts ($C_c$). (**G**) Maximum assimilation rate at ambient $CO_2$ and saturating irradiance derived from the curves in **F**. Boxes in box plots represent interquartile range (IQR), center line the mean, and the ends of the whisker are set at 1.5*IQR above and below the third and first quartiles, respectively. Asterisks show outliers. *p*-values for significant differences ($p$<0.05) are shown.

REFERENCES


1. K. Hammer, *Die Kulturpflanze*. **32**, 11–34 (1984).
2. R. Milla, C. P. Osborne, M. M. Turcotte, C. Violle, *Trends in Ecology and Evolution*. **30**, 463–9 (2015).
3. R. Milla, J. Morente-López, J. M. Alonso-Rodrigo, N. Martín-Robles, F. S. Chapin, *Proceedings of the Royal Society B*. **281**, 20141429–20141429 (2014).
4. K. Gasparini, J. dos R. Moreira, L. E. P. Peres, A. Zsögön, *Current Opinion in Plant Biology*. **60**, 102006 (2021).
5. A. Zsögön *et al.*, *Nature Biotechnology*. **36**, 1211–1216 (2018).
6. I. J. Wright *et al.*, *Nature*. **428**, 821–7 (2004).
7. T. J. Brodribb, T. S. Feild, G. J. Jordan, *Plant Physiology*. **144**, 1890–8 (2007).
8. L. Sack, N. M. Holbrook, *Annual Review of Plant Biology*. **57**, 361–381 (2006).
9. G. Haberlandt, *Jahrbücher für Wissenschaftliche Botanik*. **13**, 74–188 (1882).
10. R. B. Wylie, *American Journal of Botany*. **39**, 645–651 (1952).
11. I. Terashima, *Photosynthesis Research*. **31**, 195–212 (1992).
12. T. Kenzo, T. Ichie, Y. Watanabe, T. Hiromi, *American Journal of Botany*. **94**, 764–775 (2007).
13. J. H. McClendon, *Plant Physiology*. **99**, 1677–1679 (1992).
14. A. Zsögön, A. C. Alves Negrini, L. E. P. Peres, H. T. Nguyen, M. C. Ball, *New Phytologist*. **205**, 618–626 (2015).
15. C. M. Jones, C. M. Rick, D. Adams, J. Jernstedt, R. T. Chetelat, *American Journal of Botany*. **94**, 935–947 (2007).
16. T. Lin *et al.*, *Nature Genetics*. **46**, 1220–1226 (2014).
17. A. V. Persikov *et al.*, *Nucleic Acids Research*. **43**, 1965–1984 (2015).
18. F. Baile, W. Merini, I. Hidalgo, M. Calonje, *The Plant Cell*. **33**, 2701–2715 (2021).
19. L. Truebestein, T. A. Leonard, *Bioessays*. **38**, 903 (2016).
20. D. Cui *et al.*, *PLoS Genet*. **9**, e1003759 (2013).
21. M. Gallei, C. Luschnig, J. Friml, *Current Opinion in Plant Biology*. **53**, 43–49 (2020).
22. J. Truskina *et al.*, *Nature*. **589**, 116–119 (2021).
23. M. Sagar *et al.*, *Plant Physiology*. **161**, 1362–74 (2013).
24. L. Sack, C. Scoffoni, *New Phytologist*. **198**, 983–1000 (2013).
25. S. A. M. McAdam *et al.*, *Plant physiology*. **175**, 351–360 (2017).
26. T. N. Buckley, L. Sack, M. E. Gilbert, *Plant Physiology*. **156**, 962–973 (2011).
27. K. Kawai, R. Miyoshi, N. Okada, *Trees*. **31**, 1–11 (2017).
28. M. A. Zwieniecki, T. J. Brodribb, N. M. Holbrook, *Plant Cell & Environment*. **30**, 910–921 (2007).
29. C. Aybar *et al.*, *Hydrological Sciences Journal*. **65**, 770–785 (2020).
30. D. Nikolopoulos, G. Liakopoulos, I. Drossopoulos, G. Karabourniotis, *Plant Physiology*. **129**, 235–243 (2002).
31. C. Bellasio, M. R. Lundgren, *New Phytologist*. **212**, 485–496 (2016).
32. M. A. M. Barbosa *et al.*, *Plant, Cell & Environment*. **42**, 1575–1589 (2019).
33. A. Baresch, C. Crifò, C. K. Boyce, *New Phytologist*. **221**, 628–639 (2019).
34. J. Hu, A. Israeli, N. Ori, T. Sun, *The Plant Cell*. **30**, 1710–1728 (2018).
35. M. Arsic *et al.*, *Plant Physiology*. **183**, 1472–1483 (2020).


ACKNOWLEDGEMENTS

We thank Profs Alisdair Fernie and Ralph Bock (Max-Planck Institute, Germany), Dr Federico Scossa (CREA, Italy), Dr Karla Gasparini (University of São Paulo, Brazil) and Diego S. Reartes for valuable discussions and input on the manuscript. We also gratefully acknowledge the support and contributions of the UFV Plant Physiology Graduate Program.

**Funding**

Fundação de Amparo à Pesquisa do Estado de São Paulo (FAPESP), Brazil 2016/01128-9

Fundação de Amparo à Pesquisa do Estado de São Paulo (FAPESP), Brazil 2017/14953-0

Conselho Nacional de Desenvolvimento Científico e Tecnológico (CNPq).

Coordenação de Aperfeiçoamento de Pessoal de Nível Superior (CAPES), Brazil, Finance Code 001

Foundation for Research Assistance of the Minas Gerais State (FAPEMIG), Brazil RED-00053-16

**Author contributions**

Conceptualization: JEL, LEPP, MR, AZ

Methodology: LF, WCO, AF, LEPP, MR, AZ

Investigation: JDRM, BLR, BSL, JEL, LNS, TS

Funding acquisition: WCO, AF, LEPP, MR, AZ

Project administration: MR, AZ

Supervision: LF, WCO, AF, LEPP, MR, AZ

Writing – original draft: JDRM, AZ

Writing – review & editing: all authors

**Data and materials availability**

All data are available in the main text or the supplementary materials.

**Supplementary materials**

Materials and Methods

Figs. S1 to S12

Tables S1 to S7

References

genes

MDPI

*Article*

# Down Regulation and Loss of *Auxin Response Factor 4* Function Using CRISPR/Cas9 Alters Plant Growth, Stomatal Function and Improves Tomato Tolerance to Salinity and Osmotic Stress

**Sarah Bouzroud [1,2,†], Karla Gasparini [3,†], Guojian Hu [2], Maria Antonia Machado Barbosa [3], Bruno Luan Rosa [3], Mouna Fahr [1], Najib Bendaou [1], Mondher Bouzayen [2], Agustin Zsögön [3], Abdelaziz Smouni [1,*] and Mohamed Zouine [2,*]**

1 Laboratoire de Biotechnologie et Physiologie Végétales, Centre de biotechnologie végétale et microbienne biodiversité et environnement, Faculté des Sciences, Université Mohammed V de Rabat, Rabat 1014, Morocco; sarah.bouzroud@gmail.com (S.B.); fahrmouna@yahoo.fr (M.F.); najib.bendaou@gmail.com (N.B.)
2 GBF, Université de Toulouse, INRA, 31326 Castanet-Tolosan, France; hu.guojian0309@gmail.com (G.H.); bouzayen@ensat.fr (M.B.)
3 Departamento de Biologia Vegetal, Universidade Federal de Viçosa, Viçosa 36570-900, Brazil; karlagasparini28@gmail.com (K.G.); mabarbosa483@gmail.com (M.A.M.B.); Bruno.rosa@gmail.com (B.L.R.); agustin.zsogon@ufv.br (A.Z.)
* Correspondence: azizsmouni@gmail.com (A.S.); mohamed.zouine@ensat.fr (M.Z.)
† These authors contributed equally to this work.

Received: 23 December 2019; Accepted: 28 February 2020; Published: 3 March 2020


**Abstract:** Auxin controls multiple aspects of plant growth and development. However, its role in stress responses remains poorly understood. Auxin acts on the transcriptional regulation of target genes, mainly through Auxin Response Factors (*ARF*). This study focuses on the involvement of *SlARF4* in tomato tolerance to salinity and osmotic stress. Using a reverse genetic approach, we found that the antisense down-regulation of *SlARF4* promotes root development and density, increases soluble sugars content and maintains chlorophyll content at high levels under stress conditions. Furthermore, *ARF4*-as displayed higher tolerance to salt and osmotic stress through reduced stomatal conductance coupled with increased leaf relative water content and Abscisic acid (ABA) content under normal and stressful conditions. This increase in ABA content was correlated with the activation of ABA biosynthesis genes and the repression of ABA catabolism genes. *Cu/ZnSOD* and *mdhar* genes were up-regulated in *ARF4*-as plants which can result in a better tolerance to salt and osmotic stress. A CRISPR/Cas9 induced *SlARF4* mutant showed similar growth and stomatal responses as *ARF4*-as plants, which suggest that *arf4-cr* can tolerate salt and osmotic stresses. Our data support the involvement of *ARF4* as a key factor in tomato tolerance to salt and osmotic stresses and confirm the use of CRISPR technology as an efficient tool for functional reverse genetics studies.

**Keywords:** *ARF4*; Auxin; CRISPR-Cas9; osmotic stress; salt; tolerance; tomato

## 1. Introduction

Auxin is a key regulator of many plant growth and development processes throughout the plant life cycle [1]. Auxins regulate diverse cellular and developmental responses in plants via three types of transcriptional regulators, auxin response factors (ARFs), Aux/IAA and TOPLESS (TPS) proteins [2]. ARFs play a key role in regulating the expression of auxin response genes. In total, 23 *ARF* genes have been isolated from *Arabidopsis thaliana* [3]. Most of them share a structure with conserved domains:

an N-terminal DNA-binding domain (DBD), a variable central transcriptional regulatory region (MR), which can function as an activator or repressor domain, and a carboxy-terminal dimerization domain (CTD) that contributes to the formation of either ARF/ARF homo- and hetero-dimers or ARF/Aux/IAA hetero-dimers [4,5]. Since *ARF1*, the first *Arabidopsis ARF* gene, was cloned and its function investigated [6], the *ARF* gene family has been identified and well characterized in many crop species, including tomato (*Solanum lycopersicum*), maize (*Zea mays*), rice (*Oryza sativa*), poplar (*Populus trichocarpa*), Chinese cabbage (*Brassica rapa*), banana (*Musa* sp.) and physic nut (*Jatropha curcas* L.) [4,7–10].

In tomato, the *ARF* gene family is also involved in the control of many physiological processes [5]. Downregulation of *ARF3* decreased the density of epidermal cells and trichomes in tomato [11]. The *Slarf2A/B* mutation leads to a severe fruit ripening inhibition with dramatically reduced ethylene production, while the over-expression of *ARF2A* resulted in a blotchy ripening pattern in fruit as a result of a significant accumulation of ripening-related genes and metabolites [12]. Down-regulation of *SlARF6* and *SlARF8* in transgenic plants through the overexpression of *miR167a* may lead to floral development defects and female sterility [13]. Transcriptional down-regulation of *ARF4* expression leads to severe leaf curling along the longitudinal axis [14]. The down-regulation of *SlARF4* also resulted in ripening-associated phenotypes such as enhanced firmness, sugar and chlorophyll content leading to dark green fruit and blotchy ripening [14,15]. This phenotype was also reported in *SlARF10* gain of function mutant [16].

*ARF* genes also seem to be implicated in plant responses to environmental stresses. It has been reported that both *OsARF11* and *OsARF15* show differential expression in salt stress conditions, suggesting that they are involved in the rice response to stress [7]. In banana, the expression of many *ARF* genes was altered in response to salinity and osmotic stresses [9]. We have previously shown that, in tomato, expression levels of many *SlARF* genes are responsive to a wide range of abiotic stress conditions [17]. Interestingly, the *SlARF4* regulatory region was enriched in cis-*acting* elements specific to salinity and water deficit response [17]. Here, we extended this observation to plants subjected to salinity and osmotic stress. We investigated whether loss of *SlARF4* function in tomato could have an impact on plant growth and function under water deficit, high salinity or osmotic stress conditions. By assessing morphological, anatomical, physiological and molecular analyses, we provide evidence for the involvement of *SlARF4* in tomato response to salinity and osmotic stress. We discuss the potential role of elements of the auxin signaling network in responses to environmental stresses.

## 2. Material and Methods

### 2.1. Plant Material

Wild-type tomato (*Solanum lycopersicum*, L.) cv Micro-Tom (WT), and the following *AUXIN RESPONSE FACTOR 4* lines were used in this study: an *ARF4* antisense silenced line (*ARF4*-as), and a reporter line with the β-glucoronidase (GUS) gene driven by the native *ARF4* promoter region (pARF4::GUS). *ARF4*-as plant lines were previously generated and well-characterized by Sagar et al. (2014) [15]. The most representative plant line was chosen.

### 2.2. Generation of SlARF4-Crispr (arf4-cr) Plants

Tomato *SlARF4*-crispr (*arf4-cr*) plants were obtained by *Agrobacterium tumefasciens* mediated genetic transformation according to Wang et al. (2005) [18]. CRISPR/Cas9 mutant lines were generated following previous standard protocol [19]. Two single-guide (sg) RNAs in the Solyc11g069190 coding sequence were designed using the CRISPR-P server (http://cbi.hzau.edu.cn/cgi-bin/CRISPR) [20]. The sgRNA sequences are AATGGAGGTCACACCAGAG and GGAACTGAAAAGCCACCAT, aiming to create a 49bp deletion in the DBD domain of *SlARF4* gene. The sgRNAs were first cloned in the Level 1 vectors pICH47751 and pICH47761 driven by the *Arabidopsis* U6 promoter, respectively. The Level 1 constructs pICH47732-NOSpro::NPTII, pICH47742-35S:Cas9, pICH47751-AtU6pro:sgRNA1, and pICH47761-AtU6::sgRNA2 were then assembled into the Level 2 destination vector pAGM4723. For genotyping of the transgenic lines, genomic DNA

was extracted using ReliaPrep™ gDNA Tissue Miniprep System (Promega, Madison, United States)). The CRISPR/Cas9-positive lines were identified by PCR, then further genotyped for mutations using the primers (Fwd: ACATGGTTTCACTGTAAAGGGATCT and Rev: CTGGCCTGAAAGAAAAGCATCAAA) spanning the two sgRNAs target sequences by PCR and Sanger sequencing of ARF4-PCR products.

### 2.3. Characterization of ARF4-as and arf4-cr Plants

#### 2.3.1. Plant Growth Conditions

Plants were grown as described previously [21]. Seeds of WT, *ARF4*-as and *arf4-cr* transgenic plants were sown in germination trays with commercial substrate (Tropstrato HT Hortaliças, Vida Verde) and supplemented with 1g $L^{-1}$ 10:10:10 NPK and 4 g $L^{-1}$ dolomite limestone ($MgCO_3$ + $CaCO_3$). After the emergence of the first pair of true leaves, the seedlings were transferred to plastic pots (350 mL) with the same substrate described above, supplemented with 8 g $L^{-1}$ 10:10:10 nitrogen: phosphorus: potassium (N:P:K) and 4 g $L^{-1}$ lime. The experiment was conducted in a greenhouse localized at Universidade Federal de Viçosa (642 m asl, 20°45′ S; 42°51′ W), Minas Gerais, Brazil, under semi-controlled conditions (mean temperature of 28 °C and 450–500 µmol $m^{-2}$ $s^{-1}$ PAR irradiance). Irrigation was performed twice a day, where each plastic pot received the same volume of water.

#### 2.3.2. Growth Analyses

Growth measurements were conducted as described previously [22]. Plant height and internode length were measured 35 days after germination (DAG). At 45 DAG the plants were harvested and divided into leaves, stem and root. Leaf area was measured using leaf area meter (Li-Cor Model 3100 Area Meter, Lincoln, NE, USA). Leaf, stem and root were then packed separately in paper bags and oven dried at 70 °C for 72 h until they reached constant weight. Shoot and root biomass were measured from the dry weight of leaves, stem and root. Specific Leaf Area (SLA) was determined as described by Hunt (1982) [23].

#### 2.3.3. Microscopy

For anatomical analysis, leaf discs were collected from the medium point of the fifth lateral leaflet and fixed in FAA50 (Formaldehyde, acetic acid and ethanol 50%) for 48 h, and then stored in ethanol 70%. Samples were infiltrated with historesin (Leica Microsystems, Wetzlar, Germany) and cut in cross sections with ~5 µm (RM2155, Leica Microsystems, Wetzlar, Germany). Leaf cross sections were mounted in water on glass slides and stained with toluidine blue. Histological sections were observed using an optic microscope (AX-70 TRF, Olympus Optical, Tokyo, Japan) and then photographed using digital photo camera (Zeiss AxioCam HRc, Göttinger, Germany). Anatomical features, such as leaf thickness and thickness of cell layers, were analyzed using Image-Pro Plus® software (version 4.5, Media Cybernetics, Silver Spring, MD, USA).

#### 2.3.4. Measurements of Photosynthetic Parameters

Photosynthetic parameters were performed using an open-flow infrared gas exchange analyzer system (Li 6400XT, Li-Cor, Lincoln, USA) equipped with an integrated fluorescence chamber (Li-6400-40; Li-Cor Inc.). All measurements were made on terminal leaflets of intact and completely expanded leaves. The analysis was conducted under common conditions for photon flux density (1000 µmol $m^{-2}$ $s^{-1}$), leaf temperature (25 ± 0.5 °C), leaf-to-air vapor pressure difference (16.0 ± 3.0 mbar), air flow rate into the chamber (500 µmol $s^{-1}$), reference $CO_2$ concentration of 400 ppm using an area of 2 $cm^2$ in the leaf chamber.

*A*/Ci curves were determined initiated at an ambient $CO_2$ concentration of 400 µmol $mol^{-1}$ under a saturating photosynthetic Photon Flux Density (PPFD) of 1000 µmol $m^{-2}$ $s^{-1}$ at 25 °C under ambient $O_2$ supply. $CO_2$ concentration was decreased to 50 µmol $mol^{-1}$ of air in step changes. Upon the completion of the measurements at low $C_a$, $C_a$ was returned to 400 µmol $mol^{-1}$ of air to restore the original *A*. Next,

$CO_2$ was increased stepwise to 1600 µmol $mol^{-1}$ of air. The maximum rate of carboxylation ($V_{cmax}$), maximum rate of carboxylation limited by electron transport ($J_{max}$) and triose-phosphate utilization (TPU) were estimated by fitting the mechanistic model of $CO_2$ assimilation proposed by Farquhar et al. (1980) [24]. Corrections for the leakage of $CO_2$ into and out of the leaf chamber of the LI-6400 were applied to all gas-exchange data as described by Rodeghiero et al. (2007) [25].

#### 2.3.5. Kinetics of Stomatal Conductance

The evaluation of stomatal behavior in response to light and $CO_2$ variation was performed in WT and *ARF4*-as plants 40 DAG, under laboratory conditions (temperature 22–25 °C; relative humidity 50–60% and radiation of 150–200 µmol $^{-2}$ $s^{-1}$), using an open-flow infrared gas exchange analyzer system (Li 6400XT, Li-Cor, Lincoln, CA, USA). The variation of $g_s$ was performed on the fifth or sixth fully expanded leaf. For step-change evaluation of $g_s$ in response to light intensity, leaves were stabilized for 30 min in the dark and then radiation was increased to 1000 µmol $m^{-2}$ $s^{-1}$, and allowed to stabilize for 240 min. Subsequently, light was turned off and observations recorded for another 100 min. The alternation in the amount of light was based on the results presented by Lawson et al. (2010) [26]. The response of $g_s$ to $CO_2$ was performed in a similar manner to those described above for light response. The analysis was performed in a range of 240 min, with changes in $CO_2$ concentration (400-800-400 µmol $CO_2$ $m^{-2}$ $s^{-1}$).

#### 2.3.6. Productivity Traits

The productivity parameters were measured in eight plants per genotype (WT, *ARF4*-as and *SlARF4*-crispr). The average fruit weight was determined after individual weighing of each fruit, using a semi analytical balance with a sensitivity of 0.01 g (Shimadzu® AUY220 model, Japan)). Equatorial and polar diameter was measured using a digital pachymeter (Jomarca *STAINLESS HARDENED*, Nieuw, Vennep, Netherland). The determination of the soluble solids content (°Brix) was performed in 10 fruits per plant using a digital temperature-compensated refractometer, model RTD 45 (Instrutherm®, São Paulo, SP, USA).

### *2.4. ARF4 Expression under Salt, Drought and Osmotic Stresses*

#### 2.4.1. Plant Growth and Stress Conditions

WT tomato seeds were sterilized for 10 min in 50% sodium hypochlorite, rinsed four times with sterile distilled water and sown in pots containing peat. Then they were incubated in a culture room with 16 h light/8 h dark photoperiod and 25 ± 2 °C temperature. After 3 weeks, plants were subjected to salt and drought stresses. Salt stress was performed by watering daily the plants with 250 mM of NaCl solution. Control plants were daily watered with distilled water. Leaves and roots samples were harvested after 2 and 24 h of salt stress application. Drought stress was performed on three-week-old plants by water holding for 48 h and for 5 days. Watering continued normally throughout for control plants. Leave and root samples were collected after drought stress application. Three biological replicates were done for each condition.

#### 2.4.2. RNA Extraction

Total RNA was extracted from leaves and roots samples by using The Plant RNeasy extraction kit (RNeasy Plant Mini Kit, Qiagen, Valencia, CA, USA). To remove any residual genomic DNA, the RNA was treated with an RNase-Free DNase according to the manufacturer's instruction (Ambion® DNA-*free*™DNase, Austin, Texas, United States). The concentration of RNA was accurately quantified by spectrophotometric measurement and 1µg of total RNA was separated on 2% agarose gel to monitor its integrity. DNase-treated RNA (2 µg) was then reverse-transcribed in a total volume of 20 µL using the Omniscript Reverse Transcription Kit (Qiagen, Hilden, Germany).

#### 2.4.3. Real Time PCR

The real-time quantification of cDNA corresponding to 2 µg of total RNA was performed in the ABI PRISM 7900HT sequence detection system using the QuantiTech SYBR Green RT-PCR kit (Qiagen). The Gene-specific primers used are listed in Table S1. The reaction mixture (10 µL) contained 2 µg of total RNA, 1,2 µM of each primer and appropriate amounts of enzymes and fluorescent dyes as recommended by the manufacturer. Actin gene was used as reference. Real-Time PCR conditions were as follow: 50 °C for 2 min, 95 °C for 10 min, then 40 cycles of 95 °C for 15 s and 60 °C for 1 min, and finally one cycle at 95 °C for 15 s and 60 °C for 15 s. Three independent biological replicates were used for real-time PCR analysis. For each data point, the $C_T$ value was the average of $C_T$ values obtained from the three biological replicates.

#### 2.4.4. Histochemical Analysis of GUS Expression

Transgenic plants expressing *pARF4::GUS* were generated by *Agrobacterium. tumefaciens*-mediated transformation according to Wang et al. (2005) [18]. For that, PCR was performed on the genomic DNA of tomato Micro-Tom (10 ng.mL$^{-1}$) using specific primers. The corresponding amplified fragment was cloned into the *pMDC162* vector containing the GUS reporter gene using Gateway technology (Invitrogen). The cloned *SlARF* promoter was sequenced from both sides using vector primers in order to see whether the end of the promoter is matching with the beginning of the reporter gene. Sequencing results analyses were carried out using the Vector NTI (Invitrogen) and ContigExpress software by referring to *ARF* promoter sequences.

After being surface sterilized, *pARF4::GUS* seeds were cultivated in Petri dishes containing half strength Murashige & Skoog medium for 7 days in a growth chamber at 25 °C with 16 h light/8 h dark cycle. One-week-old plants were then grown hydroponically for two weeks in Broughton & Dillworth (BD) liquid medium [27]. Three-week-old plants were subjected to salt and osmotic treatment. Salt stress was performed by adding 250 mM of NaCl to the culture medium. After 24 h of the salt stress application, plants were incubated overnight at 37°C in GUS buffer (3 mM 5-bromo-4-chloro-3-indolyl-β-D-glucuronide (Duchefa Biochemie, Haarlem, The Netherlands), 0.1% v/v Triton X-100 (Sigma, Steinhaim, Germany) 8 mM β-mercaptoethanol, 50 mM $Na_2HPO_4/NaH_2PO_4$ [pH 7.2]) then followed by a destaining in 70% EtOH. Osmotic stress was conducted by adding 15% PEG 20000 to the liquid culture solution. Plants were collected after five days of stress application and were GUS-stained as described above. For each stress condition, control plants were cultivated in BD liquid medium for the same period.

### *2.5. Stress Tolerance Assays in the Transgenic Tomato Plants*

#### 2.5.1. Plant Growth and Stress Application

WT and *ARF4*-as seeds were first surface-sterilized for 10 min in 50% sodium hypochlorite, and then rinsed four times with sterile distilled water. They were then cultured in petri dishes containing half strength Murashige & Skoog (MS) medium for 7 days in a growth chamber at 25° with 16 h light/8 h dark cycle. One-week-old plants were then grown hydroponically in pots containing 1 L of BD aerated nutriment solution for two weeks in the same growth conditions (25° with 16 h light/8 h dark cycle) [27]. Three weeks plants were then subjected to salt and osmotic stresses. Salt stress was performed by adding 100 mM or 150 mM NaCl to the liquid BD medium. Leaves and roots samples were harvested after 2 weeks of treatment. osmotic treatment was conducted as follows: three weeks plants were subjected to osmotic stress by adding 5% or 15% PEG 20,000 corresponding to final osmotic potentials of −0.09 MPa and −0.28 MPa to the hydroponic solution for 2 weeks. Meanwhile, the control plants were grown normally in BD medium. Leaves and roots samples were collected after 2 weeks of culture for both stressed and unstressed plants. For each treatment, the hydroponic solution was renewed each 3 days.

2.5.2. Morphological Analysis

- Determination of shoot and root fresh weights

Shoot and root fresh weights were determined as followed: stressed and unstressed plants from each line were harvested and rinsed thoroughly with distilled water (DW). The plants were blot dried on blotting sheet and cut into shoots and roots. The fresh weight of each part of the plant was measured and the mean of shoots and roots weights was determined based on at least twelve plants per line in each condition.

- Determination of primary root length and lateral root density

Primary root length was determined as followed. Pictures for each plant were analyzed using ImageJ software in order to determinate the root length. Twelve independent plants from each line under control and stress conditions were used to calculate the mean.

The lateral root number was determined by counting the number of emerging roots and the mean was calculated based on at least twelve plants per line in each condition. The lateral root density (LR density) was determined using the following equation: number of LRs/the length of the root.

2.5.3. Physiological Analysis

- Determination of chlorophyll content

Determination of chlorophyll content of each line under stressful and normal conditions was performed as described in Bassa et al. (2012) [28]. A 100 mg aliquot of leaves collected from stressed and unstressed plants was weighted and ground with 1 mL of 80% acetone. The liquid obtained was centrifuged for 1 min at 10,000 rpm to remove any remaining solid tissue. Samples were analyzed by spectrophotometry at two wavelengths, 645 and 663 nm, using 80% acetone as the blank. The total chlorophyll content was determined using the following equations: Total Chlorophyll Content = 20.2 × Chl a + 8.02 × Chl b (Chl a = 0.999A663 – 0.0989A645 and Chl b = –0.328A663+1.77A645)

- Determination of soluble sugar content

Total soluble sugar content was determined as in Dubois et al. (1956) [29]. Thus, 100 mg of fresh leaves and roots of each sample were homogenized in 5 mL of 80% ethanol in test tubes. Test tubes were kept in water bath of 80 °C for 1 h, and sample extracts were transferred to another test tube, and 0.5 mL distilled water and 1 mL of 5% phenol then added and allowed to incubate for 1 h. Finally, after 1 h, 2.5 mL sulfuric acid was added to the test tubes and shaken well on an orbital shaker. Absorbance was read at 485 nm on Spectrophotometer. Sucrose was used as standard.

- Determination of leaf stomatal conductance

Leaf abaxial stomatal conductance of the youngest fully expanded leaf (usually the fifth leaf, counting from the base) of stressed and well-drained plants of each studied line were determined after two weeks of stress treatment using a hand-held leaf diffusion poromoter (SC-1 LEAF POROMETER, Decagon, Pullman, Washington, United States). For each line, three biological replicates were conducted at each condition.

- Determination of Abscisic acide (ABA) content

Three weeks ARF4-as and WT plants were exposed to salt and osmotic stress. Leaf samples were taken after 24 h for salt stress and after 48 h for osmotic. ABA measurement assays were performed as described Forcat et al. (2008) [30]. Briefly, 110 mg of frozen tissue were extracted at 4 °C for 30 min with 400 µL of $H_2O$ with 10% methanol + 1% acetic acid. The internal standard was 2H6 ABA. The extract was centrifuged at 13,000 g for 10 min at 4 °C. The supernatant was carefully removed and the pellet re-incubated for 30 min

with 400 µL of methanol-acetic acid mix. Following the centrifugation, the supernatants were pooled. Extracts were then analyzed by Liquid Chromatography- Mass Spectrometry (LC-MS) using an Acquity Ultra Performance Liquid Chromatography (UPLC) coupled to a XevoQtof (Waters, MA, USA). Analysis parameters were described in Jaulneau et al. (2010) [31].

- Determination of Relative water content (RWC):

Tomato fully expanded leaves were excised and fresh weight (FW) was recorded every 30 min. The excised leaves were then allowed to float on deionised water for about 24 h and turgid weight (TW) was recorded. Leaves were dried at 80 °C for 24 h and dry weight (DW) recorded. Finally, RWC was calculated according to Smart and Bingham (1974) [32].

#### 2.5.4. Quantitative Expression Assays

Three-weeks-old WT and ARF4-as plants grown hydroponically in BD medium were subjected to either 150 mM of NaCl or 15% of PEG. Leaves and root samples were harvested after 2 h and 24 h for salt stress and after 48 h for osmotic stress. RNA extraction, cDNA synthesis and real time PCR were performed as previously described in paragraph "ARF4 gene expression under salt and osmotic stress conditions". The gene-specific primers used are listed in Table S1.

## 3. Results

### *3.1. SlARF4 Downregulated Line Shows Altered Anatomical, Morphological and Physiological Parameters*

We analyzed a previously published *AUXIN RESPONSE FACTOR 4* antisense line (*ARF4*-as) [15]. The *ARF4*-as plants exhibit a wide range of morphogenic phenotypes, namely delayed flowering, increased height and leaf curling as compared to their isogenic Micro-Tom (wild-type, WT) counterparts (Figure 1). Stem and root dry weight, on the other hand, showed a significant reduction in *ARF4*-as plants compared to WT, along with a minor increase in leaf area and specific leaf area (Figure 2).

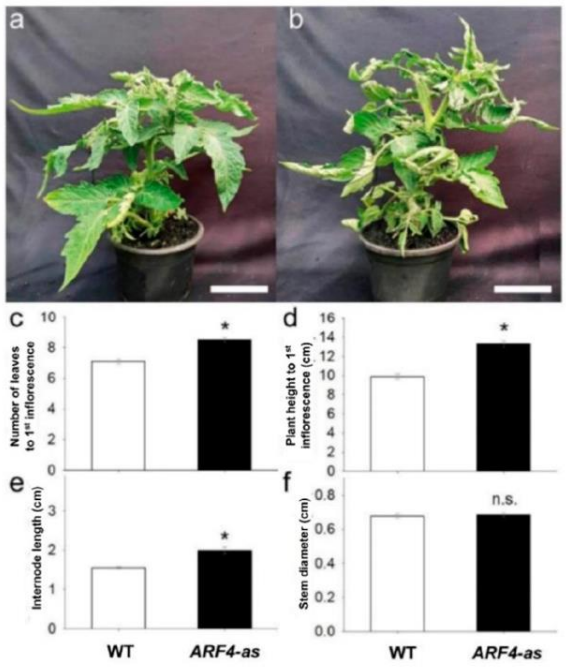


**Figure 1.** Phenotype of cv. Micro-Tom tomato plants (wild-type, WT) and isogenic *ARF4* antisense transgenic line (*ARF4*-as), 35 days after germination. (**a**) WT and (**b**) *ARF4*-as plants at the same stage of development, (**c**) number of leaves to first inflorescence, (**d**) plant height to first inflorescence, (**e**) plant internode length and (**f**) stem diameter. Bars are mean values ($n = 7$) ± s.e.m. Asterisks indicate values that were determined by Student's t test to be significantly different ($p < 0.05$) from WT.

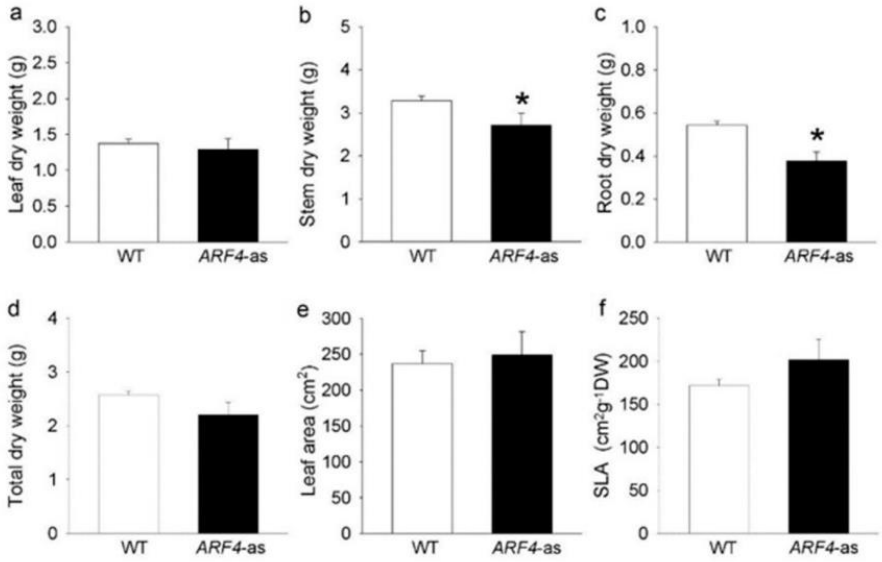


**Figure 2.** Dry weight and parameters related with leaf area for Micro-Tom (WT) and isogenic *ARF4* antisense transgenic line (*ARF4*-as), 45 days after germination. (**a**) leaf dry weight, (**b**) stem dry weight, (**c**) root dry weight, (**d**) total dry weight, (**e**) total leaf area and (**f**) specific leaf area (SLA). Values are means ± s.e.m ($n$ = 8). Asterisks indicate values that were determined by Student's $t$ test to be significantly different ($p < 0.05$) from the Micro-tom (WT).

*ARF4*-as plants displayed an upward curling along the longitudinal axis of leaves (Figure 3b–k). The extent of the changes detected in leaf morphology prompted us to check leaf ultrastructure in WT and *ARF4*-as plants. Leaf thickness was clearly reduced in *ARF4*-as plants compared to WT (Figure 3a,b). Average leaf blade thickness was 209 ± 8 μm in WT compared to 181 ± 7 μm in *ARF4*-as (Figure 3c). The palisade parenchyma (PP), spongy parenchyma (SP) and mesophyll tissue layers were thinner in *ARF4*-as plants than in WT plants (Figure 3d,e,j). The palisade:spongy mesophyll ratio was significantly higher in WT than in *ARF4*-as (Figure 3f). Meanwhile, the intracellular air spaces (IAS) were more conspicuous in *ARF4*-as compared to WT (Figure 3g), while no visible difference was observed in adaxial or abaxial epidermis between genotypes (Figure 3h,i).

Consistent with the presence of thinner leaves in the *ARF4*-as mutant plants, net $CO_2$ assimilation rate ($A$) showed lower values along with a decreased stomatal conductance ($g_s$) in *ARF4*-as plants while WT plants exhibited higher $CO_2$ assimilation rate and $g_s$ values (Figure 4a–b). It is well known that $A$ can be limited by the slowest of two biochemical processes: (1) the maximum rate of ribulose 1,5-biphosphate (RuBP) carboxylase/oxygenase (Rubisco) catalyzed carboxylation ($V_{cmax}$) and (2) regeneration of RuBP controlled by electron transport rate ($J_{max}$) [33]. Consistently, $V_{cmax}$ and $J_{max}$ exhibited a significant decrease in *ARF4*-as plants (Table S2), indicating that photosynthesis is reduced due to the silencing of *SlARF4* (Figure 5a).

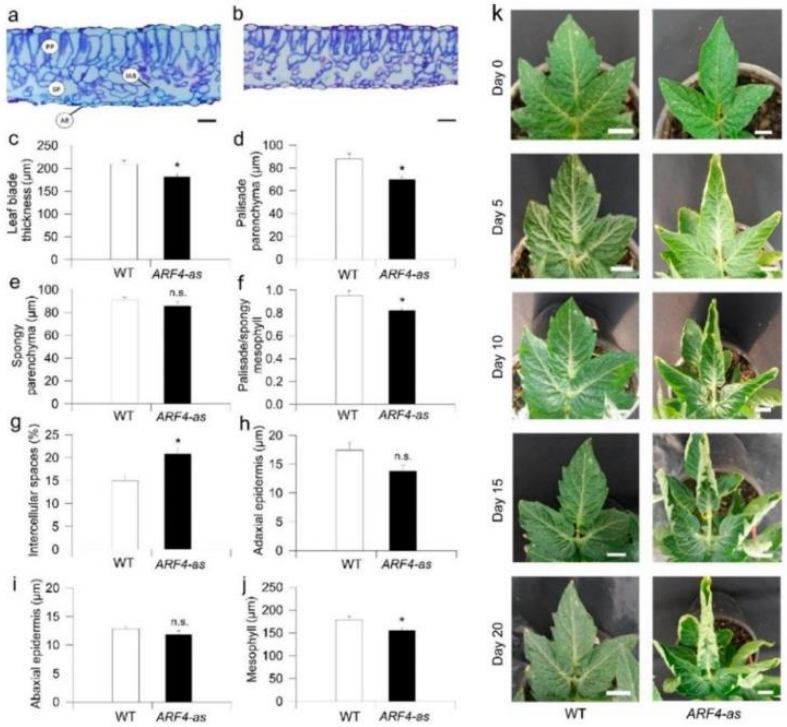


**Figure 3.** Leaf anatomy and morphology is altered in an *ARF4*-as transgenic line. Representative leaf cross-sections of (**a**) Micro-Tom (WT) and (**b**) *ARF4*-antisense line (*ARF4*-as). Scale bars= 20 µm. (**c**) Total thickness of the leaf blade, (**d**) thickness of palisade, (**e**) thickness of spongy and (**f**) ratio of palisade to spongy mesophyll, (**g**) proportion of intercellular air spaces, (**h**) adaxial epidermis and (**i**) abaxial epidermis and (**j**) mesophyll thickness in WT and *ARF4*-as plants and (**k**) Time series of a representative leaf illustrating blade curling in ARF4-as plants. Day 0 represents the day when the leaf was fully expanded. Values are means ± s.e.m ($n$ = 6). Asterisks indicate values that were determined by student's $t$ test to be significantly different ($p < 0{,}05$) from WT while n.s indicates non significant difference between *ARF4*-as and WT.

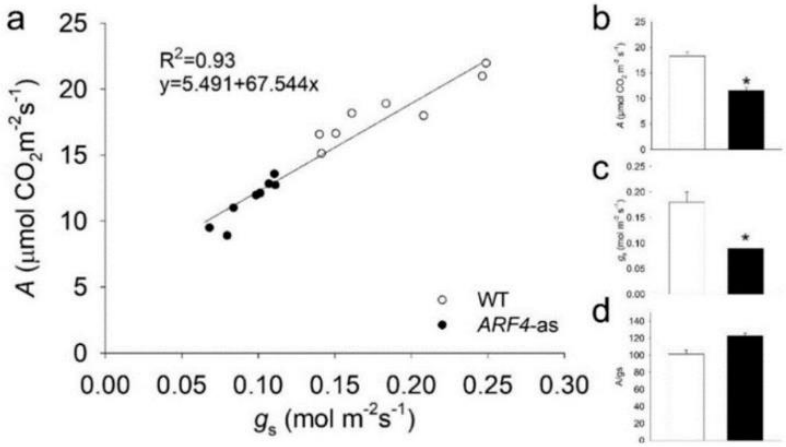


**Figure 4.** Net $CO_2$ assimilation rate (A) and stomatal conductance ($g_s$) in Micro-Tom (WT) and isogenic ARF4 antisense transgenic line (*ARF4*-as). (**a**) $CO_2$ assimilation rate (**A**) as a function of stomatal conductance (gs), each point represents one measurement on an individual plant. Line fitted by linear regression. (**b**) net CO2 assimilation rate (A). (**c**) stomatal conductance ($g_s$). (**d**) intrinsic water efficiency ($A/g_s$). Values are means ± s.e.m ($n$ = 8). Asterisks indicate values that were determined by Student's t test to be significantly different ($p < 0.05$) between genotypes.

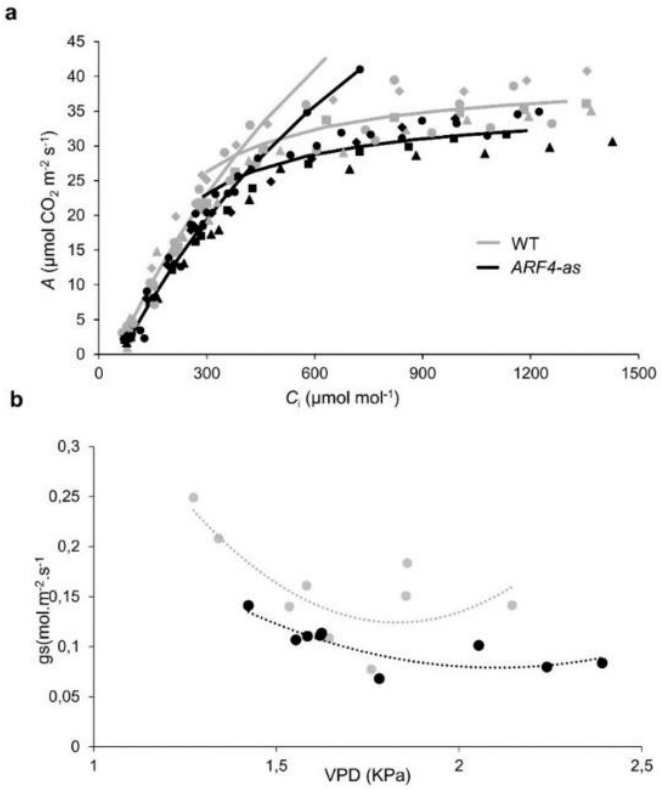


**Figure 5.** Photosynthetic assimilation rate and stomatal conductance in Micro-Tom (WT) and *ARF4*-antisense silencing line. (**a**) Net photosynthesis (*A*) curves in response to sub-stomatal ($C_i$) $CO_2$ concentration in WT and *ARF4*-as plants. Values are presented as means ± s.e.m. ($n$ = 5) obtained using the fully expanded fifth leaf. Two-branch curves: the biochemically based leaf photosynthesis model [24] was fitted to the data based on $C_i$, values of $A/C_i$ for five plants of WT (gray) and *ARF4-as* (black). (**b**) Response of stomatal conductance ($g_s$) to changes in leaf-to-air vapor pressure deficit (VPD). Vapor pressure difference was varied by changing the humidity of air, keeping leaf temperature constant. Each point represents one measurement on an individual plant.

Stomatal conductance is one of the main parameters that affect photosynthesis under osmotic stress [34]. As stomatal behavior is closely linked to $CO_2$ uptake, it is considered to be one of the main reasons for reduced photosynthesis [35]. Stomatal conductance was significantly lower in *ARF4*-as compared to WT (Figure 4c). The response of stomatal conductance ($g_s$) to changing air vapor pressure deficit (*VPD*) was determined in *ARF4*-as and WT plants. At low *VPD*, WT plants exhibited high $g_s$ and tended to reduce $g_s$ as *VPD* increased from 1.25 kPa to 2 kPa and maintained a moderate $g_s$ values at higher *VPD*s. Meanwhile, *ARF4*-as plants presented a relatively low $g_s$ values at both low and high *VPD* compared to WT plants (Figure 5b). We verified a similarly impaired stomatal response in *ARF4*-as plants in response to step changes in irradiance and $CO_2$ levels (Figure S1), suggesting that *ARF4* could be an important player in the regulation of stomatal movements. Furthermore, intrinsic water-use efficiency (WUE) was notably higher in *ARF4*-as plants (Figure 4d) suggesting that the downregulation of *SlARF4* has the potential to improve the ration of carbon assimilation to transpirational water loss.

Given this potential impact on carbon assimilation, we next sought to examine whether *SlARF4* under-expression might affect plant agronomic parameters. Yield, number of fruits and fruit fresh weight were not altered between WT and *ARF4*-as plants, whereas fruit shape was altered in *ARF4*-as plants (Figure S2), as expected, given the well-known role of auxin in fruit development [12,36].

### 3.2. *ARF4* has Altered Expression in Response to Salt and Osmotic Stresses

The expression pattern of *SlARF4* was analyzed by real-time PCR in leaves and roots exposed to salt or drought stress. *ARF4* gene expression was significantly regulated by salt and drought stresses. *SlARF4* expression was significantly repressed in leaves and roots after 2 hours of salt treatment while its expression was significantly induced in leaves and roots after 24 h (Figure 6a,b). During drought treatment, *SlARF4* gene was slightly induced after 48 h of stress application in leaves (Figure 6c). In drought stressed roots, *SlARF4* was although significantly induced after 5 days of stress exposure (Figure 6d). Tomato lines harboring *pARF4::GUS* constructs were generated and used to assay *in planta* analysis of *ARF4* expression under stress conditions. We observed strong expression in leaves, primary root and root tip after 24 h of salt stress exposure (Figure 6e). After five days of osmotic treatment, GUS activity was detected in the root system and in different parts of the leaf (Figure 6f).

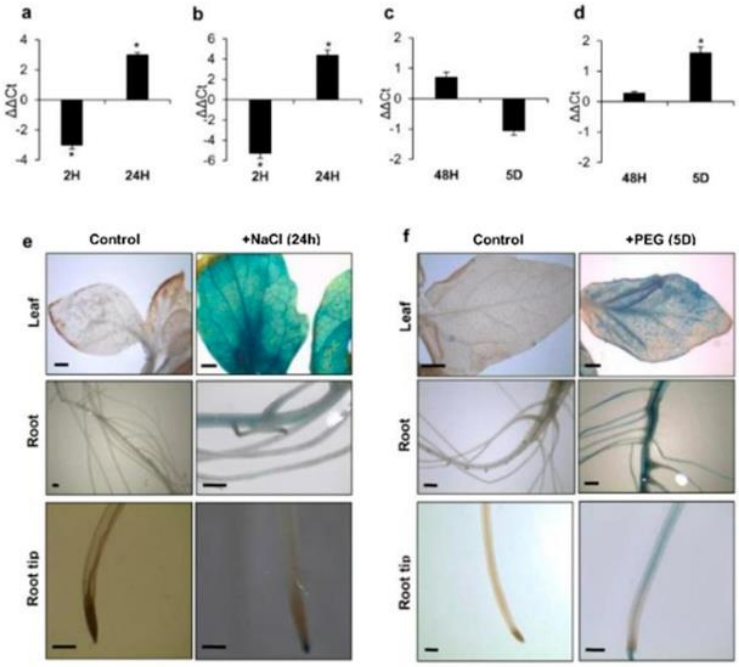


**Figure 6.** *SlARF4* expression in response to salt and drought stresses. Gene expression in leaves (**a**) and roots (**b**) of WT plants exposed to salt stress, in leaves (**c**) and roots (**d**) of WT plants exposed to osmotic stress. ΔΔCt refers to differences in gene expression relative to untreated plants. Values are mean ± SD of three biological replicates. GUS activity in *pARF4::GUS* tomato lines in salt (**e**) or osmotic (**f**) stress conditions. Bars scale (1mm). Stars (*) indicate the statistical significance ($p < 0.05$) according to Student's *t*-test.

### 3.3. *ARF4* alters the Plants Response to Salt and Osmotic Stress

#### 3.3.1. Shoot and Root Fresh Weight are Differentially Altered in ARF4 Transgenic Lines

Shoot fresh weight was investigated in WT and *ARF4-as* plants under salt and osmotic stress conditions. In the absence of stress, fresh weight was significantly higher in the *ARF4-as* as compared to WT (Figure 7a). Two levels of NaCl (100 mM and 150 mM) were applied, and both led to reductions in shoot fresh weight in both genotypes. In response to 150 mM NaCl, shoot fresh weight decreased by 60% in WT plants respectively and only by 30% in *ARF4*-as plants (Figure 7a). In roots, the reduction in the fresh weight was around 55% and 28% for WT and *ARF4*-as plants lines respectively (Figure 7c). Similarly, to salt stress, osmotic stress affected plant growth. Shoot fresh weight decreased by 66% for WT by 44% for *ARF4*-as plants when exposed to 15% of PEG 20000 (Figure 7b).

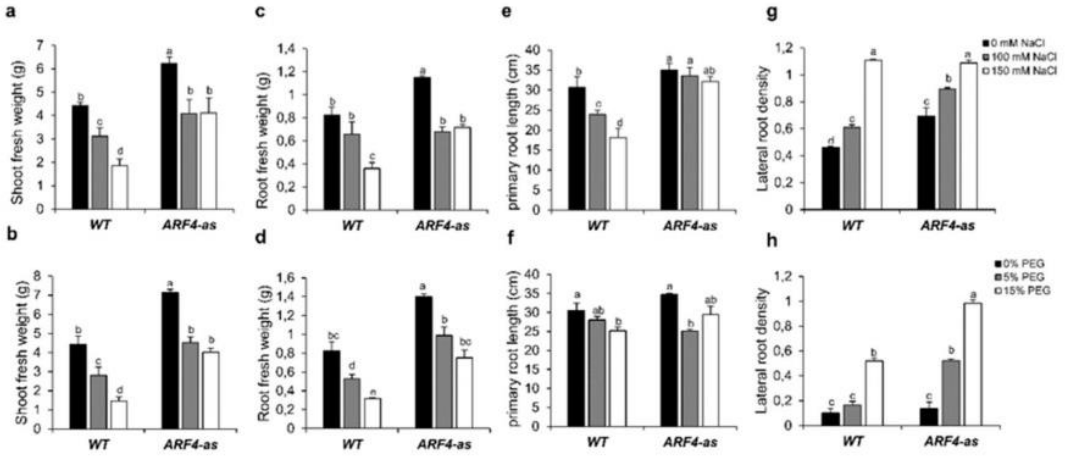


**Figure 7.** Growth parameters of tomato wildtype (WT) and *ARF4*-as in response to salt and osmotic stresses. (**a**,**b**) shoot fresh weight in salt and osmotic stress conditions respectively, (**c**,**d**) root fresh weight in salt and osmotic stress conditions respectively, (**e**,**f**) primary root length root in salt and osmotic stress conditions respectively, (**g**,**h**) root density in salt and osmotic stress conditions respectively. Salt and osmotic stresses were performed on three weeks tomato plants for two weeks by adding 100 mM of NaCl or 150 mM of NaCl for salt stress or 5% or 15% of Polyethylene Glycol (PEG) 20,000 for osmotic stress. Values are mean ± SD of three biological replicates. Bars with different letters indicate the statistical significance ($p < 0.05$) according to Student Newman-Keuls test.

Root fresh weight deceases significantly with the increase of PEG concentration. The decrease reached 57% in WT plants while the reduction was around 40% in *ARF4*-as in response to 15% of PEG20000 (Figure 7d).

#### 3.3.2. Root Development and Density are Less Affected in ARF4-as Plants

Root development was investigated in WT and *ARF4-as* plants in response to different concentrations of NaCl or PEG. Our results showed a significant reduction in primary root length in WT (by 40% in salt stress condition and by 17% in response to osmotic stress) while the decrease was nearby 8% and 12% in *ARF4*-as plants in response to salt and osmotic stress respectively (Figure 7e,f).

Root density was also investigated in the three lines under salt and osmotic stress conditions. Our results showed that root density significantly increased with the increase of NaCl or PEG concentrations in WT and in *ARF4*-as plants (Figure 7g,h). Root density increases by 57% in WT and 120% in *ARF4*-as., respectively. In response to osmotic stress, both plant lines showed a significant increase in root density. At 5% of PEG 20,000, root density increased by 50% and 130% in WT and *ARF4*-as plants respectively.

### *3.4. ARF4-as Plants are Less Affected by Salt and Osmotic Stress*

#### 3.4.1. Photosynthesis is Less Affected in ARF4-as Plants

Photosynthesis is among the primary processes to be affected by salinity and drought stress [37]. Our results showed that total chlorophyll content decreased significantly in WT plants exposed to different concentrations of NaCl while no significant changes in chlorophyll content was detected in *ARF4*-as plants (Figure S3). At 150 mM of NaCl, total chlorophyll content decreased only by 4% in the *ARF4*-as plants as compared to the control. Meanwhile, the diminution of total chlorophyll content was around 62.8% respectively in WT at 150 mM of NaCl compared to the control. The drastic decline in total chlorophyll content was also observed as a result of osmotic stress application on WT plants. The reduction in total chlorophyll content averaged the 37% in WT plants cultivated at 15% of PEG 20,000 respectively (Figure S3). Meanwhile, total chlorophyll content increased significantly*ARF4*-as in

response to osmotic stress. In fact, the average of chlorophyll content was 1.2 times higher in *ARF4*-as at 15% PEG 20,000 than at 0% PEG 20,000.

### 3.4.2. Sugars are Highly Accumulated in ARF4-as Plants in Stress Conditions

Soluble carbohydrates content was next investigated in *ARF4*-as and WT plant lines in response to different concentrations of NaCl or PEG. In response to salt stress, leaf soluble sugar content decreased by 57.5% in WT plants and was increased by 146% in *ARF4*-as line exposed to 150 mM of NaCl for 2 weeks (Figure S3). In roots, soluble sugar content was also decreased in WT by 49.4%, while an increase around the 191% in soluble sugar content was detected in *ARF4*-as plants. PEG induced osmotic stress imposed to plants significantly decreased soluble sugar contents at all the stress levels in WT and *ARF4*-as plants. Leaf soluble sugar content decreased by 42.8% and 18% respectively in WT and *ARF4*-as plants exposed to 15% of PEG 20,000. In roots, PEG application induced a significant decrease in soluble sugar content by 41.1% (at 15% of PEG 20,000) in WT plants respectively. Meanwhile, a significant increase in soluble carbohydrates content was although reported in *ARF4*-as plants and reached the 67% at 15% PEG 20,000 as compared to the control.

Carbohydrates produced in leaves during photosynthesis are transported throughout the plant by SUTs in order to support plant growth. The *SUT1* proteins are involved in the movement of sucrose into and out of the source and sink tissues and through the phloem via apoplastic pathways [38]. Investigating the expression of the sucrose transporter *SlSUT1* under salt and osmotic stresses had revealed that its expression was induced in WT and *ARF4*-as leaves and roots exposed to salt stress (Figure S4). These findings were also detected in response to osmotic stress. In osmotic stressed leaves, *SlSUT1* was significantly induced in WT and *ARF4*-as plants. In roots, the expression of *SlSUT1* was also up-regulated significantly.

### 3.4.3. ARF4-as Plants Showed Lower Stomatal Conductance

Stomata play a key role in plant response to environmental changes as they control both water loss and $CO_2$ uptake [39]. Stomatal conductance was estimated in WT and *ARF4*-as plants in salt or osmotic stress (Figure 8a,b). Under normal conditions, *ARF4*-as plants exhibited low stomatal conductance as compared to WT plants. Salt and osmotic stress application induces a significant decrease in stomatal conductance in WT. In fact, the reduction in stomatal conductance observed in the WT was around 32% and 46% in response to salt and osmotic stress respectively. Meanwhile, no significant changes in stomatal conductance were detected in *ARF4*-as plants, that still maintained the same values of stomatal conductance observed in normal conditions.

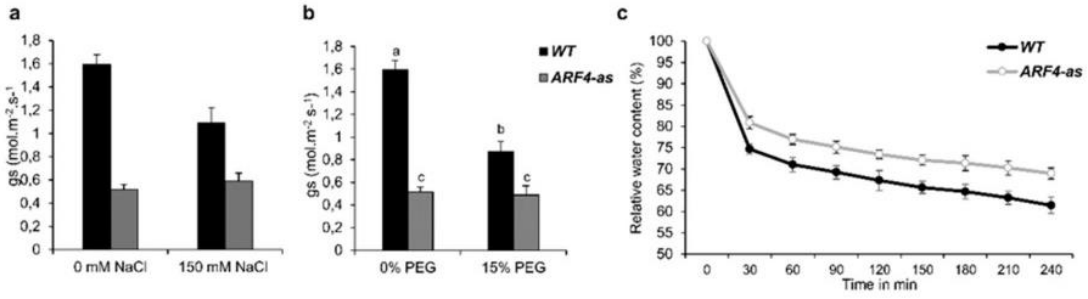


**Figure 8.** Stomatal conductance and relative water content in WT and *ARF4*-as plants. (**a**,**b**) stomatal conductance in salt and osmotic stress conditions, (**c**) relative water content in response to dehydration. Bars with different letters indicate the statistical significance ($p < 0.05$) according to Student Newman-Keuls test.

Stomatal closure can be trigged by various internal and external factors. Schultz (2003) have shown that the decline in leaf water potential can trigger stomatal closure under stressful conditions [40]. Relative water content (RWC) was investigated in WT and *ARF4*-as plants. A remarkable decrease in RWC was observed in both lines (Figure 8c). Up to 25% and 15% of water losses was recorded during the first 30 min of dehydration in WT and *ARF4*-as plants respectively. RWC reached 65% in WT and after 3 h of dehydration while a 28% decrease of water losses was found in *ARF4*-as plants.

#### 3.4.4. ARF4-as Plants Exhibited A High ABA Content

As ABA is the key hormone for regulating stomatal aperture and thus RWC [41], endogenous ABA content of 5 weeks *ARF4*-as and WT plants in normal or under salt and osmotic conditions were then measured in leaf tissues. Our results showed that the ABA content in *ARF4*-as increased by 120% and 101% under salt and osmotic stress conditions respectively whereas in WT plants increased by only 20% in salt conditions and decreased by 26% in PEG treatment (Table 1).

**Table 1.** Abscisic Acid (ABA)content (expressed in µmol/g of FW) in WT and *ARF4*-as leaves in response to salt or osmotic stress conditions. Values presented are mean ± SD of three biological replicates (except for data related to *ARF4*-as plants in osmotic stress conditions, where only two biological replicates were done).

| | **Salt Stress** | | **Osmotic Stress** | |
|---|---|---|---|---|
| | **0 mM NaCl** | **150 mM NaCl** | **0% PEG** | **15% PEG** |
| WT | 0.1272 | 0.1454 | 0.0681 | 0.05 |
| *ARF4*-as | 0.1151 | 0.2636 | 0.0636 | 0.1272 |

Endogenous ABA content is controlled by to the balance between its biosynthesis and its degradation. In tomato, two genes, *SlNCED1* and *SlNCED2*, encoding 9-cis-epoxycarotenoid dioxygenases are responsible for ABA biosynthesis, whereas *SlCYP707A1*, *SlCYP707A2*, *SlCYP707A3* and *SlCYP707A4* encoding ABA 8'-hydroxylase are responsible for ABA catabolism [42]. Investigating the expression of these genes in WT and the *ARF4*-as plants revealed that their expression was significantly regulated by salt or osmotic stress application (Figure 9). Indeed, *SlNCED1* expression was significantly induced in *ARF4*-as leaves after 2 h and 24 h of salt stress exposure while no significant changes was observed in roots. In WT, the expression of *SlNCED1* was significantly up regulated in leaves and roots after 24 h of salt treatment. In response to osmotic stress, the expression of *SlNCED1* was significantly up-regulated in *ARF4*-as roots while no significant change in *SlNCED1* expression was detected in WT plants. *SlNCED2* expression was significantly induced in the *ARF4*-as leaves after 2 h and 24 h of salt application and in WT after 24 h. A significant increase in the expression of *SlNCED2* was detected in *ARF4*-as plants in response to osmotic stress.

The expression pattern of *SlCYP707A1*, *SlCYP707A2* and *SlCYP707A3*, key ABA degradation genes was also assessed in *ARF4*-as and WT plants under salt and osmotic stress conditions (Figure 9). Quantitative RT-PCR results showed that the expression of the ABA metabolism genes was up-regulated in WT leaves after 2 h and 24 h of salt stress exposure. In roots, the expression of *SlCYP707A1* and *SlCYP707A3* was up regulated in WT plants in response to salt stress while a significant repression was reported in the expression of *SlCYP707A2*. Although, the expression of the ABA metabolism genes expression was repressed in the *ARF4*-as salt stressed roots. In response to osmotic stress, the expression of *CYP707A1*, *CYP707A2* and *CYP707A3* was repressed in *ARF4*-as plants while their expression was up regulated in WT roots and downregulated in leaves.

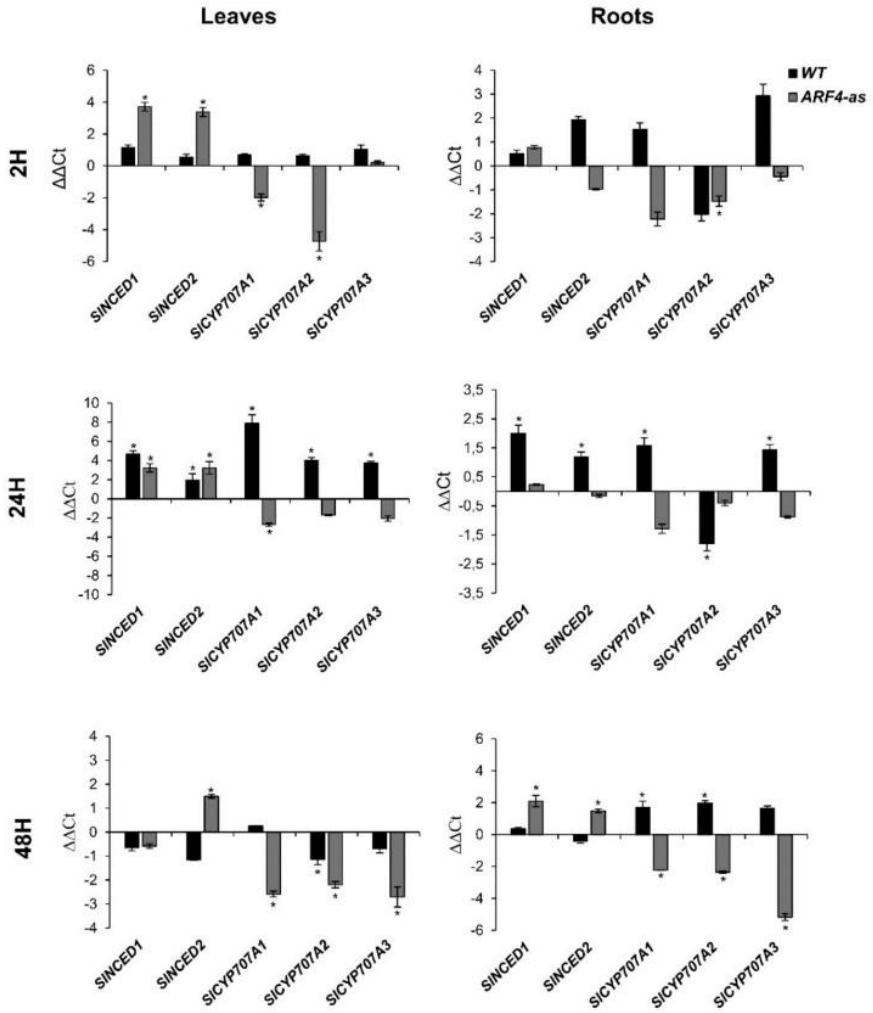


**Figure 9.** Expression of *SlNCED1*, *SlNCED2*, *SlCYP707A1*, *SlCYP707A2* and *SlCYP707A3* genes in WT and *ARF4*-as leaves and roots after 2 h and 24 h of salt stress and 48 h of osmotic stress application. ΔΔCt refers to fold differences in gene expression relative to untreated plants. Values presented are mean ± SD of three biological replicates. Asterisks (*) indicate the statistical significance ($p < 0.05$) according to Student's *t*-test.

### *3.5. Antioxidant Genes Expression is Altered in Response to Salinity and Osmotic Stress*

#### 3.5.1. Cat1 (Catalase) Expression in Response to Salt and Osmotic Stress

Catalases are tetrameric heme-containing enzymes with the potential to directly degrade $H_2O_2$ into $H_2O$ and $O_2$ and essential for ROS detoxification [43]. In angiosperms, catalase is encoded by three genes: *Cat1*, *Cat2* and *Cat3* [44]. We investigated *Cat1* expression in WT and *ARF4*-as plants exposed to salt and osmotic stresses. *Cat1* expression was induced in *ARF4*-as plants exposed to salt stress. A high up regulation in *Cat1* expression was detected in WT roots in response to salt stress (Figure S5). In osmotic stressed leaves, *Cat1* expression was significantly induced in WT while a remarkable but not significant repression was observed in *ARF4*-as plants. Meanwhile, *Cat1* gene expression was highly up regulated or repressed in WT and *ARF4*-as plant roots respectively.

#### 3.5.2. SOD (Superoxide Dismutase) Expression in Response Salt and Osmotic Stress

Superoxide dismutase (SOD) is an enzyme that belongs to the family of metalloenzymes ubiquitous in all aerobic organisms. It is one of the first defenses against ROS induced damages by catalyzing the removal of $O_2^-$ by scavenging it into $O_2$ and $H_2O_2$ [43,44]. Based on the metal ion it binds, SOD are classified into three isozymes; Mn-SOD (in mitochondria), Fe-SOD (in chloroplasts) and Cu/ZnSOD (in cytosol, peroxisomes and chloroplasts) [43]. Investigating the expression of *Cu/ZnSOD* revealed that its expression was remarkably repressed in WT plants subjected to salt and osmotic stresses. Meanwhile, *Cu/ZnSOD* gene expression was induced in *ARF4*-as leaves in response to salt and osmotic stresses while its expression was repressed in the roots (Figure S5).

#### 3.5.3. mdhar (Monodehydroxyascorbate Reductase) Expression in Response to Salt and Osmotic Stress

Monodehydroxyascorbate reductase (MDHAR) is another enzymatic antioxidant indirectly involved in the ROS scavenging through regenerating ascorbic acid, indispensable for the degradation of $H_2O_2$ by the APX enzyme [43]. Investigating the expression pattern of *mdhar* gene in salt stress conditions revealed a significant up regulation in *ARF4*-as leaves and roots while its expression was repressed in WT plants (Figure S5). In response to osmotic stress, the expression of *mdhar* was slightly upregulated in *ARF4*-as leaves. In roots, *mdhar* is significantly up regulated in *ARF4*-as plant line.

### *3.6. SlARF4-Crispr Mutant Exhibited Similar Alteration in Growth and Stomatal Functions Observed in ARF4-as Plants*

*SlARF4* mutants were also generated using CRISPR-Cas9 technology. Two target sequences were located in the *SlARF4* DBD domain and guide RNAs designed to target them. The transformants from T1 generation of line 108 were genotyped (by PCR and DNA sequencing). Based on PCR results, plants #5, #6 and #7 yielded a DNA fragment with a 49bp DNA deletion. The *Cas9* transgene was segregated out in plant #5 while still bearing the desired mutation of *SlARF4* gene. The presence of *Cas9* gene in *arf4-cr* mutants was confirmed in two of the three randomly analyzed plants (Figure 10a). DNA sequencing of *ARF4*-PCR product from plant #5 and #6 revealed that plant #5 harbored a single fragment type containing the expected 49bp DNA deletion. However, only four out of 10 PCR clones from plant #6 hold the 49bp deletion in the DBD domain while the remaining 6 PCR clones showed although a small deletion in both target regions (Figure 10b). At the morphological level, the T1 generation plants showed dramatic up curling phenotype, similar to *ARF4*-as plants (Figure 10c, d).

Besides the leaf curling phenotype, the *arf4-cr* mutant (#5) showed a significant decrease in leaf, root and stem dry weight as compared to its WT siblings (Figure 11a–c). Leaf area was also significantly lower in *SlARF4*-Crispr plants (Figure 11d). Moreover, as expected, net $CO_2$ assimilation rate ($A$) and stomatal conductance ($g_s$) was significantly lower in *arf4-cr* plants than in WT while water use efficiency was significantly higher in *arf4-cr* mutant (Figure 12). Regarding the agronomical traits, plant productivity and quality were not affected by knoking out *SlARF4* with CRISPR technology. Yield and fruit fresh weight of *arf4-cr* plants were slightly but not significantly higher as compared to WT while equatorial and polar diameter of *arf4-cr* fruits were significantly higher (Figure S6). *arf4-cr* plants showed similar growth and stomatal variations compared to *ARF4*-as plants mainly in stem weight, root weight, $CO_2$ assimilation and stomatal conductance (Figure 2, Figure 4 and Figure S3). Thus, these results pointed out the efficiency of CRISPR technology as a substitute to the antisense technology for gene manipulation.

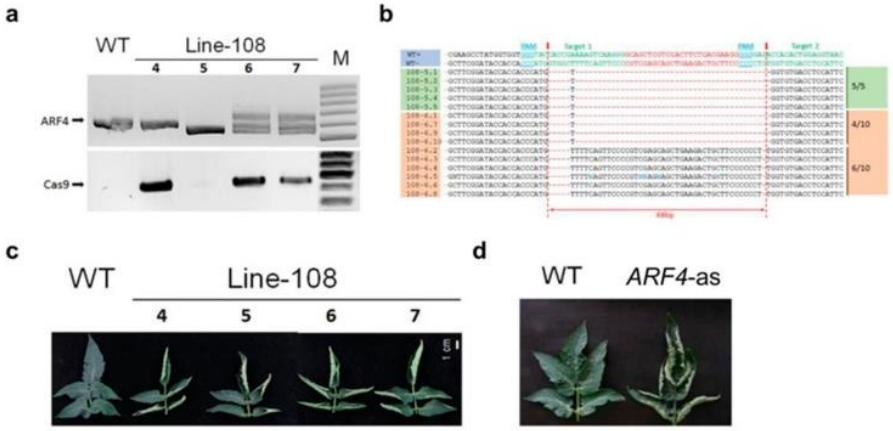


**Figure 10.** CRISPR-Cas9 mediated gene editing in tomato Micro-Tom. (**a**) PCR genotyping of plants at the T1 generation of line-108. Deletion mutations of *SlARF4* were found in plants #4, #5, #6 and #7. Among these, the T-DNA insertion (CRISPR-Cas9 transgene) was segregated out in plant #5 while still bearing the desired mutation in the *SlARF4* gene. (**b**) Sequencing data of *ARF4*-PCR products from #5 and #6 plants. The PCR products from plant #5 yielded a single fragment type containing the expected 49bp DNA deletion, whereas in the case of plant #6, only 4 out of 10 PCR clones contain the desired mutation, the remaining 6 PCR clones exhibited a small deletion in both target regions. Red dashed indicated the expected cleavage sites for CRISPR-Cas9. (**c**) Leaf phenotype of CRISPR-Cas9 generated *ARF4* mutants. (**d**) All four plants showed dramatic leaf curling, similar to the phenotype observed in *ARF4*-as plants.

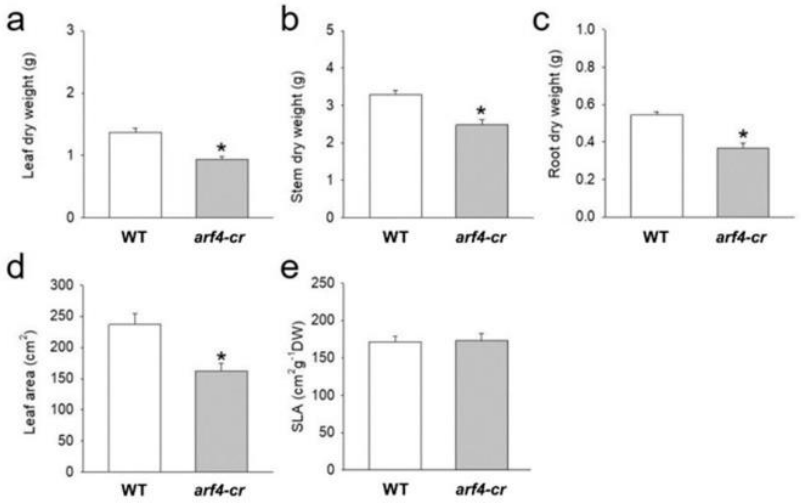


**Figure 11.** Dry weight and parameters related with leaf area for Micro-Tom (WT) and *arf4-cr*, 45 days after germination. (**a**) leaf dry weight, (**b**) stem dry weight, (**c**) root dry weight, (**d**) leaf area and (**e**) Specific leaf area (SLA). Values are means ± s.e.m ($n$ = 8). Asterisks indicate values that were determined by Student's t test to be significantly different ($p < 0.05$) from the Micro-tom (WT).

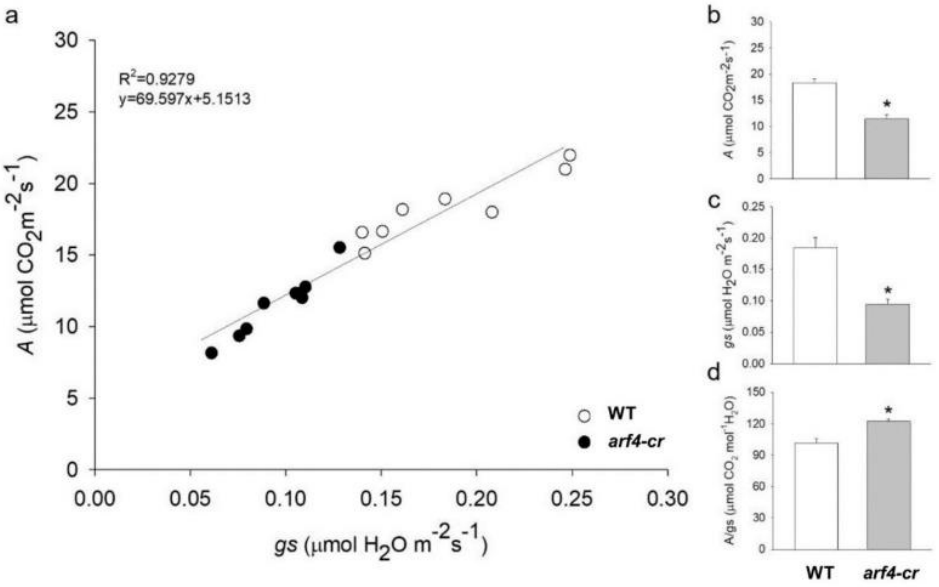


**Figure 12.** Relationship between net $CO_2$ assimilation rate ($A$) and stomatal conductance ($g_s$) for Micro-Tom (WT) and *arf4-cr*. (**a**) $CO_2$ assimilation rate ($A$) as a function of stomatal conductance ($g_s$), (**b**) net $CO_2$ assimilation rate ($A$), (**c**) stomatal conductance ($g_s$), (**d**) intrinsic water efficiency ($A/g_s$). Values are means ± s.e.m ($n$ = 8). Asterisks indicate values that were determined by Student's t test to be significantly different ($p < 0.05$) from the wild type (WT).

## 4. Discussion

In the face of a global scarcity of water resources and the increased water and soil salinization, abiotic stresses present major challenges in sustaining crop yield. Plant tolerance to these stresses relies on the implementation of molecular mechanisms for cellular adjustments, including signal perception and transduction cascades, transcriptional networks and adaptive metabolic pathways. Plant hormones such as ABA, ethylene and SA play an important role in mediating plant responses to stresses. Auxin, the key regulator of many aspects of plant growth and development, could be a key player in plant response to biotic and abiotic stress. ARFs play crucial role in auxin signaling. *ARF4* is involved in the regulation of several processes such as lateral root development, fruit quality and development [14,15,45]. Here, we demonstrated that the downregulation of *ARF4* confers tolerance to salt and osmotic stress. Interestingly, even under stress conditions, *ARF4*-as plants show (i) a normal plant development, (ii) high chlorophyll content along with a significant accumulation of sugars, (iii) an increase in ABA content and a higher WUE, (iv) a significant upregulation of antioxidants and thus (iv) an enhanced stress tolerance compared to WT plants. These multiple fitness benefits obtained by downregulating *ARF4* in plants constitute a desirable trait for horticultural crops.

Successful plant growth relies on the plasticity in leaf anatomical characteristics, which enables plants to cope with diverse stress environments [46]. The transcriptional downregulation of *ARF4* leads to severe leaf curling along the longitudinal axis which was consistent with that observed in DR12-ASL lines generated in the Kemer cultivar by Jones et al. (2002) and those obtained in Micro Tom by Sagar et al. (2013) [14,15]. Leaf rolling is a one of the most common responses to water stress [47]. It has been reported that greater leaf rolling may be an important indicator linked to osmotic tolerance and may have a positive impact on crop yield under water stress conditions [48]. Plants with a leaf rolling mechanism exhibit a resistance to osmotic and high temperature and had higher WUE. This was explained by the fact that leaf rolling reduced transpiration rate [47].

Plants' tolerance to abiotic stress depends also on their ability to adjust the relationship between water, transpiration, photosynthesis and water use efficiency through stomatal changes in order to maximize $CO_2$ assimilation [49]. In fact, the decrease in stomatal conductance can enhance plant

tolerance to osmotic stress of many plant species such as chickpea and rice [50,51]. *ARF4*-as plants showed decreased stomatal conductance coupled with an increase in WUE, suggesting that the downregulation of *ARF4* can lead to a better tolerance to abiotic stresses. Thus, the combination of a marked leaf curling phenotype associated with decreased $g_s$ and high WUE in *ARF4*-as plants suggests that these plants might tolerate better salinity and water deficit.

The auxin response has emerged recently as an active player in plant response to abiotic stresses [51]. Extensive research has shown that various environmental signals are associated with changes in auxin homeostasis, redistribution, and signaling [52]. Accumulating evidence indicates that auxin plays a role in plant responses to abiotic stresses through complex metabolic and signaling networks. Auxin coordinates plant development essentially through two groups of transcriptional regulators Aux/IAA and ARFs [3]. Genome-wide expression analyses have suggested that the expression of numerous *ARF* genes change when plants respond to abiotic stresses in many plant species [7,9,53,54]. In tomato, expression profiling of the *ARF* family under abiotic stress conditions showed that most of the tomato *ARF*s were responsive and some of them were significantly regulated [17]. Among them, *SlARF4* expression was significantly induced in tomato plants in response to salt (24 h) or drought (five days). Additionally, the *SlARF4* regulatory region was enriched in *cis*-acting elements specific to salinity and water deficit response [17]. In this work, *ARF4* expression assessed both *in vitro* and *in planta* was affected by either salt, drought or osmotic treatment, which suggests that this gene is involved in tomato response to those stresses.

Plant growth and development are heavily constrained by salinity and water deficit [55]. In the current study, plant growth evaluated through fresh weight was significantly affected in WT and *ARF4*-as transgenic plants in response to salt or osmotic stress. The reduction in fresh weight was reported in many plant species which includes barley and cabbage in response to salinity or water deficit [56,57]. The decrease in seedling growth (evaluated through the measurement of fresh weight) is due to restricted cell division and enlargement, as salt and drought stress directly reduces growth by decreasing cell division and elongation [58]. However, the reduction in fresh weight was less pronounced in the *ARF4*-as plants which suggest that *ARF4*-as plants might tolerate better salt and osmotic stress than the other plant lines.

The root system is the first organ to encounter salinity and drought stress. Root development can be severely affected by environmental stresses [59]. In *Arabidopsis*, root length and development was significantly reduced in response to salinity [60]. In this study, we had noticed a significant decrease in primary root length in WT and in *ARF4-as* plants in response to salt or osmotic stress conditions as compared with normal conditions. However, less reduction was reported in *ARF4*-as plants. In general, deeper rooting has been shown to be beneficial for plant production and survival as it increases water uptake which confer the advantage to support plant growth during adverse conditions [61]. Numerous studies have linked plant stress tolerance with the increase in root length and density for several plant species such as barley, sunflower, wheat, rice and cotton [37]. *ARF4*-as plants showed less reduction in primary root length coupled with an increase in root density. *ARF4* was found to be implicated in defining root architecture in *Arabidopsis* under optimal growth conditions through the control of lateral root emergence [45] which suggest that this gene might play an important role in root architecture in stress conditions and thus contribute to the improvement tomato tolerance to salinity and osmotic stress.

Plants' photosynthesis activity is known to be affected by abiotic stress [37]. Stress-induced decrease in chlorophyll content have been reported in several plant species including tomato [62]. Zarafshar et al. (2014) explained this decrease as the result of pigment photo-oxidation and chlorophyll degradation [63]. *ARF4*-as plants showed although a slight decrease in total chlorophyll content in response to salt stress and a slight increase in osmotic stress conditions. Tomato tolerant genotypes showed less reductions in photosynthetic pigments [64]. The lack of changes in chlorophyll content in the *ARF4*-as plants shows the capacity to preserve the photosynthetic apparatus and thus indicates their better tolerance to salinity and osmotic stress.

Metabolic activities in plant cells are very complex, and various biochemical pathways are interconnected with each other, working in coherence towards cellular homeostasis [65]. High concentration of osmolytes including sugars help plants to tolerate abiotic stresses by improving their ability to preserve osmotic balance within the cells [66]. To assess this, we studied sugars accumulation to correlate their levels with the presence or the absence of *SlARF4* function. We found that soluble sugars content (Figure S3) increased more in *ARF4*-as transgenic plants than in WT in response to salt or osmotic stresses. Besides its accumulation under stress conditions, sugars can be transported to different organs of the plant. *SUT1*; gene encoding for a sucrose transporter, was found to be upregulated in *ARF4*-as plants in response to salt or osmotic stress. Previous studies had reported an increase in *SUT1* transcript in sugarcane leaves after 24 h of osmotic treatment with PEG [67]. Thus, its upregulation in *ARF4*-as might improve tolerance to osmotic and salinity through the stimulation of sucrose transport required for the osmoregulation and for the cellular energy demands during salt or osmotic stresses.

Stomata are known for their role in the regulation of gas exchange and water loss by transpiration [68]. Their opening and closing is affected by environmental and internal parameters that maintain the water balance and functioning of complex signal transduction pathways [69]. Salt, drought and osmotic tolerance was correlated with a decline in stomatal conductance in many plant species [50,70]. In this work, we found that the downregulation of *SlARF4* resulted in reduced stomatal conductance under salt and osmotic stresses along with a high RWC, which suggests the involvement of *ARF4* in the regulation of stomatal closure in order to prevent water loss through transpiration to cope with salt or drought conditions.

ABA content is closely defined by the balance between its biosynthesis and biodegradation. In tomato, ABA biosynthesis is governed by the activity of *SlNCED1* and *SlNCED2*, whereas *SlCYP707A1*, *SlCYP707A2*, *SlCYP707A3* and *SlCYP707A4* encoding ABA 8′-hydroxylase are main genes for ABA catabolism [42]. Water stress is known to induce the expression of *NCED* genes in tomato [71]. Moreover, transgenic plants overexpressing the *NCED* gene accumulated large amounts of ABA and were more resistant to drought stress [72]. Regarding ABA biodegradation genes, *Arabidopsis* knock-out mutant *cyp707a3-1* accumulated higher endogenous ABA levels coupled with a reduced transpiration rate, thereby resulting in a phenotype exhibiting enhanced tolerance to drought stress [73]. The significant increase in *SlNCED1* expression in *ARF4*-as leaves and roots along with the repression of the three ABA catabolism genes in normal and salt stress conditions explain the increase in the concentration of ABA in leaves. This finding suggests the involvement of *ARF4* in the regulation of ABA synthesis and provides clues on the existence of a possible cross talk between auxin and ABA signaling pathways.

In plants, abiotic stresses induce the overproduction of reactive oxygen species (ROS), a highly reactive and toxic molecules that cause damage to proteins, lipids, carbohydrates and DNA and results ultimately in oxidative stress [43]. The ability of plants to mitigate the negative effects of abiotic stresses relays on the efficiency of the antioxidant defense systems to protect plant cells from oxidative damage by scavenging ROS accumulation. The key enzymatic antioxidants are catalase, superoxide dismutase (SOD), monodehydroascorbate reductase (MDHAR), dehydroascorbate reductase (DHAR) [43]. Several studies have linked abiotic stress tolerance to an overproduction of antioxydants in many plant species including tomato [74]. Genetic manipulation of genes encoding for these antioxydants increased plant tolerance to a wide range of abiotic stresses. For instance, the overproduction of a bacterial *cat1* gene improved tolerance to salinity in tomato [69]. Rice plants engineered to express a bacterial *cat1* gene showed increased tolerance to osmotic stress [75]. The overexpression of Rice cytosolic Cu/Zn-SOD in chloroplasts of tobacco plant improved their photosynthetic performance during photooxidative stresses such as high salt or drought stresses [76]. The overexpression of *mdhar* in transgenic tobacco increased the tolerance against salt and osmotic stresses [77]. Here, we found that the expression of *mdhar* and *SOD* genes was significantly upregulated in *ARF4*-as plants in response to either salt or osmotic stress, which suggest that the down regulation of *ARF4* improved tomato tolerance to salt and osmotic stresses by reducing ROS accumulation mainly through antioxidant enzymes activities.

The down regulation of *SlARF4* induced many alterations on plant growth and stomatal functions. *ARF4*-as plants exhibited leaf-curling phenotype, low stomatal conductance along with an increase in WUE. We have previously demonstrated a connection between flowering time, auxin signaling and WUE in tomato [78,79]. It will be interesting to explore the role of *ARF4* in these pathways. In response to stress, the down regulation of *ARF4* results in a better root development, an accumulation of sugars and a high chlorophyll content alongside with a low stomatal conductance, a high RWC and ABA content. The expression of some antioxidant genes and ABA biosynthesis genes was significantly induced in *ARF4*-as plants conferring to these transgenic plants a better tolerance to salinity and osmotic stress. *ARF4* CRISPR mutant shared similar growth and stomatal responses than those observed in *ARF4*-as. Thus, the use of gene-editing technology could represent a promising avenue for the incorporation of valuable abiotic stress tolerance traits in tomato and other horticultural crops [80,81].

## 5. Conclusions

This study provides clues on the involvement of *ARF4* in the acquisition of salt and drought tolerance in tomato. We found that the downregulation of *SlARF4* increases tomato tolerance to salinity and drought stress. Indeed, loss of *SlARF4* function increases root length and density resulting in improved development of the root system. Furthermore, *ARF4*-as plants displayed leaf curling, lower stomatal conductance, higher WUE under normal conditions and maintained high level of chlorophyll content even in stress conditions suggesting that their photosynthetic activity was less affected by stress. Total carbohydrates were accumulated in high proportion in photosynthetic tissues of *ARF4*-as plants. At the molecular level, the expression of the sucrose transporter *LeSUT1* was significantly up-regulated in *ARF4*-as which might explain carbohydrates accumulation in root tissues. *Cu/ZnSOD* and *mdhar* genes were found to be up-regulated in *ARF4*-as plants suggesting that *ARF4*-as mutant is more tolerant to salt and water stress. Furthermore, *SlARF4*-as plants showed a significant increase in ABA content associated with a low stomatal conductance under stressful conditions. This increase in ABA content is due to the activation of ABA biosynthesis genes and the repression of ABA catabolism genes. Besides, *ARF4* mutant generated by CRISPR technology (*arf4-cr*) displayed similar growth and stomatal responses as *ARF4*-as which enable us to confirm the role of *SlARF4*. taken together, the data presented in this work brings new elements on auxin involvement in stress tolerance in tomato and underlines the role of *ARF4* in this process providing new insights for the use of genetic editing technologies to breed abiotic stress tolerant crops.

**Supplementary Materials:** The following are available online at http://www.mdpi.com/2073-4425/11/3/272/s1, Figure S1: Stomatal responses to irradiance and $CO_2$ levels in Micro-Tom (WT) and *ARF4*-as transgenic line, Figure S2. Productive parameters in tomato Micro-Tom (WT) and *ARF4*-as transgenic line, Figure S3. Photosynthesis and sugar accumulation in WT and *ARF4*-as plants exposed to different concentrations of NaCl or PEG, Figure S4. Expression of sucrose transporter *SlSUT1* in WT and *ARF4*-as plants exposed to salt or osmotic stresses, Figure S5. Expression of *Cat1*, *mdhar* and *SOD* in WT and *ARF4*-as plants exposed to salt or osmotic stresses, Figure S6. Productive parameters in tomato Micro-Tom (WT) and *arf4-cr* transgenic line, Table S1: Gene ID and quantitative RT-PCR primers, Table S2. Characterization of photosynthetic parameters in tomato cv. Micro-Tom (WT) and isogenic *ARF4* antisense transgenic line (*ARF4*-as) Vcmax.

**Author Contributions:** All authors have read and agree to the published version of the manuscript. Conceptualization, N.B., M.B, A.Z., A.S. and M.Z.; methodology, A.Z., A.S. and M.Z.; formal analysis, S.B., K.G., G.H., M.A.M.B., B.L.R.; writing original draft preparation, S.B., A.Z., K.G, A.S. and M.Z.; writing—review and editing, N.B., M.B., M.F., A.Z., A.S. and M.Z.; supervision, A.Z., A.S. and M.Z.; funding acquisition, M.Z. All authors have read and agreed to the published version of the manuscript.

**Funding:** This research was supported by Labex TULIP (ANR-10-LABX-41), by the ANR TomEpiSet project, by Hubert-Curien partnership program Volubilis {MA/12/280-27105PL} and benefited from networking activities within the European COST Action FA1106.

**Acknowledgments:** The authors are grateful to L. Lemonnier, D. Saint-Martin and O. Berseille for genetic transformation and culture of tomato plants and I. Mila for the cloning.

**Conflicts of Interest:** All Authors have read, edited and approved the final version of the manuscript. They have declared that no competing interests exist.

## References

1. Vanneste, S.; Friml, J. Auxin: A trigger for change in plant development. *Cell* **2009**, *136*, 1005–1016. [CrossRef]
2. Szemenyei, H.; Hannon, M.; Long, J.A. TOPLESS mediates auxin-dependent transcriptional repression during Arabidopsis embryogenesis. *Science* **2008**, *319*, 1384–1386. [CrossRef] [PubMed]
3. Guilfoyle, T.J.; Hagen, G. Auxin response factors. *Curr. Opin. Plant Biol.* **2007**, *10*, 453–460. [CrossRef] [PubMed]
4. Zouine, M.; Fu, Y.; Chateigner-Boutin, A.-L.; Mila, I.; Frasse, P.; Wang, H.; Audran, C.; Roustan, J.-P.; Bouzayen, M. Characterization of the tomato ARF gene family uncovers a multi-levels post-transcriptional regulation including alternative splicing. *PLoS ONE* **2014**, *9*, e84203. [CrossRef] [PubMed]
5. Li, S.-B.; Xie, Z.-Z.; Hu, C.-G.; Zhang, J.-Z. A review of auxin response factors (ARFs) in plants. *Front. Plant Sci.* **2016**, *7*, 47. [CrossRef]
6. Ulmasov, T.; Murfett, J.; Hagen, G.; Guilfoyle, T.J. Aux/IAA proteins repress expression of reporter genes containing natural and highly active synthetic auxin response elements. *Plant Cell* **1997**, *9*, 1963–1971.
7. Jain, M.; Khurana, J.P. Transcript profiling reveals diverse roles of auxin-responsive genes during reproductive development and abiotic stress in rice. *FEBS J.* **2009**, *276*, 3148–3162. [CrossRef]
8. Xing, H.; Pudake, R.N.; Guo, G.; Xing, G.; Hu, Z.; Zhang, Y.; Sun, Q.; Ni, Z. Genome-wide identification and expression profiling of auxin response factor (ARF) gene family in maize. *BMC Genomics* **2011**, *12*, 178. [CrossRef]
9. Hu, W.; Zuo, J.; Hou, X.; Yan, Y.; Wei, Y.; Liu, J.; Li, M.; Xu, B.; Jin, Z. The auxin response factor gene family in banana: Genome-wide identification and expression analyses during development, ripening, and abiotic stress. *Front. Plant Sci.* **2015**, *6*, 742. [CrossRef]
10. Tang, Y.; Bao, X.; Liu, K.; Wang, J.; Zhang, J.; Feng, Y.; Wang, Y.; Lin, L.; Feng, J.; Li, C. Genome-wide identification and expression profiling of the auxin response factor (ARF) gene family in physic nut. *PLoS ONE* **2018**, *13*, e0201024. [CrossRef]
11. Zhang, X.; Yan, F.; Tang, Y.; Yuan, Y.; Deng, W.; Li, Z. Auxin response gene SlARF3 plays multiple roles in tomato development and is involved in the formation of epidermal cells and trichomes. *Plant Cell Physiol.* **2015**, *56*, 2110–2124. [PubMed]
12. Breitel, D.A.; Chappell-Maor, L.; Meir, S.; Panizel, I.; Puig, C.P.; Hao, Y.; Yifhar, T.; Yasuor, H.; Zouine, M.; Bouzayen, M. AUXIN RESPONSE FACTOR 2 intersects hormonal signals in the regulation of tomato fruit ripening. *PLoS Genet.* **2016**, *12*, e1005903. [CrossRef] [PubMed]
13. Liu, N.; Wu, S.; Van Houten, J.; Wang, Y.; Ding, B.; Fei, Z.; Clarke, T.H.; Reed, J.W.; Van Der Knaap, E. Down-regulation of AUXIN RESPONSE FACTORS 6 and 8 by microRNA 167 leads to floral development defects and female sterility in tomato. *J. Exp. Bot.* **2014**, *65*, 2507–2520. [CrossRef] [PubMed]
14. Jones, B.; Frasse, P.; Olmos, E.; Zegzouti, H.; Li, Z.G.; Latché, A.; Pech, J.C.; Bouzayen, M. Down-regulation of DR12, an auxin-response-factor homolog, in the tomato results in a pleiotropic phenotype including dark green and blotchy ripening fruit. *Plant J.* **2002**, *32*, 603–613. [CrossRef] [PubMed]
15. Sagar, M.; Chervin, C.; Mila, I.; Hao, Y.; Roustan, J.-P.; Benichou, M.; Gibon, Y.; Biais, B.; Maury, P.; Latché, A. Sl-ARF4, an Auxin Response Factor involved in the control of sugar metabolism during tomato fruit development. *Plant Physiol.* **2013**, *161*, 1362–1374. [CrossRef] [PubMed]
16. Yuan, Y.; Mei, L.; Wu, M.; Wei, W.; Shan, W.; Gong, Z.; Zhang, Q.; Yang, F.; Yan, F.; Zhang, Q.; et al. SlARF10, an auxin response factor, is involved in chlorophyll and sugar accumulation during tomato fruit development. *J. Exp. Bot.* **2018**, *69*, 5507–5518. [CrossRef]
17. Bouzroud, S.; Gouiaa, S.; Hu, N.; Bernadac, A.; Mila, I.; Bendaou, N.; Smouni, A.; Bouzayen, M.; Zouine, M. Auxin Response Factors (ARFs) are potential mediators of auxin action in tomato response to biotic and abiotic stress (Solanum lycopersicum). *PLoS ONE* **2018**, *13*, e0193517. [CrossRef]
18. Wang, H.; Jones, B.; Li, Z.; Frasse, P.; Delalande, C.; Regad, F.; Chaabouni, S.; Latche, A.; Pech, J.-C.; Bouzayen, M. The tomato Aux/IAA transcription factor IAA9 is involved in fruit development and leaf morphogenesis. *Plant Cell* **2005**, *17*, 2676–2692. [CrossRef]
19. Brooks, C.; Nekrasov, V.; Lippman, Z.B.; Van Eck, J. Efficient gene editing in tomato in the first generation using the clustered regularly interspaced short palindromic repeats/CRISPR-associated9 system. *Plant Physiol.* **2014**, *166*, 1292–1297. [CrossRef]

20. Lei, Y.; Lu, L.; Liu, H.-Y.; Li, S.; Xing, F.; Chen, L.-L. CRISPR-P: A web tool for synthetic single-guide RNA design of CRISPR-system in plants. *Mol. Plant* **2014**, *7*, 1494–1496. [CrossRef]
21. Barbosa, M.A.M.; Chitwood, D.H.; Azevedo, A.A.; Araújo, W.L.; Ribeiro, D.M.; Peres, L.E.P.; Martins, S.C.V.; Zsögön, A. Bundle sheath extensions affect leaf structural and physiological plasticity in response to irradiance. *Plant Cell Environ.* **2019**, *42*, 1575–1589. [CrossRef] [PubMed]
22. Gasparini, K.; Costa, L.C.; Brito, F.A.; Pimenta, T.M.; Cardoso, F.B.; Araújo, W.L.; Zsögön, A.; Ribeiro, D.M. Elevated $CO_2$ induces age-dependent restoration of growth and metabolism in gibberellin-deficient plants. *Planta* **2019**, *250*, 1147–1161. [CrossRef] [PubMed]
23. Hunt, R. Plant growth analysis: Second derivatives and compounded second derivatives of splined plant growth curves. *Ann. Bot.* **1982**, *50*, 317–328. [CrossRef]
24. Farquhar, G.D.; von Caemmerer, S.V.; Berry, J.A. A biochemical model of photosynthetic $CO_2$ assimilation in leaves of C 3 species. *Planta* **1980**, *149*, 78–90. [CrossRef]
25. Rodeghiero, M.; Niinemets, Ü.; Cescatti, A. Major diffusion leaks of clamp-on leaf cuvettes still unaccounted: How erroneous are the estimates of Farquhar et al. model parameters? *Plant Cell Environ.* **2007**, *30*, 1006–1022. [CrossRef]
26. Lawson, T.; von Caemmerer, S.; Baroli, I. Photosynthesis and stomatal behaviour. In *Progress in Botany 72*; Springer: Berlin/Heidelberg, Germany, 2010; pp. 265–304.
27. Broughton, W.; Dilworth, M. Control of leghaemoglobin synthesis in snake beans. *Biochem. J.* **1971**, *125*, 1075–1080. [CrossRef]
28. Bassa, C.; Mila, I.; Bouzayen, M.; Audran-Delalande, C. Phenotypes associated with down-regulation of Sl-IAA27 support functional diversity among Aux/IAA family members in tomato. *Plant Cell Physiol.* **2012**, *53*, 1583–1595. [CrossRef]
29. Dubois, M.; Gilles, K.A.; Hamilton, J.K.; Rebers, P.T.; Smith, F. Colorimetric method for determination of sugars and related substances. *Anal. Chem.* **1956**, *28*, 350–356. [CrossRef]
30. Forcat, S.; Bennett, M.H.; Mansfield, J.W.; Grant, M.R. A rapid and robust method for simultaneously measuring changes in the phytohormones ABA, JA and SA in plants following biotic and abiotic stress. *Plant Methods* **2008**, *4*, 16. [CrossRef]
31. Jaulneau, V.; Lafitte, C.; Jacquet, C.; Fournier, S.; Salamagne, S.; Briand, X.; Esquerré-Tugayé, M.-T.; Dumas, B. Ulvan, a Sulfated Polysaccharide from Green Algae, Activates Plant Immunity through the Jasmonic Acid Signaling Pathway. *J. Biomed. Biotechnol.* **2010**, *2010*. [CrossRef]
32. Smart, R.E.; Bingham, G.E. Rapid estimates of relative water content. *Plant Physiol.* **1974**, *53*, 258–260. [CrossRef] [PubMed]
33. Bernacchi, C.J.; Rosenthal, D.M.; Pimentel, C.; Long, S.P.; Farquhar, G.D. Modeling the Temperature Dependence of C3 Photosynthesis. In *Photosynthesis in silico: Understanding Complexity from Molecules to Ecosystems*; Laisk, A., Nedbal, L., Govindjee, Eds.; Advances in Photosynthesis and Respiration; Springer: Dordrecht, The Netherlands, 2009; ISBN 978-1-4020-9237-4.
34. Jiang, Q.; Roche, D.; Monaco, T.; Hole, D. Stomatal conductance is a key parameter to assess limitations to photosynthesis and growth potential in barley genotypes. *Plant Biol.* **2006**, *8*, 515–521. [CrossRef] [PubMed]
35. Ashraf, M.; Harris, P.J. Photosynthesis under stressful environments: An overview. *Photosynthetica* **2013**, *51*, 163–190. [CrossRef]
36. De Jong, M.; Mariani, C.; Vriezen, W.H. The role of auxin and gibberellin in tomato fruit set. *J. Exp. Bot.* **2009**, *60*, 1523–1532. [CrossRef] [PubMed]
37. Munns, R.; James, R.A.; Läuchli, A. Approaches to increasing the salt tolerance of wheat and other cereals. *J. Exp. Bot.* **2006**, *57*, 1025–1043. [CrossRef]
38. Jia, W.; Zhang, L.; Wu, D.; Liu, S.; Gong, X.; Cui, Z.; Cui, N.; Cao, H.; Rao, L.; Wang, C. Sucrose transporter AtSUC9 mediated by a low sucrose level is involved in Arabidopsis abiotic stress resistance by regulating sucrose distribution and ABA accumulation. *Plant Cell Physiol.* **2015**, *56*, 1574–1587. [CrossRef]
39. Damour, G.; Simonneau, T.; Cochard, H.; Urban, L. An overview of models of stomatal conductance at the leaf level. *Plant Cell Environ.* **2010**, *33*, 1419–1438. [CrossRef]
40. Schultz, H.R. Differences in hydraulic architecture account for near-isohydric and anisohydric behaviour of two field-grown Vitis vinifera L. cultivars during drought. *Plant Cell Environ.* **2003**, *26*, 1393–1405. [CrossRef]
41. Leymarie, J.; Lascève, G.; Vavasseur, A. Interaction of stomatal responses to ABA and $CO_2$ in Arabidopsis thaliana. *Funct. Plant Biol.* **1998**, *25*, 785–791. [CrossRef]

42. Yang, R.; Yang, T.; Zhang, H.; Qi, Y.; Xing, Y.; Zhang, N.; Li, R.; Weeda, S.; Ren, S.; Ouyang, B. Hormone profiling and transcription analysis reveal a major role of ABA in tomato salt tolerance. *Plant Physiol. Biochem.* **2014**, *77*, 23–34. [CrossRef]
43. Das, K.; Roychoudhury, A. Reactive oxygen species (ROS) and response of antioxidants as ROS-scavengers during environmental stress in plants. *Front. Environ. Sci.* **2014**, *2*, 53. [CrossRef]
44. Choudhury, S.; Panda, P.; Sahoo, L.; Panda, S.K. Reactive oxygen species signaling in plants under abiotic stress. *Plant Signal. Behav.* **2013**, *8*, e23681. [CrossRef] [PubMed]
45. Marin, E.; Jouannet, V.; Herz, A.; Lokerse, A.S.; Weijers, D.; Vaucheret, H.; Nussaume, L.; Crespi, M.D.; Maizel, A. miR390, Arabidopsis TAS3 tasiRNAs, and their AUXIN RESPONSE FACTOR targets define an autoregulatory network quantitatively regulating lateral root growth. *Plant Cell* **2010**, *22*, 1104–1117. [CrossRef] [PubMed]
46. Pereira-Netto, A.B.D.; Gabriele, A.C.; Pinto, H.S. Aspects of leaf anatomy of kudzu (Pueraria lobata, Leguminosae-Faboideae) related to water and energy balance. *Pesqui. Agropecu. Bras.* **1999**, *34*, 1361–1365. [CrossRef]
47. Kadioglu, A.; Terzi, R.; Saruhan, N.; Saglam, A. Current advances in the investigation of leaf rolling caused by biotic and abiotic stress factors. *Plant Sci.* **2012**, *182*, 42–48. [CrossRef]
48. Fen, L.L.; Ismail, M.R.; Zulkarami, B.; Rahman, M.S.A.; Islam, M.R. Physiological and molecular characterization of drought responses and screening of drought tolerant rice varieties. *Biosci. J.* **2015**, *31*, 709–718. [CrossRef]
49. Zhang, Y.; Wang, Z.; Wu, Y.; Zhang, X. Stomatal characteristics of different green organs in wheat under different irrigation regimes. *Zuo Wu Xue Bao* **2006**, *32*, 70–75.
50. Mafakheri, A.; Siosemardeh, A.; Bahramnejad, B.; Struik, P.; Sohrabi, Y. Effect of drought stress on yield, proline and chlorophyll contents in three chickpea cultivars. *Aust. J. Crop Sci.* **2010**, *4*, 580.
51. Rahman, A. Auxin: A regulator of cold stress response. *Physiol. Plant.* **2013**, *147*, 28–35. [CrossRef]
52. Navarro, L.; Dunoyer, P.; Jay, F.; Arnold, B.; Dharmasiri, N.; Estelle, M.; Voinnet, O.; Jones, J.D. A plant miRNA contributes to antibacterial resistance by repressing auxin signaling. *Science* **2006**, *312*, 436–439. [CrossRef]
53. Wang, S.; Bai, Y.; Shen, C.; Wu, Y.; Zhang, S.; Jiang, D.; Guilfoyle, T.J.; Chen, M.; Qi, Y. Auxin-related gene families in abiotic stress response in Sorghum bicolor. *Funct. Integr. Genomics* **2010**, *10*, 533–546. [CrossRef]
54. Van Ha, C.; Le, D.T.; Nishiyama, R.; Watanabe, Y.; Sulieman, S.; Tran, U.T.; Mochida, K.; Van Dong, N.; Yamaguchi-Shinozaki, K.; Shinozaki, K. The auxin response factor transcription factor family in soybean: Genome-wide identification and expression analyses during development and water stress. *DNA Res.* **2013**, *20*, 511–524. [CrossRef] [PubMed]
55. Guóth, A.; Tari, I.; Gallé, Á.; Csiszár, J.; Pécsváradi, A.; Cseuz, L.; Erdei, L. Comparison of the drought stress responses of tolerant and sensitive wheat cultivars during grain filling: Changes in flag leaf photosynthetic activity, ABA levels, and grain yield. *J. Plant Growth Regul.* **2009**, *28*, 167–176. [CrossRef]
56. Farooq, M.; Wahid, A.; Kobayashi, N.; Fujita, D.; Basra, S.M.A. Plant Drought Stress: Effects, Mechanisms and Management. In *Sustainable Agriculture*; Lichtfouse, E., Navarrete, M., Debaeke, P., Véronique, S., Alberola, C., Eds.; Springer: Dordrecht, The Netherlands, 2009; pp. 153–188. ISBN 978-90-481-2666-8.
57. Fayez, K.A.; Bazaid, S.A. Improving drought and salinity tolerance in barley by application of salicylic acid and potassium nitrate. *J. Saudi Soc. Agric. Sci.* **2014**, *13*, 45–55. [CrossRef]
58. Akıncı, Ş.; Lösel, D.M. Plant water-stress response mechanisms. In *Water stress*; InTech: Rijeca, Croatia, 2012.
59. Kurth, E.; Cramer, G.R.; Läuchli, A.; Epstein, E. Effects of NaCl and CaCl2 on cell enlargement and cell production in cotton roots. *Plant Physiol.* **1986**, *82*, 1102–1106. [CrossRef]
60. Burssens, S.; Himanen, K.; Van de Cotte, B.; Beeckman, T.; Van Montagu, M.; Inzé, D.; Verbruggen, N. Expression of cell cycle regulatory genes and morphological alterations in response to salt stress in Arabidopsis thaliana. *Planta* **2000**, *211*, 632–640. [CrossRef]
61. Comas, L.; Becker, S.; Cruz, V.M.V.; Byrne, P.F.; Dierig, D.A. Root traits contributing to plant productivity under drought. *Front. Plant Sci.* **2013**, *4*, 442. [CrossRef]
62. Dogan, M.; Tipirdamaz, R.; Demir, Y. Salt resistance of tomato species grown in sand culture. *Plant Soil Env.* **2010**, *56*, 499–507. [CrossRef]
63. Zarafshar, M.; Akbarinia, M.; Askari, H.; Hosseini, S.M.; Rahaie, M.; Struve, D.; Striker, G.G. Morphological, physiological and biochemical responses to soil water deficit in seedlings of three populations of wild pear (Pyrus boisseriana). *Gembloux Agro-Bio Tech* **2014**, *18*, 353–366.

64. Hernandez, J.; Jimenez, A.; Mullineaux, P.; Sevilia, F. Tolerance of pea (Pisum sativum L.) to long-term salt stress is associated with induction of antioxidant defences. *Plant Cell Environ.* **2000**, *23*, 853–862. [CrossRef]
65. Hasegawa, P.M.; Bressan, R.A.; Zhu, J.-K.; Bohnert, H.J. Plant cellular and molecular responses to high salinity. *Annu. Rev. Plant Biol.* **2000**, *51*, 463–499. [CrossRef] [PubMed]
66. Atkinson, N.J.; Urwin, P.E. The interaction of plant biotic and abiotic stresses: From genes to the field. *J. Exp. Bot.* **2012**, *63*, 3523–3543. [CrossRef] [PubMed]
67. Patade, V.Y.; Bhargava, S.; Suprasanna, P. Transcript expression profiling of stress responsive genes in response to short-term salt or PEG stress in sugarcane leaves. *Mol. Biol. Rep.* **2012**, *39*, 3311–3318. [CrossRef] [PubMed]
68. Xie, C.; Zhang, R.; Qu, Y.; Miao, Z.; Zhang, Y.; Shen, X.; Wang, T.; Dong, J. Overexpression of MtCAS31 enhances drought tolerance in transgenic Arabidopsis by reducing stomatal density. *New Phytol.* **2012**, *195*, 124–135. [CrossRef]
69. Mohamed, E.-A.; Iwaki, T.; Munir, I.; Tamoi, M.; Shigeoka, S.; Wadano, A. Overexpression of bacterial catalase in tomato leaf chloroplasts enhances photo-oxidative stress tolerance. *Plant Cell Environ.* **2003**, *26*, 2037–2046. [CrossRef]
70. Brugnoli, E.; Lauteri, M. Effects of salinity on stomatal conductance, photosynthetic capacity, and carbon isotope discrimination of salt-tolerant (*Gossypium hirsutum* L.) and salt-sensitive (*Phaseolus vulgaris* L.) C3 non-halophytes. *Plant Physiol.* **1991**, *95*, 628–635. [CrossRef]
71. Burbidge, A.; Grieve, T.M.; Jackson, A.; Thompson, A.; McCarty, D.R.; Taylor, I.B. Characterization of the ABA-deficient tomato mutant notabilis and its relationship with maize Vp14. *Plant J.* **1999**, *17*, 427–431. [CrossRef]
72. Wan, X.-R.; Li, L. Regulation of ABA level and water-stress tolerance of Arabidopsis by ectopic expression of a peanut 9-cis-epoxycarotenoid dioxygenase gene. *Biochem. Biophys. Res. Commun.* **2006**, *347*, 1030–1038. [CrossRef]
73. Umezawa, T.; Okamoto, M.; Kushiro, T.; Nambara, E.; Oono, Y.; Seki, M.; Kobayashi, M.; Koshiba, T.; Kamiya, Y.; Shinozaki, K. CYP707A3, a major ABA 8′-hydroxylase involved in dehydration and rehydration response in Arabidopsis thaliana. *Plant J.* **2006**, *46*, 171–182. [CrossRef]
74. Gondim, F.A.; Gomes-Filho, E.; Costa, J.H.; Mendes Alencar, N.L.; Prisco, J.T. Catalase plays a key role in salt stress acclimation induced by hydrogen peroxide pretreatment in maize. *Plant Physiol. Biochem. PPB* **2012**, *56*, 62–71. [CrossRef]
75. Moriwaki, T.; Yamamoto, Y.; Aida, T.; Funahashi, T.; Shishido, T.; Asada, M.; Prodhan, S.H.; Komamine, A.; Motohashi, T. Overexpression of the Escherichia coli catalase gene, katE, enhances tolerance to salinity stress in the transgenic indica rice cultivar, BR5. *Plant Biotechnol. Rep.* **2008**, *2*, 41–46. [CrossRef]
76. Badawi, G.H.; Yamauchi, Y.; Shimada, E.; Sasaki, R.; Kawano, N.; Tanaka, K.; Tanaka, K. Enhanced tolerance to salt stress and water deficit by overexpressing superoxide dismutase in tobacco (Nicotiana tabacum) chloroplasts. *Plant Sci.* **2004**, *166*, 919–928. [CrossRef]
77. Eltayeb, A.E.; Kawano, N.; Badawi, G.H.; Kaminaka, H.; Sanekata, T.; Morishima, I.; Shibahara, T.; Inanaga, S.; Tanaka, K. Enhanced tolerance to ozone and drought stresses in transgenic tobacco overexpressing dehydroascorbate reductase in cytosol. *Physiol. Plant.* **2006**, *127*, 57–65. [CrossRef]
78. Robledo, J.M.; Medeiros, D.; Vicente, M.H.; Azevedo, A.A.; Thompson, A.J.; Peres, L.E.P.; Ribeiro, D.M.; Araújo, W.L.; Zsögön, A. Control of water-use efficiency by florigen. *Plant Cell Environ.* **2020**, *43*, 76–86. [CrossRef]
79. Silva, W.B.; Vicente, M.H.; Robledo, J.M.; Reartes, D.S.; Ferrari, R.C.; Bianchetti, R.; Araújo, W.L.; Freschi, L.; Peres, L.E.P.; Zsögön, A. SELF-PRUNING Acts Synergistically with DIAGEOTROPICA to Guide Auxin Responses and Proper Growth Form. *Plant Physiol.* **2018**, *176*, 2904–2916. [CrossRef]
80. Zsögön, A.; Cermak, T.; Voytas, D.; Peres, L.E.P. Genome editing as a tool to achieve the crop ideotype and de novo domestication of wild relatives: Case study in tomato. *Plant Sci.* **2017**, *256*, 120–130. [CrossRef]
81. Zsögön, A.; Čermák, T.; Naves, E.R.; Notini, M.M.; Edel, K.H.; Weinl, S.; Freschi, L.; Voytas, D.F.; Kudla, J.; Peres, L.E.P. De novo domestication of wild tomato using genome editing. *Nat. Biotechnol.* **2018**, *36*, 1211–1216. [CrossRef]

# GENERAL CONCLUSION AND PERSPECTIVES

In light of current and future concerns surrounding the effects of adverse weather factors on food production. Our data provide a detailed characterization of leaf morphological and physiological traits that can significantly aid in the process of improving tomato resistance to drought conditions. The identification of genes responsible for leaf traits such as succulence, mesophyll cell anatomy, stomatal and vein density, and vascular bundle sheath extension is an important step toward understanding how plants control these traits under stressful conditions and how we can utilize them to produce more resilient plants. Finally, we suggest the existence of important *S. pen* genes responsible for changes in leaf traits that may improve the resistance of commercial tomato plants to water deficit conditions. Furthermore, we demonstrate the important, yet understudied, the role of the auxin signaling network on resistance to abiotic stresses.

In the first chapter of this work, we characterized IL2-5, IL4-3, and IL2-5/4-3 and demonstrated that the leaf anatomical and morphological traits of these ILs can enhance the drought resistance capacity of tomato plants. After removal of irrigation, these ILs showed delayed leaf wilting, improved maintenance of leaf water status and leaf gas exchange, reduced damage to photosynthetic machinery and increased resilience. We attribute these behaviors during drought to increased leaf thickness and succulence, as well as reduced leaf area and stomatal density. We saw that, relative to its parents, IL2-5/4-3 showed an additive phenotype with greater leaf thickness, also exhibiting better root system development under drought conditions. Both ILs showed higher drought resistance compared to cv. M82. In this work, we also demonstrated that the anatomical changes manifested by these ILs do not alter the ability to perform leaf gas exchange. On the other hand, we demonstrated that these changes may benefit the increase in the photosynthetic capacity of the plants. By analyzing the responses of the parental ILs alone, we saw that IL4-3 can significantly contribute to the maintenance of tomato yield after a period of drought. In the future, the use of sub-lineages of IL2-5 and IL4-3 may help in accurately mapping the genetic basis of phenotypes with increased leaf thickness and succulence.

In the second chapter, we identified allelic variation in the *OBV* gene in tomato, which is responsible for controlling the development of BSEs. We showed that BSEs play an important role in the physiological and hydraulic functions of leaves, increasing hydraulic conductivity and photosynthesis. In this work, we saw that mutation of this gene disrupts a C2H2 zinc finger motif in the *OBV* protein, resulting in the absence of BSEs in leaves. Here,

we also show that *OBV* can generate changes in leaf insertion angle, leaf margin serration, smaller vein density, and fruit shape through changes in auxin signaling. The discovery of the *OBV* gene enables an improved understanding of the role of BSEs in plant ecophysiological responses and is also a key step towards insertion and exploitation of the key benefits of BSEs in agronomically important species.

Finally, in the third chapter, we explore the involvement of *ARF4* in tomato responses to drought, salinity, and osmotic stress and confirm its role in resistance to these stresses using CRISPR technology. Here, we show that negative regulation of *SlARF4* can enhance tomato resistance to salinity and water stress. Loss-of-function of *ARF4* enhances root system development through changes in length and density. We demonstrated that the *ARF4-as* leaf curl phenotype comes accompanied by lower stomatal conductance, higher *WUE*, as well as reduced stress damage to photosynthetic pigments. Here, we saw that *ARF4-as* showed an expressive increase in ABA content in drought, which was caused by activation of biosynthesis-related genes as well as repression of ABA catabolism genes in this genotype. Thus, we demonstrate that an *ARF4* mutant generated by CRISPR technology exhibits similar responses to *ARF4-as*, thus confirming the role of *ARF4* in resistance to the stresses discussed.